

Probe Modelling and Experimentation for Advancing Atrial Fibrillation Treatment using Irreversible Electroporation Therapy

A dissertation presented by:

Hamza Benchakroun

To:

College of Science and Engineering, University of Galway,

in fulfilment of the requirements for the degree of
Doctor of Philosophy.

Supervised by:

Martin O'Halloran and Declan O'Loughlin

23 August 2023

Contents

<i>Declaration of Originality</i>	5
<i>Acknowledgements</i>	6
<i>List of Figures</i>	7
<i>List of Tables</i>	10
<i>Abstract</i>	11
<i>Chapter 1: Introduction</i>	12
1.1 Introduction	12
1.2 Motivation	14
1.3 Thesis Contributions	15
1.4 Journal and Conference Publications	17
1.5 Thesis Structure	19
<i>Chapter 2: Literature Review</i>	21
2.1 Introduction	21
2.2 Atrial fibrillation	22
2.3 Anatomy and Physiology of the LAA	24
2.4 Current Treatment for AF	25
2.4.1 Pharmacological treatments	25
2.4.2 Cardioversion treatments.....	26
2.4.3 Surgical Treatments.....	27
2.4.4 Catheter-based ablation treatments	29
2.5 Electroporation	29
2.6 Conductivity of biological tissue	31
2.6.1 Model for the Passive Electrical Properties of Cells and Tissues.....	31
2.6.2 Conductivity of biological tissue below 100 kHz	33
2.7 Measurement techniques	35
2.7.1 Electromagnetic wave propagation method (free space)	37
2.7.2 Resonant-based measurement.....	38
2.7.3 Inductance-based method	39
2.7.4 Transmission line	40
2.7.5 Capacitive-base method.....	41
2.8 Protocol for conductivity acquisition	42
2.9 Conductivity of the cardiac tissue	45
2.10 Conclusions	47

<i>Chapter 3: Evaluation of Tetrapolar Probes: Investigating the Impact of Probe Typology and Electrode Size on Conductivity Measurements for the Left Atrial Appendage from 0.1 Hz to 100 kHz</i>	48
3.1 Introduction	48
3.2 Background	50
3.2.1 Operating frequency of the tetrapolar probe	50
3.2.2 Design process of a tetrapolar probe	51
3.2.3 Typology of the tetrapolar probe	52
3.2.4 Electrode spacing	52
3.2.5 Electrode size	53
3.2.6 Electrode material	53
3.3 Methodology	54
3.3.1 Probe description	54
3.3.2 Data acquisition	57
3.3.3 Measurement accuracy	60
3.3.4 Repeatability of measurement	61
3.4 Results	62
3.4.1 Effect of the typology and electrode size of the probe on the accuracy of the acquired conductivity	62
3.4.2 Effect of the typology and electrode size of the probe on the repeatability of the acquired conductivity	66
3.5 Conclusion	67
<i>Chapter 4: Assessing Conductivity of Ex-vivo Left Atrial Appendage from 0.1 Hz to 100 kHz</i>	69
4.1 Introduction	69
4.2 Background on Probes used or cardiac tissue electrical characterisation	70
4.3 Methodology of Left atrial appendage measurement	70
4.3.1 Data acquisition of the electrical properties below 100 kHz	70
4.3.2 Probe description	71
4.3.3 Sample acquisition and tissue handling of the LAA	72
4.4 Assessing the conductivity of ten ex-vivo samples of LAA from 0.1 Hz to 100 kHz at room temperature	74
4.5 Conclusion	76
<i>Chapter 5: The Effect of Contact Force on Conductivity Measurement of Ex-vivo Left Atrial Appendage of from 10 Hz to 100 kHz</i>	78
5.1 Introduction	78
5.2 Background	79
5.3 Methodology	80
5.3.1 Forward experiment description	81
5.3.2 Reverse experiment description	81
Hyperhydration experiment description	82
5.3.4 Data acquisition	82

5.3.5	Force Monitoring	83
5.3.6	Statistical analyses.....	83
5.3.7	Tissue handling	84
5.4	Results: Assessing the conductivity of the LAA change due to probe contact force	85
5.5	Conclusion.....	90
<i>Chapter 6: Effects of IRE on Conductivity of Hydrogel with Cells: IRE Implications for Atrial Fibrillation</i>		91
6.1	Introduction	91
6.2	Methodology	92
6.2.1	Cell culture	92
6.2.2	Hydrogel	93
6.2.3	Conductivity acquisition.....	94
6.2.4	Statistical analysis.....	94
6.2.5	Hydrogel testing.....	95
6.2.6	Hydrogel validation stress test	95
6.2.7	Hydrogel validation test	96
6.2.8	Ablation protocol.....	97
6.3	Results and Discussion	99
6.4	Conclusion.....	101
<i>Chapter 7: Conclusions and Future Work</i>		102
7.1	Summary of the main conclusions	102
7.2	Future work	105

Declaration of Originality

I, the Candidate **Hamza Benchakroun**, certify that this thesis entitled “**Advancing Irreversible Electroporation Therapy for Atrial Fibrillation through Comprehensive Analysis of Electrical Conductivity of Left Atrial Appendage: Probe Design, Contact Force, and Treatment Validation**”:

- is all my work.
- has not been previously submitted for any degree or qualification at this University or any other institution.
- and where any work in this thesis was conducted in collaboration, appropriate reference to published work by my collaborators has been made and the nature and extent of my contribution has been clearly stated.

Name: Hamza Benchakroun

Acknowledgements

I would like to thank Pr. Dr Martin O'Halloran for allowing me to work in his lab with friendly people and to supervise my work with the fundamental support of Declan O'Loughlin. I would like to thank Declan for his dedication to my work and his crucial feedback throughout these four years, I thank you for your patience and your way of working, I learned immensely from you. You deservedly earned my respect forever, and I used "deservedly" because you hate that word. I would also like to thank all my colleagues and friends, who gave me technical support during the PhD. To Niko Ištuk, Camille O'Malley, Nuno Silva, Anna Bottiglieri, Laura Farina, Nadia Muhammad Hussain, Stuart Dean, and Cristoforo Decaro for the endless coffee breaks, cigarette breaks, and moral support provided during the PhD. Finally, from the lab, I would like to thank Adam Elahi, Barry McDermott, Eoghan Dunne, Bilal Amin, and Jara Maria Baena Montes, who made my working hours more pleasant. Out of the lab, I would like to particularly thank my family (Anas, Hanane, Zhor, Chama, Maha, and Aissa) for their constant support in my life. I would like to also thank myself for finishing the PhD, it was not easy, but you did it. Congratulation, and let's start writing a new chapter.

List of Figures

Figure 2. 1 illustration compares the normal heart rhythm to the irregular pattern seen in the heart..... 23

Figure 2. 2 The transesophageal echocardiography image illustrates the elliptical configuration of the LAA in relation to the heart [85] with two distinct diameters in A' and B' 25

Figure 2. 3 Complete set of atrial lesions as done in the cox-maze procedure..... 28

Figure 2. 4 Electrical model for a suspended cell viewed from electrodes: Extracellular and intracellular media are resistances, while the cell membrane is a capacitance. Combined as R_e (extracellular resistance) in parallel with C_m (membrane capacitance) and R_i (intracellular resistance) [30]..... 31

Figure 2. 5 (a) Representation of low-frequency (left) and high-frequency (right) current flow through a cell suspension or tissue, illustrating the restriction of low-frequency currents to extracellular spaces and the unhindered passage of high-frequency currents..... 32

Figure 2. 6 Measurement setup configurations (a) two electrodes, (b) three electrodes and (c) four electrodes..... 44

Figure 2. 7 Conductivity acquired from the literature review of conductivity of cardiac tissue..... 46

Figure 3. 1 Flow of electrical current through biological tissue. At lower frequencies (A), the current moves between the cells and through the extracellular fluid. However, at higher frequencies (B), the current can penetrate the cell membrane 48

Figure 3. 2 diagram of the parameters to consider when designing a tetrapolar probe, that includes electrode size, electrode spacing, electrode material and he probe typology..... 51

Figure 3. 3 Diagram showing the dimensions of the two proposed typologies of tetrapolar probe used in this paper (a) collinear probe (b) polar probe (c) small collinear probe (d) Small asymmetric collinear probe (e) small asymmetric and unequal collinear probe (f) unequal polar prob 55

Figure 3. 4 Measurement setup with the probe, the laptop running NOVA 2.1 software in the foreground. PGSTAT204 potentiostat/galvanostat and the probe holder used to lift and keep the probe fixed 58

Figure 3. 5 Results for the small collinear probe, including its correlation factor and cell constant from three NaCl solutions from frequency 0.1 Hz to 100 kHz 59

List of Figures

Figure 3. 6 Pearson correlation coefficient (R) as a function of the frequency range for the proposed probes. R represents the experimental response of the probes to the calibration solutions and reflects the working frequency of the probes	60
Figure 3. 7 The electric field distribution by the proposed probes focusing on points A and B. (a) filed distribution of the polar probe (V m-1). (b) electric field distribution of the collinear probe (V m-1). (c) electric field distribution of the small collinear65	65
Figure 3. 8 Coefficient of variation (CV) of the polar probe, collinear probe, small collinear probe, unequal collinear probe, asymmetric and unequal probe, and the unequal polar probe. CV shown in the totality targeted frequency range from .1 Hz to 100 kHz	67
Figure 4. 1 Measurement setup with the probe, the laptop running NOVA 2.1 software in the foreground. PGSTAT204 potentiostat/galvanostatic and the probe holder used to lift and keep the probe fixed	71
Figure 4. 2 Diagram showing the dimensions of the proposed collinear probe with small electrodes. The illustration shows the footprint of the probe on the surface of the LAA, (b) Photo of the manufactured prototype of the proposed collinear probe with small electrodes	72
Figure 4. 3 Left picture shows the first sample bovine heart with the LAA highlighted. The right picture shows the dissected LAA from sample one. The yellow square shows the position of the LAA pectinate muscle where the measurements were taken. The yellow dot shows part of the membrane	74
Figure 4. 4 Conductivity acquired from ten bovine LAA samples at room temperature 20 °C and the reference cardiac conductivity	75
Figure 5. 1 (a) Left picture shows the first sample bovine heart with the LAA highlighted; (b) The right picture shows the dissected LAA from sample one. The yellow square shows the position of the LAA pectinate muscle where the measurements were taken.	85
Figure 5. 2 The average variation of the conductivity with the contact force for (a) forward experiment (b) reverse experiment (c) hyperhydration experiment	86
Figure 5. 3 The average variation of the conductivity with the force for the forward, reverse, and hyperhydration experiment at 10 Hz, 100 Hz, 1 kHz, 10 kHz, and 100 kHz.....	87
Figure 5. 4 The percentage variation of the conductivity from the proposed experiment at 10 Hz, 100 Hz, 1 kHz, 10 kHz, and 100 kHz (a) Forward experiment with ten LAAs, contact force from 2 N to 10 N (b) Reverse experiment with five LAAs, contact force from 10 N to 1 N (c) the hyperhydration experiment with five LAAs, contact force from 1 N to 10 N	89

List of Figures

Figure 6. 1 The figure shows the effects of probe contact force on the surface of the hydrogel during the stress test. The photos illustrate that the hydrogel starts exhibiting damage at 4N, with more pronounced indentations at higher contact forces. The first sample of hydrogel shown in this figure is breaks at 8N 96

Figure 6. 2 shows visible marks on the surface of all three hydrogel samples following IRE. These marks are from the electrodes used for the treatment and were not present prior to treatment. (a) shows the marks on sample 1 (b) shows the probe used for IRE 97

Figure 6. 3 compares pre- and post-IRE conductivity measurements with the standard deviation of the hydrogel. The results show that there was no significant change in conductivity between pre- and post-IRE 97

Figure 6. 4 Schematic diagram of the IRE setup, consisting of a two-electrode probe connected to a signal generator. The probe is composed of two 50 μm thick copper electrodes with dimensions of 3×5 mm and a 5 mm gap 98

Figure 6. 5 3D scanned images of three hydrogel samples with cells after IRE treatment, as visualized by the EVOS M7000 Imaging System. The green area indicates living cells, and the red area indicates dead cells in the treated zone. The ablation parameters, including area, perimeter, and diameter, match the expected results from a successful treatment protocol..... 98

Figure 6. 6 hydrogel sample with and without cells (a) hydrogel with cells the pink tint is introduced by the cells and cell media (b) hydrogel without cells 99

Figure 6. 7 shows the comparison of the mean conductivity with the standard deviation of the hydrogel with cells before and after IRE. The graph displays the conductivity measurements from ten different samples at various frequencies ranging from 10 Hz to 100 kHz..... 100

List of Tables

Table 2.1 the different measurement techniques to acquire electrical properties of biological tissues	36
Table 2.2 Summary of the tetrapolar probe used to characterize biological tissue with their respective size. the two most common probes are the collinear probe and the polar probe	45
Table 3.1 Characteristics of the six probes used in chapter 3, including the probe type, electrode configuration, electrode diameter, and distance between electrodes. The table also lists the number of electrodes and the total length of the probe.....	57
Table 3.2 The table provides the values of k (m) for various types of probes within the frequency range from 0.1 Hz to 100 kHz.	59
Table 3.3 Average conductivity plus SD of NaCl phantom acquired with the proposed probes with the reference conductivity values	63
Table 4.1 Average electrical conductivity of ten bovine LAA samples compared to literature values	76
Table 5.1 Contact force reported by the ten studies investigating heart muscle conductivity from the IT'IS Foundation database and how the contact pressure during the measurement is described	79
Table 5.2 Percentage change of the electrical properties of cervix, lung, and liver with monotonically increasing contact force.....	80
Table 5.3 The measured conductivity changes by -21% and -2.5% due to the increase of force contact for the set of samples in the forward and the hyperhydration experiment, respectively, +1.3% change is seen in the conductivity in the samples in the reverse experiment	87
Table 5.4 p-Values from the two tests conducted to assess the significance of the variation between the forward experiment, the reverse, and the hyperhydration experiment.....	88

Abstract

Atrial fibrillation (AF) poses a significant global health challenge, with the left atrial appendage (LAA) identified as a frequent source. Irreversible electroporation (IRE) has emerged as a promising non-thermal ablation technique for AF treatment. This research focuses on understanding LAA conductivity, crucial for estimating IRE outcomes through experimental work and numerical simulations.

The study investigates the impact of confounding factors on LAA conductivity, addressing probe design and contact force monitoring's significance. A tetrapolar probe and protocol are developed, characterizing LAA conductivity below 100 kHz and providing the first in literature LAA conductivity of ex-vivo bovine LAA from 0.1 Hz to 100 kHz. The findings underscore the importance of tailored probe designs for accurate and repeatable conductivity measurements.

Additionally, the research proposes a benchtop LAA model with living myocardial cells to assess IRE outcomes through pre- and post-conductivity measurements. Results indicate the potential use of conductivity as a validation method for IRE treatment effectiveness. This thesis serves as a valuable guide for future research into IRE as an AF treatment, emphasising the application of conductivity measurements for validation purposes. The insights gained contribute to advancing the understanding of AF treatment strategies and the role of conductivity in assessing the success of innovative interventions.

Chapter 1: Introduction

1.1 Introduction

Atrial fibrillation (AF) is the most frequent cardiac arrhythmia worldwide [1]–[4]. In 2017, over 3 million new cases worldwide were diagnosed with AF. Predictions estimate that 6–12 million people will suffer from AF in the US by 2050 and 17.9 million in Europe by 2060 [5]–[7]. AF increases the risk of blood clots, stroke, heart failure, and other heart-related complications [1]–[4].

AF is characterized by the irregular activation of the atria, where the normal electrical activity directed by the sinus node is not synchronized with the different impulses firing from other locations in the atria [1], [4], [8]. The left atrial appendage (LAA) has been identified as a frequent source of these aberrant impulses [9], [10]. The result is a disordered heartbeat primarily in the atria, disturbing the blood flow from the atria to the ventricles [1]. The aberrant impulse propagation can be controlled to a certain extent by the atrioventricular node and therefore the activity of the ventricles is typically less affected [11].

The current methods used to treat AF are pharmacological, cardioversion, catheter-based management, and surgical treatments [4]. Pharmacological options are frequently the first-line treatment to restore normal heart rhythm and control the heart rate. If pharmacological treatments are not effective, other options may be indicated to control AF, including cardioversion (electric shock to restore rhythm), catheter treatments (including ablation), and surgery (ranging from pacemaker implantation to Cox-maze procedure) [3], [12]. In addition to the current treatments, new potential treatments are being investigated and proposed [1], [4], [13], including non-thermal ablation using Irreversible electroporation (IRE) [14]–[17].

Non-thermal ablation using IRE has shown promising results in preclinical trials [13], [14], [17], and several medical device companies are investigating non-thermal ablation using IRE as a treatment for AF. Henceforth, non-thermal ablation

utilizing IRE will be referred to as "IRE" throughout the remainder of this thesis. Similarly to existing treatments, such as radio-frequency treatment [18], IRE aims to disturb the cell membrane ultimately leading to apoptosis and necrosis of the targeted tissue cells [3], [16], [19].

IRE is achieved through the creation of a supraphysiological transmembrane potential across some, or all, of the cell membrane [10], [19], [20]. Typically, a pulsed electric field (PEF) is applied, commonly characterized in the clinical literature by the "pulse strength" and "pulse duration" [21], even though the precise impact of the waveform shape on the IRE result is not well understood [21]. The evidence suggests that a minimum threshold transmembrane potential is required to ensure apoptosis [19]–[22]. To estimate the transmembrane potential, numerical electromagnetic simulations can be used to calculate the field strength at points in the targeted tissue. Although some studies have looked at the electrical properties of heart tissues, the range of realistic electrical properties for cardiac muscle and particularly the LAA is not specifically studied.

Similar electromagnetic simulations are used to support the design of biomedical device design and treatment planning, across diverse applications including electrical impedance tomography [16], [23]–[44], and in applications related to oncology, it is used to differentiate between normal and cancerous tissues [31], [45], [46]. Historically, electrical properties of biological tissue have been studied [31], [32], [36], [41], [47]–[54] and have been synthesized into several freely available databases [55], [56]. The characterization of biological tissue is a growing research field since 1759 [57]. However, despite the substantial number of tissues summarized in the literature, multiple biological tissues are not reported such as LAA as an anatomical section of cardiac tissue was never investigated specifically.

The potential of IRE in treating AF and the role of electrical properties of the LAA in AF treatment planning have motivated this research. The thesis investigates an accurate and repeatable measurement protocol for the LAA and identifies the confounders that need to be controlled and measured to ensure the accuracy of the measurements.

1.2 Motivation

IRE involves using an electric field to modify cell membranes and ultimately induce apoptosis. Understanding the electrical properties of various tissues and adjusting pulse parameters accordingly to the targeted tissue e.g. LAA is needed for effective AF treatment. However, there is limited research on the electrical properties of the LAA. Gaining accurate knowledge of the electrical characteristics of the LAA would be valuable for optimizing and potentially monitoring IRE procedures. The initial exploration related to this thesis has led to the identification several unresolved questions that are distinct from the primary research questions that will be addressed in this study. These open questions include:

- What is the importance of understanding the electrical properties of tissues for the advancement of IRE for AF treatment?
- Given the multiple data acquisition protocols for the electrical properties of tissue available in the literature, can standardization be achieved?
- Is it possible to achieve repeatable and accurate measurements of the electrical properties of complex biological tissues?
- What is the impact of confounding factors on the acquisition of electrical properties of biological tissues?
- Can these electrical properties be utilized as a means of validating cardiac IRE treatments?

These unanswered questions motivate the research objectives of this thesis, preceded by an extended literature review. Upon conducting a comprehensive literature review, a substantial amount of information was found regarding the data acquisition of electrical properties of different biological tissues. The resulting data has been compiled and summarized in several papers and online databases [55], [56]. While the literature offers extensive knowledge, they often fall short in including all biological tissues.

The difficulty in characterizing a previously uninvestigated tissue like the LAA can be attributed, in part, to differences in acquisition hardware, protocols, and associated metadata of the original data. Therefore, researchers face challenges in determining the most suitable approach to analyse and understand this complex

Chapter 1. Introduction

tissue. The complexity of the tissue refers to the structural and functional complexity. The effect of these differences on the electrical properties of tissue remains largely unexplored, further complicating the process of characterizing a new tissue like the LAA. These gaps in knowledge have led to the formulation of research questions that will be addressed in the thesis. Research questions that will be addressed in the thesis are as follows:

- 1) What are the best methods for characterizing the electrical properties of the LAA for the frequency range below 100 kHz?
- 2) How does the design of probes used during the electrical characterization measurement of the tissue impact the accuracy and the repeatability of acquired electrical properties of the LAA for frequencies below 100 kHz?
- 3) What are the electrical properties of ex-vivo LAA below 100 kHz, and how do they compare to existing research on cardiac tissue electrical properties?
- 4) What is the impact of probe contact force on the acquired electrical properties of the LAA below 100 kHz?
- 5) Could the electrical properties of the LAA be utilized as a means to validate IRE in a benchtop LAA model?

The specific contributions described in this thesis are summarised in the following section. 1.3.

1.3 Thesis Contributions

The primary objective of this thesis is to investigate the impact of different tetrapolar probes and external factors related to probe contact force on the electrical properties of the LAA, and the corresponding implications for potential treatment planning in AF. Additionally, the thesis will evaluate the ability to validate IRE through the monitoring of electrical properties. Specifically, the contributions of this thesis are as follows:

- 1) Evaluates the feasibility of custom-made tetrapolar probes for electrical characterization of the LAA in the IRE frequency below 100 kHz.

- 2) Proposes an optimized tetrapolar probe design for measuring the electrical properties of the LAA.
- 3) Provides the first ex-vivo measurement of bovine LAA properties at room temperature at the frequency range from 0.1 Hz to 100 kHz.
- 4) Enhance the understanding of the probe contact force dependency of electrical properties measurements in the case of the LAA.
- 5) Design a benchtop LAA model using hydrogel embedded with myocardial cells.
- 6) Monitor cell behaviours under IRE in a benchtop LAA model and assess the impact on electrical properties, as a platform for treatment planning.

The central research objectives necessary to fulfil the contribution of the thesis are accomplished through the following phases:

- Conducting a fundamental analysis of the limitations of tetrapolar probe design for electrical property measurements of the LAA, designing, building, and characterizing a tetrapolar probe for measuring the electrical properties of the LAA, and extending the limited understanding of the impact of tetrapolar probe design limitations on the reliability of electrical properties acquisition.
- Developing and characterizing an optimized tetrapolar probe for electrical measurement of the LAA and the assessment of the LAA electrical properties in relation to existing research on cardiac tissue. To the best of our knowledge, this study provides the first ex-vivo measurement of the electrical properties of bovine LAA at room temperature in the frequency range from 0.1 Hz to 100 kHz.
- Expanding the understanding of the effect of contact force on the electrical properties of the LAA over the frequency range below 100 kHz. The study also assesses the role of tissue extracellular fluid in tissue electrical properties and provides a mechanism to investigate the influence of probe contact force on these properties.

- Utilizing hydrogel and myocardial cells as a benchtop LAA model to assess the cell deaths due to IRE as a potential method to validate IRE treatment.

The specific contributions described in this thesis are summarised in the following section, including the publications arising from these contributions.

1.4 Journal and Conference Publications

The present study aims have been summarised and successfully presented at conferences and published in peer-reviewed journals. The research findings have been published in three journals and presented in seven conference papers. The journal first author publications are:

- **H. Benchakroun**, N. Ištuk, E. Dunne, A. Elahi, T. O'Halloran, M. O'Halloran and D. O'Loughlin, "Design of a Tetrapolar Probe for Electrical Characterization of the Left Atrial Appendage From 0.1 Hz to 100 kHz". 2023, IEEE Sensors Journal, 23(1), 741-749
<https://doi.org/10.1109/JSEN.2022.3218534>
- **H. Benchakroun**, N. Ištuk, E. Dunne, A. Elahi, T. O'Halloran, M. O'Halloran and D. O'Loughlin, "Probe Contact Force Monitoring during Conductivity Measurements of the Left Atrial Appendage to Support the Design of Novel Diagnostic and Therapeutic Procedures", 2022, Sensors, 22, 7171.
<https://doi.org/10.3390/s22197171>

The work in this thesis has been presented at the following conferences:

- **H. Benchakroun**, D. O'Loughlin, N. Ištuk, M. O'Halloran and A. La Gioia, "Evaluation of the Feasibility of Three Custom-made Tetrapolar Probes for Electrical Characterization of Cardiac Tissue," 2021 15th European Conference on Antennas and Propagation (EuCAP), pp. 1-5
<https://doi.org/10.23919/EuCAP51087.2021.9410978>
- **H. Benchakroun**, E. Dunne, D. O'Loughlin and M. O'Halloran, "Measurement of the Left Atrium Appendage Electrical Conductivity with a Tetrapolar Probe over 0 . 1 Hz to 100 kHz" 2021, 21st International

Chapter 1. Introduction

Conference on Biomedical Applications of Electrical Impedance Tomography.

Published collaborative work in this thesis is listed below:

- N. Ištuk, A. La Gioia, **H. Benchakroun**, A. Lowery, B. McDermott and M. O'Halloran, "Relationship Between the Conductivity of Human Blood and Blood Counts," 2022, IEEE Journal of Electromagnetics, RF and Microwaves in Medicine and Biology, vol. 6, no. 2, pp. 184-190, <https://doi.org/10.1109/JERM.2021.3130788>.
- N. Ištuk, R. Matta, **H. Benchakroun**, J. M. Baena-Montes, L. Quinlan, D. Moreau, R. O'Connor, E. Dunne, A. Elahi and M. O'Halloran, "Miniaturised Four-Electrode Conductivity Probe with PEDOT:PSS Coating" 2023, URSI GASS 2023, Sapporo, Japan.
- N. Ištuk, A. La Gioia, **H. Benchakroun**, A. Lowery, B. McDermott and M. O'Halloran, "Measurement of Electrical Conductivity of Human Blood at Frequencies Below 100 kHz with Four-electrode Probe Method". 2021, XXXIVth General Assembly and Scientific Symposium of the International Union of Radio Science (URSI GASS), 1–4. <https://doi.org/10.23919/URSIGASS51995.2021.9560424>, Galway, Ireland.
- N. Ištuk, **H. Benchakroun**, M. A. Elahi and M. O'Halloran, "The Effect of Contact Pressure on Ex-vivo Measurements of the Conductivity of Liver," 2022, 16th European Conference on Antennas and Propagation (EuCAP), 2022, pp. 1-3, <https://doi.org/10.23919/EuCAP53622.2022.9769625>, Madrid, Spain.
- N. Ištuk, **H. Benchakroun**, E. Dunne, M. O'Halloran, "Pressure Dependency of Conductivity Measurements: The Specific Case of the Lung". 2021, 21st International Conference on Biomedical Applications of Electrical Impedance Tomography, Galway, Ireland.
- S. Burke, K. Polak-Kraśna, **H. Benchakroun**, P. Vazquez, M. O'Halloran, A. Shahzad, W. Wijns, M. Kraśny, "Feasibility study of plaque detection using electrical impedance techniques". 2022, 16th European Conference on Antennas and Propagation (EuCAP), IEEE. <https://doi.org/10.23919/EuCAP53622.2022.9769600>, Madrid, Spain.

1.5 Thesis Structure

The remainder of this thesis is organized as follows. Chapter 2 presents an overview of the current state of knowledge on AF, including a description of AF and the current treatment options for AF. It also introduces an overview of the anatomy, physiology, and electrical properties of the LAA. Chapter 2 also highlights a lack of knowledge of the electrical properties of the LAA. Additionally, it highlights the importance of understanding these properties for treatment planning for IRE. Chapter 2 introduces different measurement methods for the measurement of electrical properties of biological tissue. Finally, chapter 2 discusses the understudied influence of the probe design and probe contact force on the electrical properties of tissue.

Chapter 3 provides background on the design of probes used for measuring the electrical properties of biological tissue, specifically focusing on probes used in the characterization of cardiac tissue. Chapter 3 describes the methodology used, including the process for acquiring and characterizing electrical properties, as well as the rationale behind the proposed probe design. It also includes a comparison of different probes that can be used for characterizing the electrical properties of the LAA. This comparison highlights the effect of the probe on the data acquisition and identifies the best-fit probe for characterizing the LAA electrical properties.

Chapter 4 presents a novel contribution to the field of cardiac tissue electrical properties. Specifically, it provides the first published electrical properties of the LAA including the description of the sample acquisition, LAA dissection, and measurement procedures. Furthermore, chapter 4 provides the LAA electrical properties in relation to current knowledge on cardiac tissue electrical properties in the literature. Chapter 4 provides a valuable addition to the current understanding of the LAA electrical properties and its potential implications for the treatment planning of AF.

Chapter 5 reviews the current literature on electrical properties measurement and the impact of contact force on electrical properties. It describes the methodology of the study, including the electrical properties acquisition process, setup design, and sample handling. Chapter 5 evaluates the influence of contact force on the electrical properties acquired from LAA samples. It also analyzes the

Chapter 1. Introduction

significance of extracellular fluids in the tissue as a contributing factor to the effects observed.

Chapter 6 explores the monitoring of the electrical properties change in a benchtop LAA model due to IRE. Chapter 6 introduces a benchtop LAA model using a hydrogel embedded with myocardial cells. The electrical properties of the model are investigated before and after IRE. Chapter 6 is structured as follows: it describes the methodology used during the study, including the development of the benchtop LAA model using cultured human cardiomyocyte cells, the description of the hydrogel and how the cells are embedded in it, the conductivity measurement process, the protocol for IRE, and the assessment of hydrogel robustness and stability. Furthermore, chapter 6 includes a statistical analysis of the significance of conductivity change and assesses the validity of using electrical property monitoring as a validation tool for IRE.

Finally, chapter 7 summarizes the main conclusions of the research presented in the previous chapters and provides suggestions for future work.

Chapter 2: Literature Review

2.1 Introduction

The investigation of the electrical properties of biological tissues has been an area of ongoing research since 1894, with numerous studies conducted and published in the literature [28], [29], [49], [58]. The electrical properties of a variety of biological tissues have been examined [27], [28], [31]–[34], [51], [59]–[62], and these studies have been utilized in the development of various therapeutic and diagnostic technologies [16], [59], [63]–[70]. Synthesized data on the electrical properties of biological tissues is available in a number of papers and freely available online databases, the most cited in the literature are the Italian National Research Council database [55] and the IT’IS Foundation database [56]. Despite the information available in the literature, there are still some biological tissues that have yet to be characterized. The present thesis focuses on the LAA, which has not been investigated and has been recognised as a region of the heart associated with AF [1]–[3].

Chapter 2 provides a comprehensive literature review on AF, detailing the current understanding of the condition, as well as an overview of the current and potentially novel treatments that have been proposed. It also explores the significance of the electrical properties of the LAA in the context of developing treatment planning for AF [1]–[3]. Chapter 2 provides an analysis of the available databases and identifies the gap in knowledge for tissue characterisation and especially the electrical properties of the LAA. Furthermore, chapter 2 reviews methods of measuring the electrical properties of tissues, including the advantages and disadvantages of each method, and provides a discussion on the most appropriate method for measuring the electrical properties of the LAA.

2.2 Atrial fibrillation

AF is a cardiac arrhythmia characterized by the lack of coordination between the normal electrical activity directed by the sinus node and the impulses firing from other locations in the atria, as shown in Fig 2.1 [8], [71].

AF is defined as an intermittent or persistent pattern of disordered electrical activity in the atria, and consequentially, disruption in blood flow from the atria to the ventricles [34], [35]. The triggers of AF can differ among individuals, with the pulmonary veins being the most commonly associated area. However, recent studies have identified the LAA as a frequent source of these abnormal impulses that lead to AF [9], [72], [73]. Therefore, the treatments for AF presented in this thesis will include methods that target AF caused by the pulmonary vein, as well as those that address AF originating from the LAA [36].

The management of AF is often multifaceted and may involve a combination of pharmacological, cardioversion, and/or surgical interventions. The choice of treatment depends on various factors such as the underlying cause, the duration and frequency of episodes, and the patient's overall health status. This introduction provides an overview of the various treatment options available for AF, including their indications, benefits, and potential risks. AF is often classified into three distinct subtypes: paroxysmal, persistent, and long-standing persistent [1], [74].

- Paroxysmal AF is characterized by episodes of irregular cardiac rhythm lasting less than one week, which typically resolves spontaneously without the need for treatment [74].
- Persistent AF, on the other hand, is defined as continuous or recurrent episodes of irregular cardiac rhythm lasting for more than one week and requires intervention with anti-arrhythmic therapy or other forms of treatment [74].
- Lastly, long-standing persistent AF is characterized by the presence of continuous or recurrent episodes of irregular cardiac rhythm lasting for more than one year and is often considered resistant to treatment, requiring more advanced therapeutic options [74].

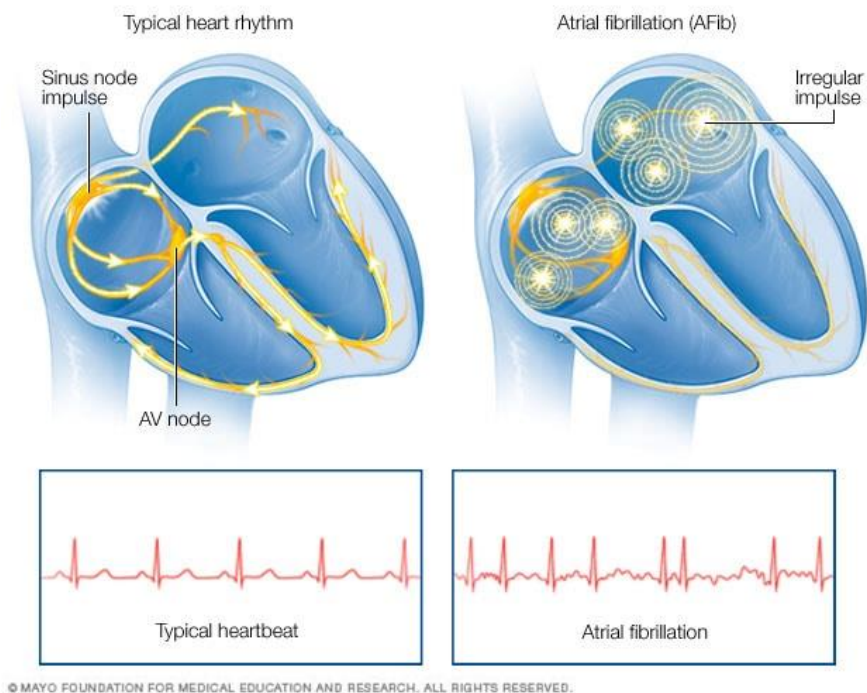


Figure 2. 1 illustration compares the normal heart rhythm to the irregular pattern seen in the heart

Pharmacological therapy is frequently used as first-line treatment and aims to restore normal heart rhythm and control heart rate [75]. Concurrently, patients may be prescribed anticoagulant medication to reduce the risk of secondary complications, such as stroke [75]. In cases where pharmacological therapy is not sufficient to control AF, additional treatment options such as cardioversion (the application of controlled electrical shocks to restore normal rhythm) [12], [76], catheter-based procedures (such as Radiofrequency Ablation) and surgery (such as pacemaker implantation or the cox-maze procedure) [77] may be employed. Recently, new technologies using catheter-based procedures have gained attention as a potential treatment option for AF [78]. These procedures, such as pulmonary vein isolation [79] and left atrial appendage closure (LAAC) [80], involve the use of catheters to ablate areas of the heart tissue that are causing the abnormal rhythm [81]. These procedures have been shown to be effective in reducing the recurrence of AF, for Pulmonary Vein Isolation (PVI) 61% reduction is seen in 367 patients [82] and for LAAC 48% reduction is seen in 1,240 patients [83]. In both cases for PVI and LAAC, the treatment is less invasive than traditional surgical options [10], [16], [19], [22], [30], [73], [84].

2.3 Anatomy and Physiology of the LAA

The heart, an intricate organ at the core of the circulatory system, coordinates the continuous circulation of oxygenated blood throughout the human body. Positioned within the thoracic cavity, left of the midline, the heart assumes the form of a muscular pump. Comprised of four chambers—two atria and two ventricles—the heart contracts rhythmically to facilitate blood flow. Its myocardial walls consist of specialized cardiac muscle tissue, endowed with contractile properties driven by electrical impulses. Within the anatomical structure of the heart, specific components play pivotal roles in maintaining cardiac function and efficiency. One such component is the LAA, an anatomical extension originating from the left atrium.

The LAA is an anatomical structure located in the left wall of the primary atrium, which forms during the fourth week of embryonic development [85]. The LAA is a long, tubular, hooked structure, usually crenellated, with a narrow junction to the venous component of the atrium as shown in Fig 2.2. In contrast to the LAA, the right atrial appendage is broad and triangular with a wide junction. The anatomy of the LAA can vary in shape and size, a study by Ernst et al., 1995 [86] provides a detailed description of the varied morphology of the LAA from 220 cases using synthetic resin casts made at necropsy. According to the study, the shape of the human LAA is predominantly elliptical (major and minor axes are *A* and *B* respectively shown in Fig 2.2), accounting for 68% of its shape, and its volume varies from 0.7 mL to 19.2 mL. Additionally, the shape of the LAA can vary depending on its depth, with *A* ranging from 16 to 51 mm, and its diameter, with *B* ranging from 10 to 40 mm [87].

Currently, the LAA is recognized as a structure with important pathological associations with AF, as LAA is now recognized as a frequent source of aberrant impulses in the heart causing AF [10], [14], [69], [73], [82], [83], [85].

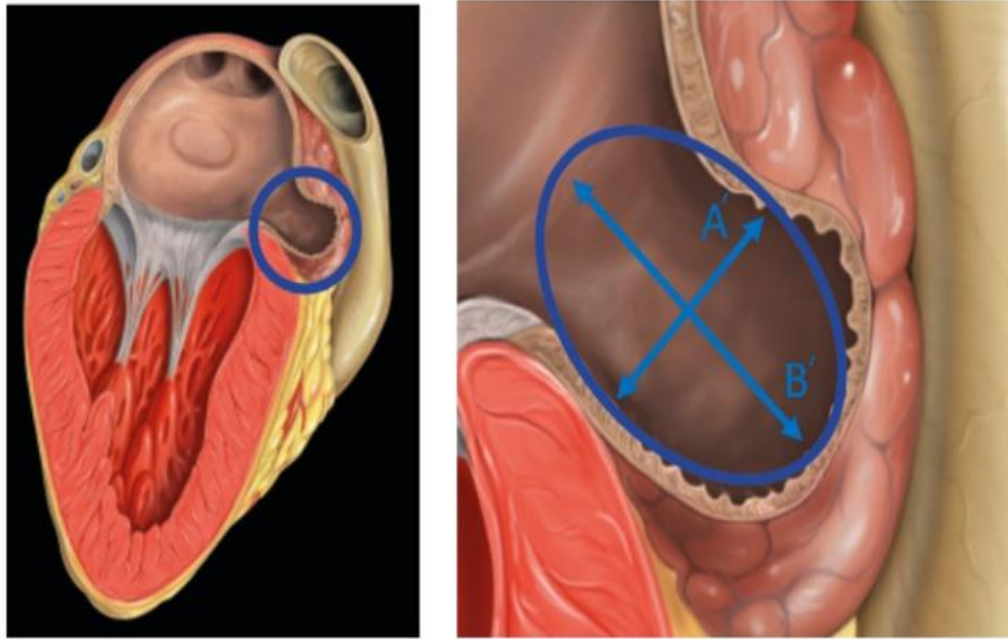


Figure 2. 2 The transesophageal echocardiography image illustrates the elliptical configuration of the LAA in relation to the heart [85] with two distinct diameters in A' and B'

2.4 Current Treatment for AF

Managing atrial fibrillation (AF) involves diverse approaches. Medications like beta-blockers are commonly used initially. Cardioversion, both electrical and chemical, restores normal heart rhythm, and surgical options like the maze procedure may be considered if initial treatments are ineffective. Minimally invasive catheter procedures, such as pulmonary vein ablation and left atrial appendage closure, offer alternatives. Electroporation, disrupting cell membranes with pulsed electric fields, holds promise. The ease of these approaches and their specific considerations will be discussed in the following sections, providing insights into precision and effectiveness in AF treatment.

2.4.1 Pharmacological treatments

Pharmacological treatments are commonly used for AF, summarised by Xu et al, 2006 [4]. The medication is primarily prescribed to control heart rate and rhythm and may also be used in conjunction with other treatments [75]. Medication options for treating AF may include [4]:

- **Rate control medications** prevent the ventricles from beating too fast (Beta-blockers (e.g., metoprolol, atenolol), Calcium channel blockers (e.g., diltiazem, verapamil), Digoxin).
- **Rhythm control medications** help restore a normal sinus rhythm (Amiodarone, Dronedarone, Flecainide, Propafenone, Sotalol).
- **Blood thinners** (anticoagulant medications) reduce the risk of blood clots and stroke (Warfarin, Dabigatran, Rivaroxaban, Apixaban).

Pharmacological treatments are often used to control the heart rate and rhythm and are often used as the first course of action. However, typically, the choice of treatment is based on many factors including clinical history, physical examination, allergies or drug interactions and side effects. Common side effects can include excessive bleeding, weakness, dizziness, and others [75].

2.4.2 Cardioversion treatments

Cardioversion is used to restore normal cardiac rhythm in cases of AF [12], [76]. Cardioversion has demonstrated high effectiveness with an overall success rate of 96.2% in 419 cases [88]. The study, which included individuals with irregular heartbeats, noted a male predominance of 69% among those undergoing cardioversion. The average age of participants was 61 years, with a slight variation of ± 13 years. Success rates were reported at 95.4% for women and 96.5% for men, highlighting the procedure's efficacy in achieving normal heart rhythm restoration [88]. Cardioversion is the treatment of choice in severely haemodynamically compromised patients with new-onset AF [76].

Cardioversion may be prescribed for AF patients at different stages, depending on factors such as the duration and severity of the AF, the patient's overall health status, and their ability to tolerate the procedure. Cardioversion treatments may be considered in cases of recent-onset or persistent AF, long-standing persistent AF, and paroxysmal AF [12], [76].

Cardioversion treatments are often characterised as electrical or chemical [76], [89]. The electrical cardioversion uses an external defibrillator, which delivers a shock to the heart through handheld paddles or electrode patches applied to the chest and back [76], [90], and the use of an implanted defibrillator, which can be classified as a surgical treatment [90].

Additionally, chemical cardioversion may be utilized, in which medication is administered orally or intravenously [91]. According to a study published in the Journal of the American College of Cardiology, electrical cardioversion is successful in restoring normal sinus rhythm in approximately 90-95% of patients [89], [92]. A meta-analysis published in the European Journal of Internal Medicine found that chemical cardioversion with antiarrhythmic drugs had a success rate of approximately 75% in restoring normal sinus rhythm in patients [92], [93].

Cardioversion is associated with certain risks, including skin irritation or damage from electrodes, bruise formation, and potential dislodgment of pre-existing blood clots which can lead to stroke, exacerbation of abnormal cardiac rhythm, and allergic reactions to medication [76], [89]. A study published in the Journal of the American College of Cardiology found that the use of prophylactic anticoagulation therapy in conjunction with electrical cardioversion increased the success rate of restoring normal sinus rhythm, while also reducing the risk of thromboembolic complications [12]. Another study published in the European Heart Journal found that the use of oral anticoagulant therapy in conjunction with chemical cardioversion such as Quinidine, Disopyramide, Flecainide, Propafenone, Atenolol and Digoxin in 197 different cases, showed an increase in the success rate of restoring normal sinus rhythm, while also reducing the risk of thromboembolic complications [94]. The specific risks associated with cardioversion may vary depending on factors such as the patient's age, type of abnormal cardiac rhythm, and other underlying medical conditions [95].

2.4.3 Surgical Treatments

In cases where medications and cardioversion are ineffective in reducing or resolving AF, a surgical procedure may be necessary [4]. These procedures are typically considered as a last resort option, as they may come with higher risks and complications compared to non-surgical methods [13], [96].

Current surgical options for AF include the implementation of a permanent pacemaker and the maze procedure [13], [96]. The permanent pacemaker procedure is performed when the patient has a slow heart rate and external electrical cardioversion has not been effective. This procedure is typically implemented if the patient has multiple arrhythmias in addition to AF [97], [98][42], [69].

The maze procedure is a type of surgical treatment for AF [77], [99]. It is usually considered for patients who have not responded to cardioversion treatments or are not candidates for non-surgical treatments such as medications or catheter ablation [77], [97], [98], [100].

During the maze procedure, the surgeon makes several small incisions in the atria (the heart's upper chambers) and creates a pattern of scar tissue. This scar tissue blocks the abnormal electrical signals that cause AF and directs the electrical impulses to follow a specific pathway, which can help restore normal heart rhythm [77], [97], [98], [100].

The pattern of scar tissue created during the maze procedure can take several forms, including the traditional "maze" pattern or a simpler pattern called the "mini maze" procedure that is shown in Fig 2.3. The maze procedure can be performed using open-heart surgery or minimally invasive techniques using a catheter-based treatment [100].

The maze procedure has success rates ranging from 75-95% [77], [97]. In [97] the maze was performed in 41 selected patients who had long-standing AF. At discharge, 35 patients (85%) were arrhythmia free, and 6 patients (15%) showed paroxysmal atrial fibrillation and paroxysmal atrial tachycardia. However, it is a more invasive procedure than other treatments for AF and carries a greater risk of complications [77].

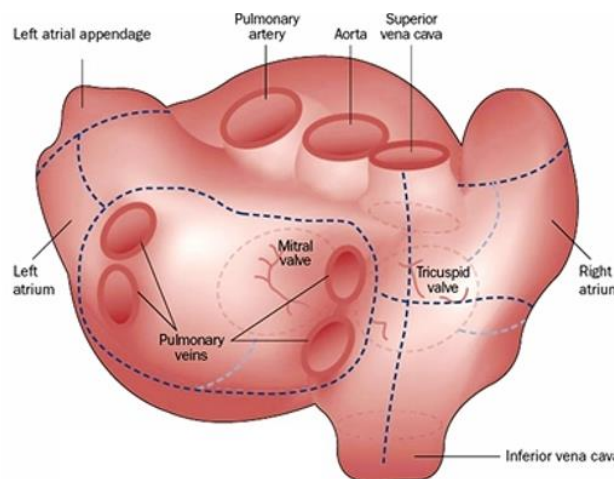


Figure 2. 3 Complete set of atrial lesions as done in the cox-maze procedure

2.4.4 Catheter-based ablation treatments

New minimally invasive catheter-based methods have been proposed to treat AF [4]. These procedures typically involve the use of catheters to deliver treatment, with several commercialized options now available, including pulmonary vein ablation and LAAC [78], [79], [101], [102].

Pulmonary vein ablation is a treatment procedure that uses a catheter-based method inserted into the heart to deliver energy inside the pulmonary veins. Two types of treatment are commonly used: radiofrequency ablation, which delivers heat using radio waves to stimulate the targeted tissue areas [101], and cryoablation, which uses extreme cold to temporarily freeze and promote apoptosis/necrosis and ultimately scarring of the targeted tissue areas [103]. Studies have shown that pulmonary vein ablation leads to better patient responses to AF medications [65], [79], [102]. In [102] AF was achieved in 61.7% of 60 patients (32 men [53.3%]; mean age 45.8±15.5 years) with paroxysmal AF in the study that lasted 27 to 89 months depending on the patient.

This procedure is often combined with medication until normal heart rhythm is restored, and in some cases, the patient may not even need medication long-term [79].

LAAC is another alternative procedure to treat AF, which reduces the risk of blood clots and stroke by blocking the opening of the LAA. The goal is to keep blood clots that form in the LAA from entering the bloodstream [80]. Two types of devices have been proposed for the closure of the LAA: devices that introduce an implant to close the opening of the LAA, such as WATCHMAN™ [80], Amulet™ [104], and WaveCrest™ [72], [105]. The second type of device proposed for closure uses a band or suture loop to close off the LAA; commercialized devices include Lariat™ [106] and Sierra™ [107]. As new treatment methods and technologies continue to be developed, new procedures for treating AF are emerging, such as non-thermal pulsed-field ablation.

2.5 Electroporation

Electroporation is similar to other catheter-based techniques, seeking to cause regions of apoptosis and necrosis but with minimal thermal effects [14], [15]. In the last 25 years, multiple in vitro studies have been presented, with these using energy

sources (electroporation) that disrupt the cell membrane [10], [14], [19], [22] [24], [66]. Electroporation offers precise targeting, sparing surrounding structures like blood vessels and nerves [10], [19], [20].

The field of electroporation has been an area of research since the 1950s [30], [84], and has been proposed as a modality for the manipulation of cells and tissues [10], [16], [22], [24]. Electroporation induces changes in the nature of the cellular membrane, forming pores in the membrane due to the applied, external electric field (electropermeabilization) [19]. These changes in membrane permeability can be reversible or irreversible [30]. Reversible electroporation creates transient pores in the cell membrane. The pores generated in the membrane and the time it takes for the membrane to recover its integrity after electroporation depends on the cell type being treated. Reversible electroporation can introduce molecules or genetic material into cells that would otherwise be impermeable to them, allowing for a wide range of applications in fields such as biotechnology, medicine, and genetic engineering. [19], [30]. Irreversible electroporation permanently disrupts the cell membrane and causes cell death [15]. The fundamental principles of reversible and irreversible electroporation are the same in terms of mechanism of action, however, there are long-lasting effects with irreversible electroporation [10], [14].

The changes induced by electroporation, whether reversible or irreversible, are brought about by the application of PEF, commonly known as pulses [21]. Additionally to the pulse, factors such as cell membrane thickness, permeability, and electrical conductivity all play a role in determining the optimal pulse for a given tissue type [24], [30]. Taking into consideration all those parameters, the electroporation outcomes remain unclear [20]. The literature suggests that a minimum threshold transmembrane potential is necessary for apoptosis [19]–[22]. Based on the electrical properties of the targeted tissue, numerical electromagnetic simulations can be used to estimate the outcome of electroporation using field strength at points.

Many studies investigated the electrical properties of tissues, and have been synthesized into several freely available databases [55][56]. In recent versions of the online databases (February 2022), the reported conductivity has changed by a factor of two for several tissues [31], [51], [56], [108] and these changes in the properties reported suggest that further work is required to investigate the

electrical properties especially frequencies below 100 kHz [31], [51], [56], [108].

2.6 Conductivity of biological tissue

The electrical properties of biological tissues are determined by the movement of ions, such as sodium, potassium, and calcium, and the concentration of these ions [31], [32], [109]. These properties are commonly used in biomedical device design and treatment planning, in diverse applications including electrical impedance tomography [53], [110]–[112], human blood count monitoring [26], [59], [113], neuron-stimulation systems [25], [114], devices for obstetric applications which compare the electrical impedance of the gravid and non-gravid uterus and cervix [27]–[29], and in applications related to oncology comparing normal to cancerous tissues [29], [31]–[34], [39], [45], [115]–[117].

2.6.1 Model for the Passive Electrical Properties of Cells and Tissues

In 1925, Fricke made a significant contribution to the analysis of the passive electrical properties of red blood cells; Fricke made a successful hypothesis regarding the thickness of the cell membrane, suggesting a range from 30 nm to the actual measurement of 7 nm [30]. This hypothesis was derived from an electrical model, where the cell membrane was conceptualized as a dielectric layer, and the extracellular and intracellular media were represented as conductive materials. Fricke's model can be represented by a simplified circuit diagram in Fig. 2.4.

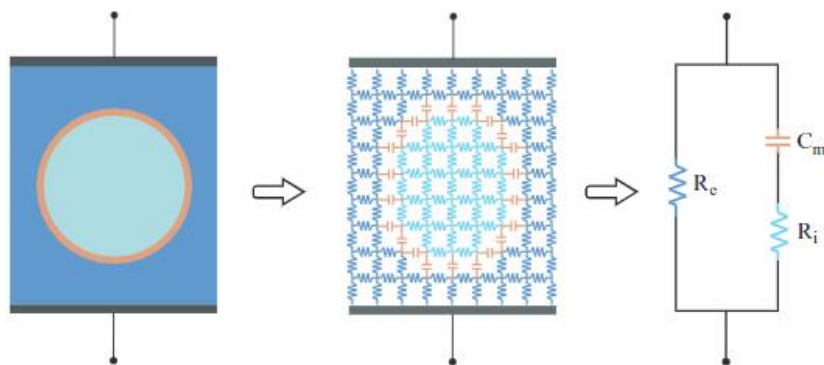


Figure 2. 4 Electrical model for a suspended cell viewed from electrodes: Extracellular and intracellular media are resistances, while the cell membrane is a capacitance. Combined as R_e (extracellular resistance) in parallel with C_m (membrane capacitance) and R_i (intracellular resistance) [30]

In the model proposed by Fricke, every infinitesimal portion of the extracellular

and intracellular media can be envisaged as a resistance, while each infinitesimal portion of the membrane can be conceived as a capacitance. The resistive behaviour of the extracellular and intracellular media primarily arises from their ionic constituents, given that both media essentially consist of ionic solutions (electrolytes). The extracellular medium is predominantly composed of anions (such as Cl^-) and cations (such as Na^+), whereas the intracellular medium is dominated by potassium ions (K^+) [30].

In contrast, the cell membrane primarily comprises a thin lipid bilayer, which is approximately 7 nm in thickness. This lipid bilayer is selectively permeable to lipids and water molecules, but effectively impermeable to ions. Consequently, it exhibits a very low intrinsic electrical conductance and can be reasonably regarded as a high-quality dielectric. Therefore, the overall structure encompassing the extracellular medium, the lipid bilayer, and the intracellular medium can be viewed as a conductor-dielectric-conductor configuration, effectively behaving as a capacitance[30].

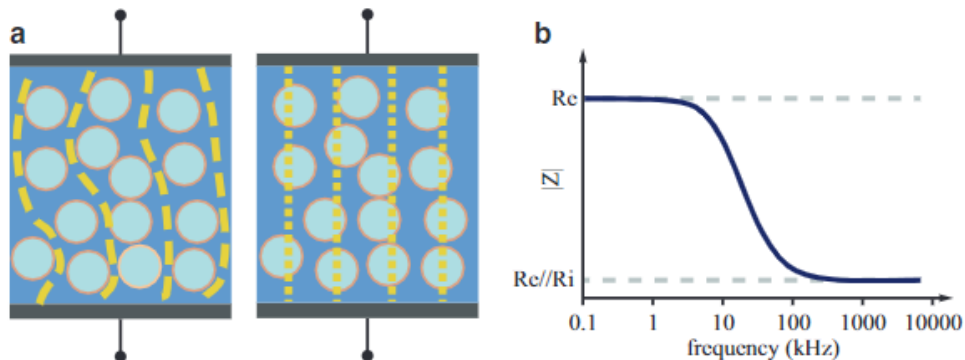


Figure 2. 5 (a) Representation of low-frequency (left) and high-frequency (right) current flow through a cell suspension or tissue, illustrating the restriction of low-frequency currents to extracellular spaces and the unhindered passage of high-frequency currents

The model consists of a resistance symbolizing the extracellular medium (R_e) in parallel with a series combination of a capacitance (C_m) representing the membrane, and another resistance denoting the intracellular medium (R_i). This model is actively applied to describe the passive electrical properties of cell suspensions and tissues. It is noteworthy that, owing to the capacitive nature of the membrane, low-frequency currents are unable to penetrate the cell, while high-frequency currents can freely traverse it [30]. Typically, for most animal tissues, the transition between the low-frequency behaviour and the high-frequency behaviour occurs within a frequency range spanning approximately from 10 kHz to 1 MHz as

seen in Fig 2.5 [30].

Within the transition range from low-frequency behaviour to high-frequency behaviour, the value 100 kHz is often used as a reference point in literature. However, it is important to note that the exact reference value can vary depending on the specific tissue and experimental conditions.

Above 100 kHz, the behaviour of the electrical current changes, and the current can cross the barrier of the cell membrane and flow through the extracellular fluid [30], [118], [119]. At higher frequencies, the electrical field causes the polar molecules within the cells (β -dispersion), such as proteins and nucleic acids, to rotate and oscillate, resulting in a flow of current through the extracellular fluid [120], [121]. The extracellular fluid still conducts the majority of the current, but some current can pass through the cell membrane and flow through the extracellular fluid [122]–[124].

Below 100 kHz, the cell membranes, which have high resistance, act as a barrier to the flow of current, preventing the charged ions from penetrating the cell space. This behaviour is known as the "extracellular" or "volume conductor" model of current flow, it is commonly used in bioelectromagnetic modelling and simulation [125], [126]. At lower frequencies, the concentration and movement of ions determine the electrical conductivity, which is a measure of how easily electric current can pass through the tissue.

In addition to the conductivity being the direct assessment of ion mobility and concentration, conductivity provides several advantages [127]. The conductivity is less affected by variations in tissue structure and composition [127], making it a more consistent measure of tissue properties [127]–[130]. Additionally, conductivity can be measured non-invasively and in real-time [127], making it a useful tool for monitoring tissue properties during medical procedures or treatment [36], [54], [130], [131]. Furthermore, conductivity is easy to interpret and can provide valuable information about tissue health and disease [31], [45], [116].

2.6.2 Conductivity of biological tissue below 100 kHz

Many studies investigated the electrical properties and have been synthesized into several freely available databases, which can be accessed online, including the Italian National Research Council database [55] and the IT'IS Foundation database [56]. Despite the detailed information about the sources of these databases, there

are differences in the original data's acquisition hardware, protocols, and associated metadata. The databases present continuous data between 10 Hz and 100 GHz, even though, in many cases, the data are acquired using different techniques in different studies, even for the same tissue type [56].

Despite the availability of these databases, there are still many unanswered questions regarding the optimal measurement protocols and important confounders that should be controlled, measured, and recorded. These issues are particularly prevalent below 100 kHz, as fewer studies are available in this frequency range. As a result, the synthesized data can frequently change as new studies become available [56].

In recent versions of the online databases (February 2022), the reported conductivity has changed by a factor of two for several tissues, including bone (cortical), brain (grey matter), brain (white matter), eye (vitreous tumour), fat, medulla oblongata, midbrain, muscle, pons, spinal cord, and thalamus [31], [51], [56], [108]. These changes in the properties reported in the literature in recent years alone suggest that further work is required to investigate the electrical properties below 100 kHz [31], [51], [56], [108].

These changes in reported electrical properties below 100 kHz could have impacted previous therapeutic technologies. Therefore, research into methods to accurately acquire and report electrical properties below 100 kHz remains of interest, and improvements in acquisition methods are required to investigate the electrical properties below 100 kHz [31], [51], [56], [108].

The acquisition methods are communally affected by external confounders, that can be characterised into setup-related confounders and tissue-related confounders.

The measurement setup-related confounders are generally controlled or monitored [60], [132], as environmental changes may impact measurement results [133], [134]. These confounders can include the type of probe used, the characterization of the probe [47], [118], the probe contact force [135], [136], cable management and stability of the setup [132], as well as imperfect connections and probe contact [136]–[139], which can all result in poor calibration and unreliable measurements [127], [129], [130], [140], [141].

The tissue-related confounders may introduce measurement uncertainty, as these confounders are primarily related to the complex structure of biological tissues [31], [33], [34], [119]. These confounders can include the type of measurement (in-vivo or ex-vivo), the type of tissue (animal or human), tissue temperature, and the specific region of the tissue being measured (such as the endocardium, epicardium, or myocardium). Furthermore, tissue preparation and handling will vary in each case, highlighting the need for a strong tissue handling protocol.

Many of the tissue handling-related confounders have been extensively studied, as the correlation between external factors such as temperature, and humidity with tissue properties are extensively studied [142]–[145]. The monitoring of some setup-related confounders is standard procedure, such as calibration and validation of the setup with standard liquids [48], [55], [146], [147], to monitor any drift of the measurement setup.

Despite the wealth of information on the impact of confounders on the measurement of conductivity of biological tissue, few studies have examined the measurement probes or determined the important confounders related to the probe that should be controlled, measured, and recorded. For example diverse approaches have been taken in electrical characterization studies of cardiac tissues, a variety of probe typologies in terms of electrode configuration and electrode size have been used [47], [118]. No study has investigated if the diverse range of probes used in the literature affects the acquired data. Furthermore, no study has proposed an optimum probe design for the electrical characterization of cardiac tissues, particularly a probe that will best fit the LAA.

2.7 Measurement techniques

Various methods have been employed to determine the electrical properties of biological tissues, in the frequency range of GHz and kHz [148]. These methods can be broadly categorised into five main groups based on the method of action and the acquisition hardware. The five categories are as follows:

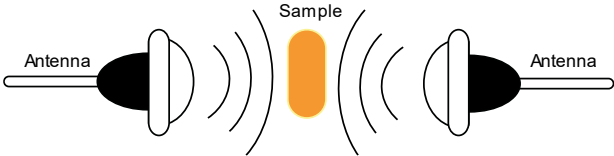
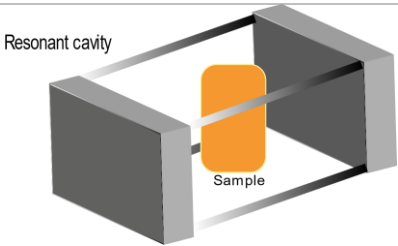
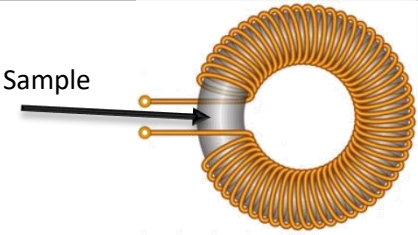
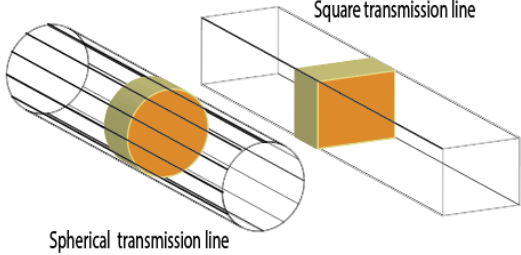
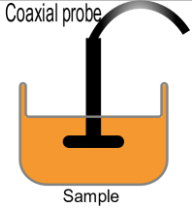
- transmission line.
- electromagnetic wave propagation method (free space).
- resonant-based method.

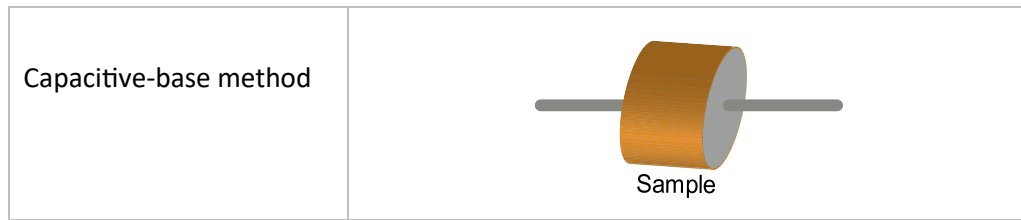
Chapter 2: Literature review

- capacitance-based method (parallel plates).
- inductance-based measurements.

These techniques are depicted in Table 2.1 and are subsequently analysed in the following sections, with an emphasis on the benefits and limitations of each for the targeted frequency range below 100 kHz. The selection of the most appropriate measurement technique is dependent on a variety of factors, such as the sample characteristics or the measurement system requirements.

Table 2. 1 the different measurement techniques to acquire electrical properties of biological tissues

<p>Electromagnetic wave propagation method</p>	
<p>Resonant-based method</p>	
<p>Inductance-based method</p>	
<p>Transmission line method</p>	
	



2.7.1 Electromagnetic wave propagation method (free space)

The methodology of measuring electromagnetic wave propagation (free space) represents an invaluable non-invasive approach within the domain of tissue analysis. This method facilitates the assessment of both the physical and electrical properties inherent to biological tissues. The basic setup involves placing a sample of the tissue under investigation between two antennas (commonly a horn antenna [147], [149], [150]) and measuring the transmission and reflection characteristics of the radio waves passing through the sample [149]. In general, this method is used in frequencies in the range of kilohertz (kHz) to megahertz (MHz). The information obtained from the free space measurement system can be used to calculate tissue parameters such as permittivity and conductivity.

It is important to note that the antennas used in free space measurement are frequency-dependent, which means that the antenna characteristics, such as impedance and radiation pattern, are dependent on the frequency of the radio waves being transmitted and received [151], [152]. As a result, the choice of antenna and its frequency response impacts the accuracy and reliability of the measurement results [153]. Proper selection and calibration of the antennas can ensure that the free space measurement system provides accurate and consistent information about the tissue under investigation [154]. The limitation of this method is related to the antenna size [155].

The size of the antenna is one of the key factors that determine the radiation frequency of an antenna [150], [156], [157]. The length of an antenna is directly proportional to the wavelength of the electromagnetic waves it is designed to radiate. As the size of an antenna increases, the lower its resonant frequency becomes [158]–[160]. Conversely, a smaller antenna size results in a higher resonant frequency. Therefore, to operate at lower frequencies, the antenna is usually very big (optimized pyramid antenna at 800 MHz is 4.5 cm by 4 cm [150]).

Furthermore, the correlation between the size of the antenna and the frequency makes it difficult to accommodate small and complex biological tissues using the free space measurement method [147].

2.7.2 Resonant-based measurement

Resonant-based measurement techniques, which utilize resonant circuits, can be employed to characterize the electrical properties of tissues. [44], [161], [162]. These methods involve applying electromagnetic fields at specific frequencies and analysing the resulting response to extract information about the tissue's composition and properties [44].

The tissue will oscillate with maximum amplitude at its resonant frequency, which is related to its stiffness, viscosity, and damping [44], [163]. By measuring the resonant frequency and response of the tissue, it is possible to determine its mechanical and electrical properties and assess the health of the tissue and its function [163]. This method is commonly used in medical applications, such as diagnostic imaging and monitoring of disease progression [164], [165], [166].

However, there are some limitations to the resonant measurement method [167], [168]. It requires specialized equipment and technical expertise to perform, which can make it difficult to implement in some settings [167], [168]. The measurement is typically limited to the surface of the tissue and may not provide accurate information about deeper tissues [166]–[168]. Other factors such as temperature, pressure, and humidity can affect the resonant frequency and response of the tissue, potentially leading to inaccurate results [166], [168]. The method assumes that the tissue is homogeneous, which may not be the case for complex biological tissues such as the LAA [166]–[168]. Specially, the results may not accurately reflect the electrical properties of the tissue [43], [169]. The method is typically limited to small sample sizes, which can make it challenging to accurately represent the properties of large tissue volumes [166]–[168]. Overall, while resonant measurement is a useful tool for characterizing the electrical properties of biological tissues, it is important to consider these limitations and carefully interpret the results in light of the specific application and sample being studied.

2.7.3 Inductance-based method

The inductance-based method for tissues involves using inductance measurements to characterize the electrical properties of tissues [170]–[172]. In the inductance-based method, a coil or sensor with known inductance is placed in proximity to the tissue of interest [170], [171], [173]. Changes in the electrical properties of tissue, such as conductivity and permittivity, can affect the inductance of the coil or sensor. By measuring the resulting changes in inductance, information about the electrical properties of the tissue can be obtained [170], [171], [173].

Inductance-based measurements can be made using an electrical circuit known as an alternating current (AC) impedance measurement circuit [170]. This circuit is made up of an AC signal generator, an inductor, and an electrical measurement device [170]. The AC signal is applied to the tissue, and the resulting voltage and current are measured. The impedance of the tissue can then be calculated from these measurements [170].

Inductance measurement can also be used in combination with other techniques such as magnetic resonance imaging (MRI) to provide more information about the structure and function of biological tissues [166], [174]. For example, Magnetic Resonance Electrical Impedance Tomography (MREIT) is a technique that uses MRI and inductance-based measurements to visualize the electrical conductivity of tissues in three dimensions [166], [174].

Inductance-based measurement methods have several limitations that must be considered when using them to study biological tissues [175], [176]. For example, the measurement requires special equipment and is difficult to interpret. Additionally, inductance-based measurements are not always accurate and can be influenced by factors such as tissue properties, electrical noise, and instrumentation limitations [177], [178]. Interference from other sources can also impact the accuracy of these measurements, particularly in medical imaging applications [177], [178].

Furthermore, measurements have limited depth, which can make it challenging to obtain measurements from larger biological tissues [179]. Some methods, such as MREIT, also involve the use of strong magnetic fields, which can pose safety concerns for certain patient populations, such as those with implanted devices [180]–[182].

2.7.4 Transmission line

A transmission line uses a probe to transmit a frequency-dependent electrical signal that travels through the tissue [183]. Two types of transmission line probes that are often used for this purpose are open-ended coaxial cables [132], [137], [184] and electrical impedance measurement probes [62], [118], [185]–[187].

- Coaxial cables are cylindrical transmission lines that consist of a central conductor surrounded by a concentric layer of insulation, which is then covered by a conductive shield [188]–[190]. The central conductor and the shield form the two electrodes for the measurement [188]–[190]. Coaxial cables provide a simple and reliable method making them suitable for characterizing the electrical properties of the tissue sample [132], [137], [184], [188]–[190].
- The electrical impedance measurement method uses the tetrapolar probes, 3-electrode probes, and bipolar probes [47], [118], [136], [187], [191]. They are used to determine the electrical properties of biological tissues, by injecting a current (or voltage) into the tissue and measuring the resulting voltage [31], [32], [36], [59]. The specific configuration of the electrodes, the way the current and voltage are measured, and the type of measurement setup used will depend on the requirements of the measurement and the properties of the material being studied.

In both cases, the methods infer the electrical properties of the tissues using changes caused by reflections and transmission of the waveform in the tissue, which can be measured by the probe [192]. The transmission line method is widely used in medical applications such as the characterization of tissues for diagnosis and monitoring of diseases [164], [193]. In addition, applications of the transmission line method can be seen in various forms such as open-ended coaxial probes, bipolar probes, three-electrode probes, and tetrapolar probes [27]–[29], [62], [118], [132], [135], [137], [184], [185], [187], [194]–[201]. The major differences between open-ended coaxial probes, bipolar probes, three-electrode probes, and tetrapolar probes lie in their designs and configurations, which impact their applications in electrical measurements, particularly in studies involving tissues or materials.

A limitation of the transmission line is the correlation between its size and the operating frequency [202]. The size of the transmission line and the operating frequency are interrelated, and they both affect the accuracy and spatial resolution of the measurement results obtained using the transmission line method [202], [203]. In general, smaller transmission lines provide higher spatial resolution but lower sensitivity, while larger transmission lines provide deeper penetration depth but lower spatial resolution [184], [204].

Recently, the transmission line and particularly the electrical impedance measurement method have gained interest due to advances in probe optimization. These optimizations have enabled an improvement in accuracy and higher spatial resolution compared to previous measurements performed in the frequency range below 100 kHz [26], [32], [36], [59], [60], [62], [205], [206].

2.7.5 Capacitive-base method

The capacitance-based method uses the capacitance between two parallel electrodes to measure the electrical properties of tissue [207]–[210]. The basic setup involves placing a tissue sample between two parallel metal plates, which serve as electrodes [208], [210], [211]. An alternating voltage is applied to the electrodes, and the capacitance between the electrodes is measured [208], [210], [211]. The electrical properties of the tissue sample can then be derived from the measured capacitance values [210].

The capacitance-based method is a simple and direct way to measure the dielectric properties of biological tissues at low frequencies [51], [212]. The parallel plate geometry is well suited for low-frequency measurements as the capacitance between the electrodes is directly proportional to the electrical properties of the tissue [51], [213]. This makes it possible to accurately determine the electrical properties of biological tissues without the need for complex models or measurements at multiple frequencies and especially for frequencies below 100 kHz [51], [213]. However, the capacitance-based method display limitations [68], [213], [214]:

- Geometry dependence: The capacitance-based method is highly dependent on the geometry of the measurement setup, including the plate

separation and plate size. This can make it difficult to accurately compare results between different studies.

- **Complex tissue structures:** The parallel plate geometry assumes a homogeneous tissue sample, but biological tissues are often heterogeneous in nature, with complex structures such as blood vessels and nerves that can affect the measured capacitance.
- **Electrode-tissue interface:** The capacitance-based method also relies on good contact between the electrodes and the tissue, which can be challenging to achieve in practice, especially for soft, wet, or moving tissues.
- **Electrode polarization:** The electrodes employed in this technique have the potential to undergo polarization, introducing the possibility of errors in the measurement. This phenomenon can result in inaccuracies or deviations in the recorded data, particularly in terms of shifts in capacitance values or other alterations in the measured electrical characteristics.
- **Limited frequency range:** The capacitance-based method is most accurate for low frequencies, and the measurement accuracy can decrease at higher frequencies, making it less suitable for the study of tissues with higher frequency-dependent electrical properties.

Among the various methods for determining the dielectric properties of biological tissues, the capacitance-based method using parallel plates is frequently utilized for frequencies below 100 kHz.

2.8 Protocol for conductivity acquisition

The acquisition of conductivity using the electrical impedance measurement method typically involves measuring the frequency-dependent complex impedance of the tissue. There are two main methods for measuring complex impedance: the galvanostatic mode, in which the ratio of the applied AC current to the measured AC voltage is calculated, and the Potentiostatic mode, in which the ratio of the AC voltage to the measured AC current is calculated. The AC current and voltage are described using equations 2.4 and 2.5. In general, the choice of measurement mode will depend on the specific application and the properties of the tissue under study.

$$V = V_m \cdot \sin(\omega t + \theta) \quad (2.4)$$

$$I = I_m \cdot \sin(\omega t + \theta) \quad (2.5)$$

where, ω is the angular frequency, I_m is the maximum amplitudes of current, V_m is the maximum amplitudes of voltage and θ is the phase shift between the voltage and current waveform. The ratio between V and I is the impedance (Z) which is represented with equation 2.6:

$$Z = R + jX \quad (2.6)$$

Z is represented as a complex number, comprising a real component, resistance (R), and an imaginary component, reactance (X). These values can be determined through the use of experimental techniques, The common setup to measure impedance typically involves the use of specialized instruments such as an impedance analyser or an LCR meter (to measure the ratio between I and V) in conjunction with a function generator which is often used to generate the AC signal.

In the measurement of conductivity, electrode polarization effects can significantly impact the accuracy of the results [215]. This phenomenon occurs due to the interaction between the charged electrode surface and free charges in the tissue under study and is particularly pronounced at low frequencies (below 100 kHz) [215]–[218]. To mitigate these effects, low current amplitudes are used to reduce the introduction of charges from the electrodes and thus reduce electrode polarization [216], [218] Additionally an optimized probe (number of electrodes, electrode surface, electrode material, electrode configuration) could be implemented to mitigate electrode polarization as well [215].

In the literature, various probe typologies have been proposed to investigate the electrical conductivity of tissue, as detailed in Table 2.2 and shown in Fig. 2.6. One of the earliest designs was the bipolar probe, which was introduced in the 1800s [135]. This probe consists of a pair of electrodes that inject the current across them, with the resulting voltage measured by the same electrode pair [45].

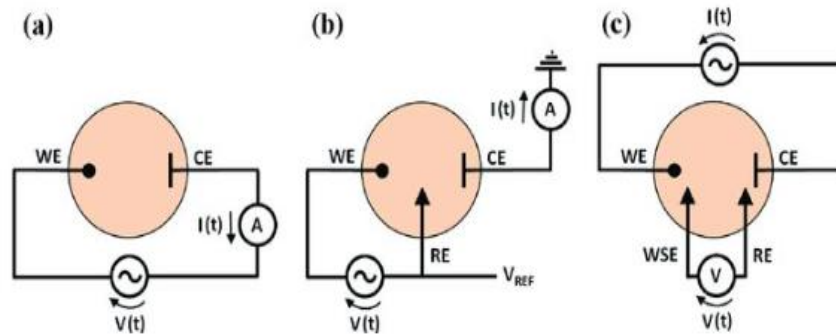


Figure 2. 6 Measurement setup configurations (a) two electrodes, (b) three electrodes and (c) four electrodes

Another design that employs a similar concept to the bipolar probe is the three-electrode probe. This probe also utilizes three electrodes, with one electrode shared for injecting and measuring. The third common electrode is used to mitigate electrode polarization by allowing the measured voltage to bypass the source electrode [32], [219].

The tetrapolar probe, first introduced by Bouty in 1884 [220], utilizes four electrodes. One pair injects the stimulus current, and the other inner pair measures the resulting voltage [42]. The tetrapolar probe has been used in various studies, such as the use of a polar probe (electrodes in a square arrangement) for the characterization of biological tissue in [27] and [42], a four concentric electrodes probe for identifying skin cancer in [116], [117], [200], and a collinear probe for distinguishing normal and cancerous human hepatic tissue [45].

The tetrapolar probe is less affected by electrode polarization or charging currents at the electrode interface compared to the two or three-electrode method. Therefore, the probes proposed in this study are tetrapolar probes [196], [221]. Among the probes used in literature for tissue, the collinear probe (four electrodes in a line) and the polar probe (four electrodes in a square configuration) are commonly employed [27], [118], [205]. Many tetrapolar probes have been proposed to characterise cardiac tissues, the most common tetrapolar probe typologies used for cardiac tissue characterization, namely the collinear and polar typologies shown in Table 2.2.

Table 2. 2 Summary of the tetrapolar probe used to characterize biological tissue with their respective size. The two most common probes are the collinear probe and the polar probe

Ref	Typology	Electrode size	Tissue type
Cinca et al. [21]	Collinear	0.2 mm radius	coronary artery (porcine)
Ellenby et al. [22]	collinear	3.1 × 0.6 mm ²	left ventricle (dog)
Gabriel et al. [27]	Collinear	-	Atrial (porcine)
Hahn et al.[24]	9 needles	0.35 mm radius	Cardiac muscle (porcine)
Jokhi R. et al. [29]	Polar	0.6 mm radius	Cervix (human)
B. Filho [30]	Polar	1 mm radius	Forearm Skin (human)

2.9 Conductivity of the cardiac tissue

After conducting a comprehensive analysis of the available literature, including research publications compiled in the databases of the Italian National Research Council and the IT'IS Foundation [55][56], the conclusion drawn from this review can be summarized as follows:

Cinca et al., 1997 [67], [222] conducted a study in which they characterized cardiac tissue by measuring myocardial electrical impedance induced by coronary artery occlusion in 13 in-vivo porcine samples. The study employed a tetrapolar probe, which consisted of four platinum electrodes (5 mm in length, 0.4 mm in diameter) arranged in a linear array on an insulating substrate, with an interelectrode distance of 2.5 mm. The use of a tetrapolar probe was chosen as it was found to have a lesser effect on tissue measurements compared to the use of a single pair of electrodes for both current injection and potential measurement.

Ellenby et al., 1987 [223] reported a similar study in which they aimed to detect reversible myocardial ischemic injury through the measurement of myocardial electrical impedance in the ex-vivo left ventricle obtained from 12 dogs. The study employed a four-electrode method, using gold-plated brass pins that were 3.125 mm long and 0.625 mm in diameter. The four-electrode method was utilized to separate current induction (outer electrodes) and voltage monitoring (inner electrodes). Additionally, the study employed a technique where the local ambient electrical activity of the myocardium was monitored by turning off the injected current while using amplifier and filter components to record bipolar electrograms between the inner two voltage-sensing electrodes.

Gabriel et al., 2009 [36] conducted a study in which they investigated the electrical conductivity of various biological tissues, including the heart (atrial) from

in-vivo porcine samples. The study updated previous data reported by Gabriel et al., 1996 [31]–[33], with a focus on conductivities at frequencies below 1 MHz. The study utilized a colinear four-electrode probe design, with specifications tailored for the tissue in question. The probe employed is collinear four platinum-coated pin electrodes embedded in synthetic fluoropolymer of tetrafluoroethylene.

Hahn et al., 1980 [38], [224] investigated the electrical conductivity of porcine cardiac tissue to evaluate heat transfer problems associated with heating by ultrasound, microwaves, and radio frequency. The assessment of electrical conductivity was performed using a nine-needle electrode probe, with eight electrodes arranged in a circle centred around the ninth electrode. The outer eight needles formed a grounded coaxial guard with respect to the inner active electrode, and the measurement was taken using the 2-electrode method to acquire the complex frequency-dependent impedance. The outer eight needles were 1.5 cm long and the inner needle was 1.0 cm long. The needles were selected to be able to penetrate multilayer tissues and monitor heat diffusion inside the multilayer tissue.

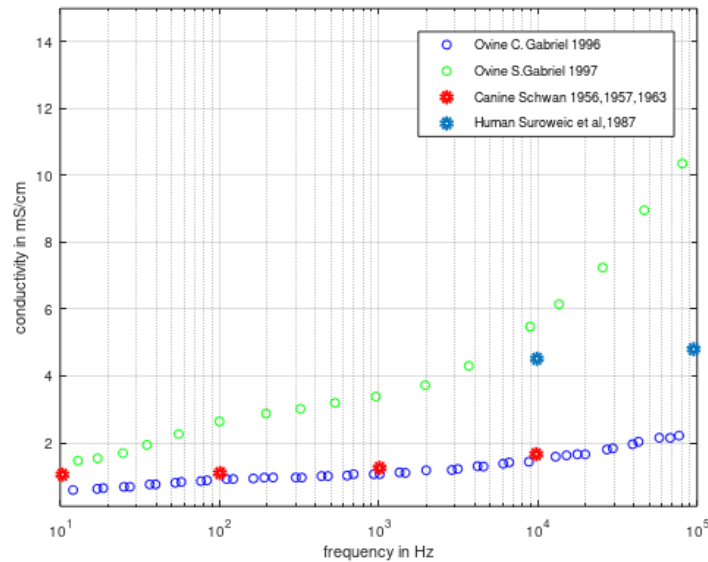


Figure 2. 7 Conductivity acquired from the literature review of conductivity of cardiac tissue

The literature on cardiac tissue conductivity displays a range of values, varying from 0.5 mS cm⁻¹ to 9 mS cm⁻¹ shown in Fig 2.7. These variations can be attributed to the origin of the samples, such as whether they were obtained ex-vivo or in-vivo, as well as the source of the samples, which can include different animals or human subjects.

Additionally, the conductivity can vary depending on the specific species of the tissue sample that were measured (human, bovine, ovine, ...), and in different parts of the heart (left ventricle, right ventricle, the atrial, ...). However, when considering only ex-vivo animal studies, the average conductivity is $3 \pm 0.5 \text{ mS cm}^{-1}$ in the frequency range from 10 Hz to 100 kHz. Despite the information available in the literature regarding the electrical properties of cardiac tissue, there is a lack of research specifically investigating the conductivity of the LAA.

2.10 Conclusions

Chapter 2 provides a foundation for the experimental design, data collection and analysis in the subsequent chapters and introduces information including the anatomy and physiology of the LAA. Current treatment options for AF have also been discussed. Additionally, IRE has been proposed as a new potential treatment for AF. The outcome of IRE on the LAA relies on understanding the electrical conductivity of the LAA. However, currently, the conductivity of the LAA has not been specifically reported in the literature. As such, further research needs to focus on investigating the conductivity of the LAA and its role in optimizing IRE treatment planning. Additionally, it is necessary to develop a reliable method to measure tissue electrical conductivity while controlling for various confounders related to the measuring probe design. This will be the aim of chapter 3. Chapter 3 will evaluate the effect of probe typology and electrode size on electrical conductivity measurements in the frequency range of 0.1 Hz to 100 kHz. The study identifies the most accurate and repeatable probe design, which will be used to assess the conductivity of the LAA.

Chapter 3: Evaluation of Tetrapolar Probes: Investigating the Impact of Probe Typology and Electrode Size on Conductivity Measurements for the Left Atrial Appendage from 0.1 Hz to 100 kHz

3.1 Introduction

The behaviour of electrical current in biological tissue varies across frequency ranges. Below 100 kHz, it is influenced by the extracellular fluid and tissue ionic composition and the current mainly flows in the extracellular fluid [15], [19], [22], [24], [30], [225]. Above 100 kHz, the current behaviour changes due to factors like capacitive properties of cell membranes [15], [19], [22], [24], [30], [225]. The threshold can vary based on tissue and experimental conditions. At higher frequencies, the current can cross the cell membrane barrier, and flow through the extracellular fluid. A representation of the current behaviour is shown in Fig 3.1.

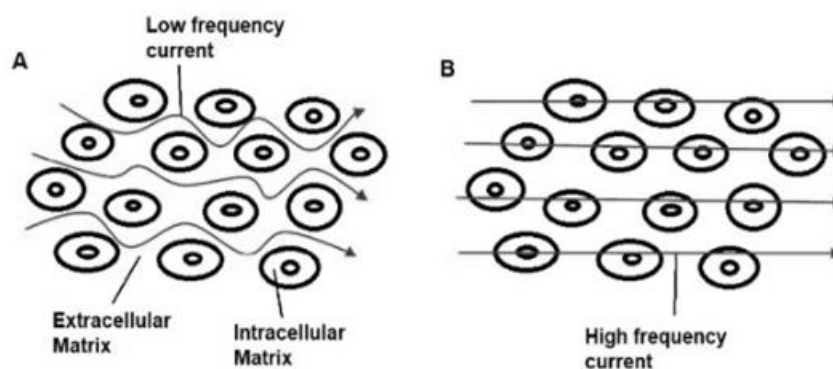


Figure 3. 1 Flow of electrical current through biological tissue. At lower frequencies (A), the current moves between the cells and through the extracellular fluid. However, at higher frequencies (B), the current can penetrate the cell membrane

Chapter 3: Evaluation of Tetrapolar Probes: Investigating the Impact of Probe Typology and Electrode Size on Conductivity Measurements for the Left Atrial Appendage from 0.1 Hz to 100 kHz

Following the extensive literature review in chapter 2 combined with the need to target the frequency range below 100 kHz [122]–[124], it was determined that the 4-electrode probe measurement method is the most suitable method for examining the conductivity of the LAA below 100 kHz. The 4-electrode method is preferred for measuring conductivity due to its reduced susceptibility to polarization or charging currents at the electrode interface compared to two or three-electrode methods [196], [221]. As a result, the 4-electrode measurement method provides a larger measurement range compared to other configurations [196], [221]. As seen in electrical characterization studies of cardiac tissues, a range of tetrapolar probe typologies in terms of electrode configuration and size have been employed [9], [27]–[29], [31], [32], [36], [191], [224], [226]. The use of multiple probe designs can be advantageous in adapting to different tissue types. However, no study has examined whether the diversity of probes used in the literature influences the obtained data. Additionally, no study has suggested a probe design for the electrical characterization of the LAA. Thus, the objective of chapter 3 is to evaluate the effect of the probe typology and electrode size on the accuracy and repeatability of electrical conductivity measurements and propose a tetrapolar probe to assess the conductivity of the LAA.

The present study in chapter 3 evaluates the accuracy and repeatability of six different probe designs using liquid phantoms in the frequency range of 0.1 Hz to 100 kHz. This frequency range was selected for analysis, as the lower end of the frequency range (0.1 Hz) was defined by the limits of our electrochemical measurement system PGSTAT204 (Autolab, Kanaalweg Den Haag, The Netherlands). The instrument includes a base potentiostat/galvanostat with a compliance voltage of 20 V and a maximum current of 400 mA. The threshold of 100 kHz where the current would mainly flow in the extracellular fluid. The most accurate and repeatable probe, as determined from the results of the study, is proposed for testing on the LAA. The electrical characterization of the LAA at low frequencies below 100 kHz is relevant to IRE design and treatment planning studies, and the probe is employed for the first-ever LAA electrical characterization, as presented in chapter 4.

The remainder of chapter 3 is organized as follows: The second section provides a background on probe design used for the characterization of biological

tissue. The third section outlines the methodology, including the electrical conductivity acquisition process and the rationale for the probe design. The fourth section presents the results, which assess the influence of different probe typologies and electrode sizes on the accuracy and repeatability of the acquired data. Moreover, the results highlight the most appropriate probe for measuring the conductivity of the LAA in ex-vivo bovine samples. Finally, the closing section summarizes the conclusions of the study and suggests directions for future research.

3.2 Background

3.2.1 Operating frequency of the tetrapolar probe

A tetrapolar probe is typically used for electrical impedance measurements, and its working frequency depends on several factors, including the size and geometry of the probe, the material properties of the probe, the surrounding medium, the desired measurement spatial resolution and accuracy.

The operating frequency of a tetrapolar probe can vary, but it typically ranges from kilohertz (kHz) to megahertz (MHz), to determine the operating frequency of a custom-made tetrapolar probe, not many approaches are available. The most suitable method to determine the operating frequency for custom-made probes is the experimental approach using reference material.

In this thesis, the operating frequency is defined as when the data acquired from a reference material (NaCl liquid phantom) correlates with the literature data. The correlation factor R was used as a metric ($R > 0.95$). The experimental approach aims to determine the frequency range of the probe using a frequency sweep experiment in which the probe is driven by an AC current at a range of frequencies, and the resulting impedance is measured [118], [227].

To determine the working frequency range of a tetrapolar probe, the following steps were taken. First, the probe was connected to an impedance analyser or an equivalent device for this thesis the PGSTAT204 (Autolab, Kanaalweg Den Haag, The Netherlands) is used. The analyser is set to sweep a frequency range of interest, which for this thesis, was between 0.1 Hz and 100 kHz. Next, the impedance values at each frequency point were recorded using a reference material (NaCl at 0.1 M, 0.05 M, and 0.01 M concentration). The recorded

impedance values were plotted as a function of frequency. Subsequently, the frequency range over which the impedance values remained relatively constant and reliable was identified using statistical analyses, specifically a correlation factor R was computed by comparing the acquired data to reference data from the literature on NaCl phantoms.

3.2.2 Design process of a tetrapolar probe

Designing an effective tetrapolar probe for tissue characterization requires consideration of several variables and characteristics that can affect its performance and accuracy [62], [118], [187], [227]. When designing a tetrapolar probe, the parameters to consider include electrode size and shape, electrode spacing, electrode material, and probe typology (geometry). Fig. 3. 2 summarises and shows the parameters to consider when designing a tetrapolar probe.

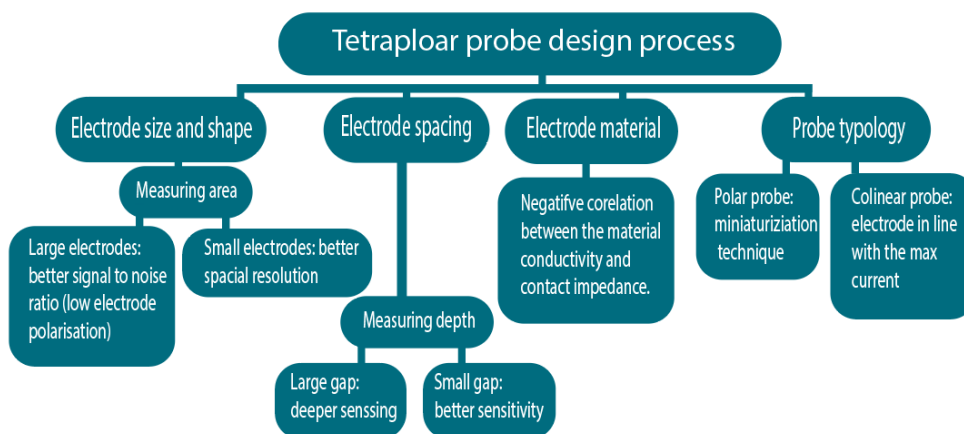


Figure 3. 2 diagram of the parameters to consider when designing a tetrapolar probe, that includes electrode size, electrode spacing, electrode material and he probe typology

In addition to geometrical characteristics, the frequency and intensity of the electromagnetic field applied to the tissue can affect the probe's sensitivity and spatial resolution. Sensitivity refers to a measurement ability of the probe to accurately measure small changes or variations in the quantity being measured. Sensitivity enables the detection of even the slightest fluctuations in properties like impedance or conductivity, facilitating precise measurements. In contrast, spatial resolution relates to the capability of the probe to distinguish fine details or small-scale variations in a specific spatial domain. It enables the detection of localized variations within the measured medium, differentiating between closely spaced

features or changes. Both sensitivity and spatial resolution are important considerations for evaluating measurement probes.

Higher frequencies typically provide greater spatial resolution but may not penetrate as deeply into the tissue. Lower frequencies can penetrate deeper into the tissue but may have lower spatial resolution [228].

Other important factors to consider when designing a tetrapolar probe for tissue characterization include the signal-to-noise ratio, the temperature sensitivity, and the mechanical stability of the probe [229]. By carefully considering these variables and characteristics, an effective tetrapolar probe can be designed to characterize the electrical properties of tissues accurately and reliably.

3.2.3 Typology of the tetrapolar probe

The typology describes the size and shape of the probe which can affect how much tissue is included in the measurement and the depth of penetration into the tissue [228]. Larger probes can cover a larger area of tissue and may provide more accurate measurements of the average tissue properties [230], [231]. However, larger probes may also have lower spatial resolution and may not be able to detect small variations in tissue properties [228]. In addition, the shape of the probe should be chosen to optimize the field distribution around the probe.

3.2.4 Electrode spacing

Electrode spacing refers to the distance between the individual electrodes on a tetrapolar probe. The spacing affects the depth of penetration into the tissue and can also affect the spatial resolution of the measurement [118], [227], [228]. Larger electrode spacing can provide deeper penetration into the tissue but may have lower spatial resolution. Smaller electrode spacing can provide higher spatial resolution but may not penetrate as deeply into the tissue [228]. In biological tissue, the calculation of the sensing depth of a tetrapolar probe is more complex, as the electrical properties of the tissue can vary spatially. The depth of sensing in this instance is contingent upon the distinct distribution of electrical properties within the tissue and can be classified based on assumptions about the tissue.

When the tissue is assumed homogenous, the sensing depth of tetrapolar probe is calculated using the following equation [221], [232]:

$$D = \left(\frac{\pi}{2}\right) \times \frac{a^2}{\rho} \quad (3.1)$$

where D is the sensing depth, a is the radius of the outer electrode, and ρ is the resistivity of the medium being measured. Equation 3.1 assumes that the tetrapolar probe is used in a homogenous medium and that the electrodes are perfectly spherical.

When the tissue is non-homogeneous, the approach to estimating the sensing depth is to use numerical simulations, such as finite element analysis, to model the electrical field generated by the tetrapolar probe and the resulting voltage measurements. By incorporating the spatial variations in tissue conductivity, permittivity, and geometry, the simulation can provide an estimate of the sensitivity and depth of the probe in the specific tissue being studied. In the case of this thesis, estimating the sensing depth for the probe on the LAA becomes particularly challenging using the second approach, since the electrical properties of the LAA are not known. A general rule of thumb is that the sensing depth of the probe is proportional to the spacing between the measuring electrode [27].

3.2.5 Electrode size

Electrode size refers to the physical dimensions of the individual electrodes on a tetrapolar probe. Larger electrodes can cover a larger area of tissue and may provide more accurate measurements of the average tissue properties. However, larger electrodes can also increase the distance between the electrodes, which can decrease the sensitivity of the measurement. Smaller electrodes, on the other hand, can improve the sensitivity of the measurement by reducing the distance between the electrodes, but may not cover as large an area and volume of tissue. the size of the electrode and its effect on the accuracy and the repeatability of the acquired data is further discussed in section 3.4.

3.2.6 Electrode material

The material of the electrodes in a tetrapolar probe can be chosen regarding different factors. The conductivity of the electrode material can affect the impedance of the probe, which in turn can affect the accuracy of the measurements [233]–[235]. Electrode materials that are prone to corrosion can degrade over time and affect the accuracy and reliability of the measurements [233]–[235]. The

durability of the electrode material is important for ensuring that the electrodes remain functional over time. Materials that are resistant to wear and tear can help extend the lifespan of the probe. These factors collectively guide the material selection process. Common considerations include the electrical conductivity of the material, its compatibility with the target medium or tissue, stability, and biocompatibility. Evaluating these factors will help determine the most suitable electrode material for a given application [233]–[235].

3.3 Methodology

3.3.1 Probe description

Chapter 3 aims to investigate the impact of typology and electrode size on the conductivity acquired through the use of different probe configurations. From the literature two types of probes are observed to be used, collinear and polar, therefore the two typologies are utilized with varying electrode configurations to cover diverse potential typologies. Fig 3. 3 illustrates the probes proposed in this study, and Table 3.1 presents their characteristics. All the proposed probes were made using pure copper (Standards BS2874/C101(1986); BS EN 12164 CW 004A), with a thickness of 0.5 mm due to its low cost, adequate conductivity, and robustness. To ensure uniformity in the manufacturing process, a 3D printed holder was designed to mount the electrodes flush to the holder, maintain the same level, and ensure a constant spacing between the electrodes in the final probe prototypes.

The probes used in the study include six different designs (two typologies). The first probe (Fig 3. 3(a)) is a collinear probe with equidistant electrodes measuring 3mm in diameter. The second probe (Fig 3. 3(b)) is a polar probe also with 3mm diameter electrodes. The third type (Fig 3. 3(c)) is a small collinear probe with equidistant smaller electrodes measuring 1.5mm in diameter, which is half the size of the collinear probe. The fourth probe (Fig 3. 3(d)) is a small asymmetric probe with small electrodes measuring 1.5mm in diameter. The non-equidistant positioning of the outer electrodes causes asymmetry. The fifth probe (Fig 3. 3(e)) is a small unequal and asymmetrical collinear probe with small electrodes. The inner electrodes are smaller than the outer electrodes, and the asymmetry is due to the non-equidistant positioning of the electrodes. Finally, the sixth probe

Chapter 3: Evaluation of Tetrapolar Probes: Investigating the Impact of Probe Typology and Electrode Size on Conductivity Measurements for the Left Atrial Appendage from 0.1 Hz to 100 kHz

(Fig. 3. 3(f)) is an unequal and asymmetrical polar probe with small electrodes. The inner electrodes are smaller than the outer electrodes, and the asymmetry is also due to the non-equidistant positioning of the electrodes.

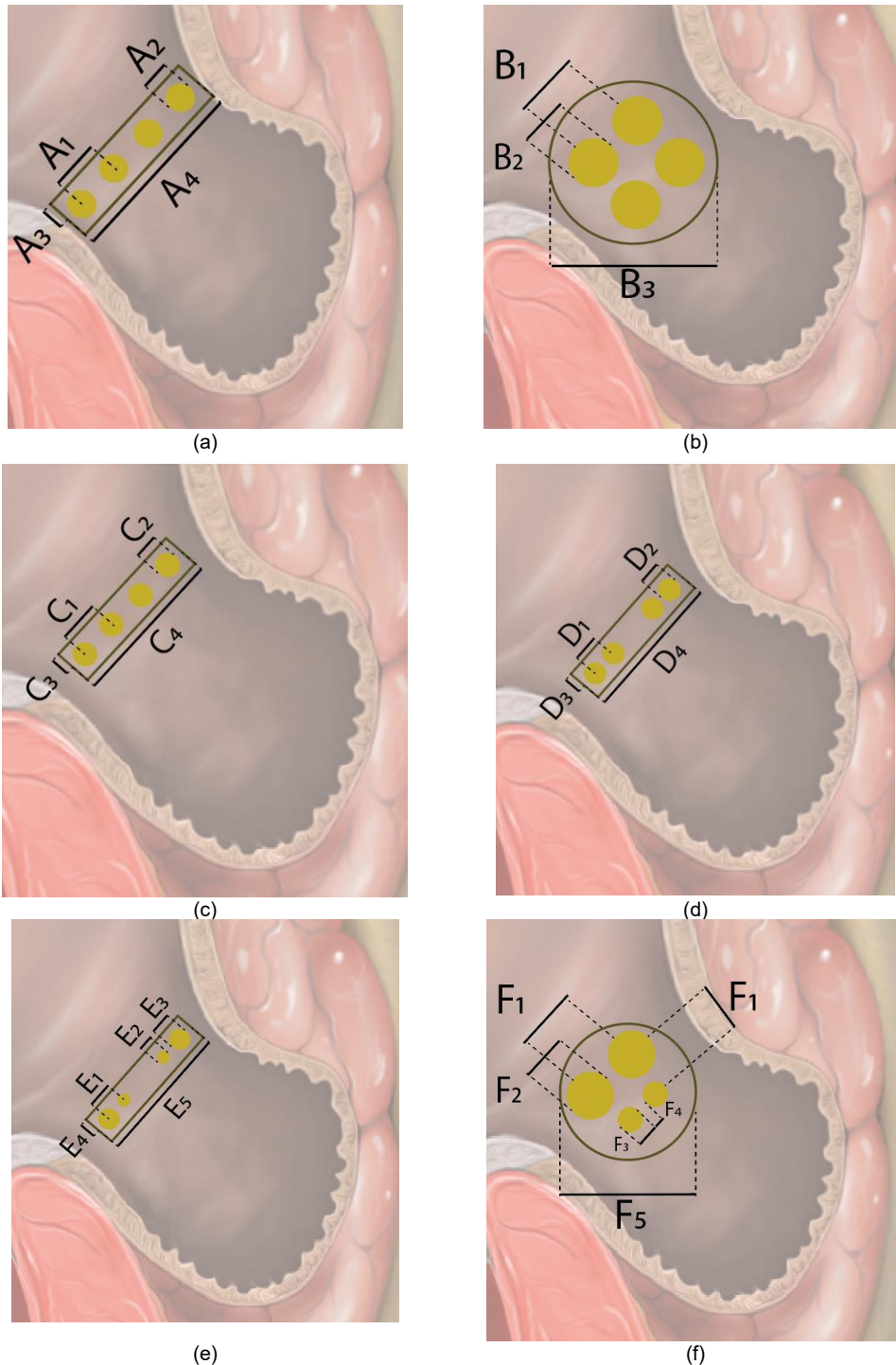


Figure 3. 3 Diagram showing the dimensions of the two proposed typologies of tetrapolar probe used in this thesis (a) collinear probe (b) polar probe (c) small collinear probe (d) Small asymmetric collinear probe (e) small asymmetric and unequal collinear probe (f) unequal polar probe

Chapter 3: Evaluation of Tetrapolar Probes: Investigating the Impact of Probe Typology and Electrode Size on Conductivity Measurements for the Left Atrial Appendage from 0.1 Hz to 100 kHz

All the probe designs were specifically intended to fit the typical dimension of the LAA [118], [221]. The size of the electrodes and the size between the electrodes were restricted by the length and the thickness of the opening of the LAA (40 mm and 5mm respectively). The total length occupied by the four electrodes ($4d$), plus the minimum distance between the electrodes (5 mm) will be:

$$4d + 3 \times 5 \text{ mm} = 4d + 15 \text{ mm} \quad (3.2)$$

To fit within the 4 cm length:

$$4d + 15 \text{ mm} \leq 40 \text{ mm} \quad (3.3)$$

Combining equation 3.2 and 3.3 then solving for d :

$$d \leq (40 \text{ mm} - 15 \text{ mm}) \times 0.25 = 6.25 \text{ mm} \quad (3.4)$$

where d is the diameter of each circle. Therefore, the maximum diameter of each circle should be 6.25 mm or less in order to fit the limitation introduced by the LAA measuring area (section 3.2).

The largest electrode size is considered to be a 6 mm diameter as the design of the total length of the probe needs to take into consideration a gap on the sides of the outer electrodes [236]. Conversely, the smallest size of the electrodes was chosen to be greater than 1 mm diameter, as electrodes with a radius greater than 1 mm can reduce non-linearities, electrode impedance, and electrode polarization [118], [221], [236], [237]. Conversely, electrodes with a radius less than 1 mm can introduce parasitic effects of comparable significance to the impedance exhibited by the sample under investigation [118], [221]. Therefore, a small electrode size of 3 mm diameter was selected to assess the effect of electrode size on the accuracy and repeatability of the acquired data. This size is larger than a 1 mm radius and represents a 50% reduction in size compared to the largest electrodes used on the collinear probe.

Chapter 3: Evaluation of Tetrapolar Probes: Investigating the Impact of Probe Typology and Electrode Size on Conductivity Measurements for the Left Atrial Appendage from 0.1 Hz to 100 kHz

Table 3.1 Characteristics of the six probes used in this study, including the probe type, electrode configuration, electrode diameter, and distance between electrodes. The table also lists the number of electrodes and the total length of the probe showed in Fig. 3. 3

Probe		Specification in mm
Collinear probe	Fig 3. 3(a)	$A_1 = 10 \text{ mm}, A_2 = 6 \text{ mm}, A_3 = 4 \text{ mm}, A_4 = 40 \text{ mm}$
Polar probe	Fig 3. 3(b)	$B_1 = B_2 = 10 \text{ mm}, B_3 = 25 \text{ mm}$
Small collinear probe	Fig 3. 3(c)	$C_1 = 5 \text{ mm}, C_2 = 3 \text{ mm}, C_3 = 2 \text{ mm}, C_4 = 20 \text{ mm}$
Small asymmetrical collinear probe	Fig 3. 3(d)	$D_1 = 2.5 \text{ mm}, D_2 = 3 \text{ mm}, D_3 = 2 \text{ mm}, D_4 = 20 \text{ mm}$
Small unequal and asymmetrical collinear probe	Fig 3. 3(e)	$E_1 = 2.5 \text{ mm}, E_2 = 1.5 \text{ mm}, E_3 = 3 \text{ mm}, E_4 = 2 \text{ mm}, E_5 = 20 \text{ mm}$
unequal and asymmetrical polar probe	Fig 3. 3(f)	$F_1 = 10 \text{ mm}, F_2 = 3 \text{ mm}, F_3 = 1.5 \text{ mm}, F_4 = 2 \text{ mm}, F_5 = 20 \text{ mm}$

3.3.2 Data acquisition

The conductivity measurement process involved the acquisition of the frequency-dependent complex impedance, which was carried out using the method described in [31], [59], [62]. A PGSTAT204 (Autolab, Kanaalweg Den Haag, The Netherlands) in galvanostat mode was used to acquire the impedance data at room temperature, with Nova 2.1 software used to control the PGSTAT204. A galvanostatic mode was employed with a current of 100 μA flowing between the inducing electrodes. The 100 μA induced current in the electrode is the lowest current possible provided by the PGSTAT204 in the targeted frequency range. Low inducing current insure lower electrode polarisation.

The measurement setup consisted of the PGSTAT204 connected to the proposed probe, which included a working electrode, a counter electrode, a reference electrode, and a sensing electrode. The probe was designed to fit into a holder attached to a retort stand to maintain the stability of the setup. The full setup used for the measurement is shown in Fig 3. 4.

Chapter 3: Evaluation of Tetrapolar Probes: Investigating the Impact of Probe Typology and Electrode Size on Conductivity Measurements for the Left Atrial Appendage from 0.1 Hz to 100 kHz

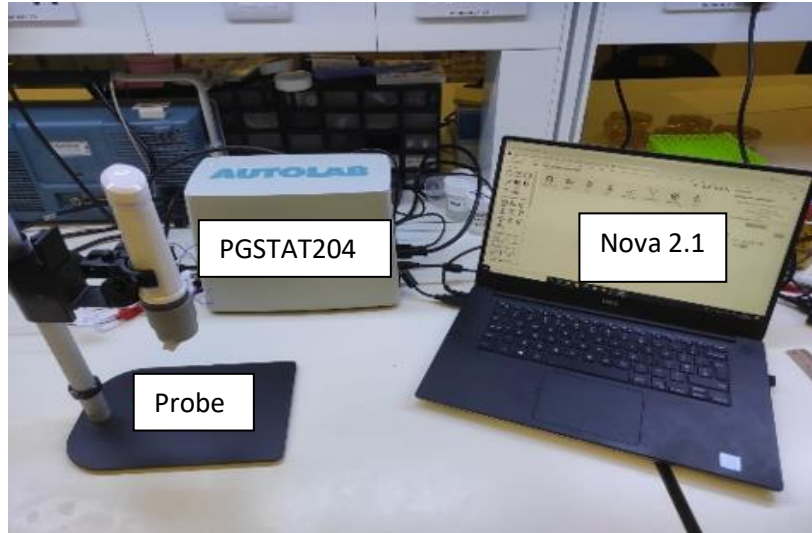


Figure 3. 4 Measurement setup with the probe, the laptop running NOVA 2.1 software in the foreground. PGSTAT204 potentiostat/galvanostat and the probe holder used to lift and keep the probe fixed

The first step in computing the electrical conductivity is determining the cell constant (k), which relates the measured conductance and the corresponding reference conductivity. For our study three NaCl solutions with known conductivity were used and by measuring their complex impedance k was derived. Calculating the electrical conductivity from the measured impedance data and the cell constant uses equation (3.5) [21], [127], [129].

$$k = \frac{G}{\sigma} \quad (3.5)$$

where σ is the electrical conductivity of the standard liquids and G is the measured conductance of the probe in the targeted frequency range. For this study, 0.01 M, 0.05 M and 0.1 M of NaCl solutions at room temperature (21 ± 0.5 °C) are used as reference liquids to find k , as the conductivity of the targeted tissue (LAA) is assumed to range within the conductivity of the reference liquids from the literature review in section 2.9. In theory, the NaCl solutions are chosen to determine k as there are no dielectric dispersions in ionic aqueous solutions at frequencies below 1 MHz [35]. Therefore, the measured complex impedance is frequency independent and only varies with the concentrations of the aqueous NaCl solution [59], [118]. This method is used for all proposed probes to determine their k .

Chapter 3: Evaluation of Tetrapolar Probes: Investigating the Impact of Probe Typology and Electrode Size on Conductivity Measurements for the Left Atrial Appendage from 0.1 Hz to 100 kHz

Fig 3.4 shows the results for the small collinear probe with the linear regression line (dashed red line), the conductance acquired vs the reference conductivity at different mole concentrations (blue dots), and the correlation factor and cell constant of the probe.

Table 3.2 The table provides the values of k (m) for various types of probes within the frequency range from 0.1 Hz to 100 kHz

Probe		$k(m)$
Collinear probe	Fig 3. 3(a)	0.066
Polar probe	Fig 3. 3(b)	0.039
Small collinear probe	Fig 3. 3(c)	0.032
Small asymmetrical collinear probe	Fig 3. 3(d)	0.02
Small unequal and asymmetrical collinear probe	Fig 3. 3(e)	0.15
unequal and asymmetrical polar probe	Fig 3. 3(f)	0.15

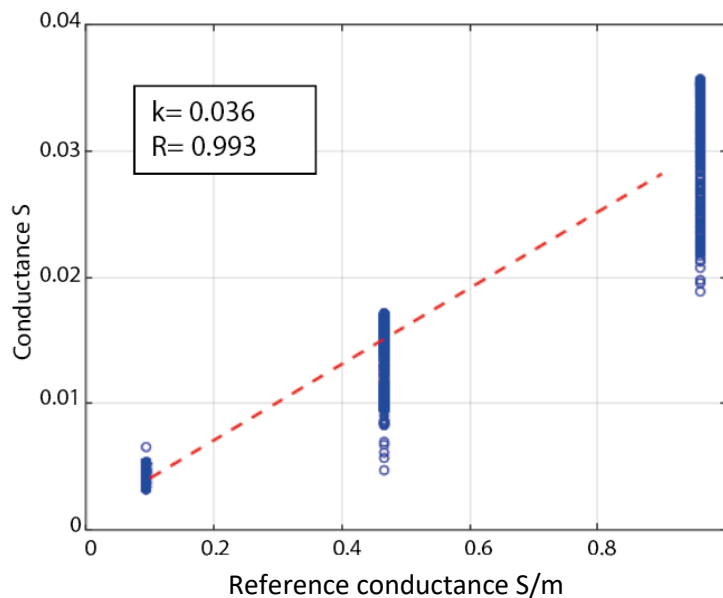


Figure 3. 5 Results for the small collinear probe, including its correlation factor and cell constant from three NaCl solutions from frequency 0.1 Hz to 100 kHz

The Pearson correlation coefficient (R) between the measured conductance and the reference conductivity was found to be a variable value and it depends on the frequency range. R is defined using equation (3.6).

$$R = \frac{\sum_{i=1}^n (x_i - \bar{x})(y_i - \bar{y})}{\sqrt{[\sum_{i=1}^n (x_i - \bar{x})^2 * \sum_{i=1}^n (y_i - \bar{y})^2]}} \quad (3.6)$$

Chapter 3: Evaluation of Tetrapolar Probes: Investigating the Impact of Probe Typology and Electrode Size on Conductivity Measurements for the Left Atrial Appendage from 0.1 Hz to 100 kHz

where x_i and y_i are the individual data points for variables x and y . \bar{x} and \bar{y} are the means of the variables x and y , respectively.

R is the experimental response of the probes to the calibration solutions and that reflects the working frequency of the probes. The observation seen in Fig 3. 6 from the proposed probes is that the lower frequency ranges from 0.1 Hz to 10 Hz are highly noisy and drive the correlation factor to be lower making the data acquired between 0.1 Hz and 10 Hz unreliable [59], [238], [239]

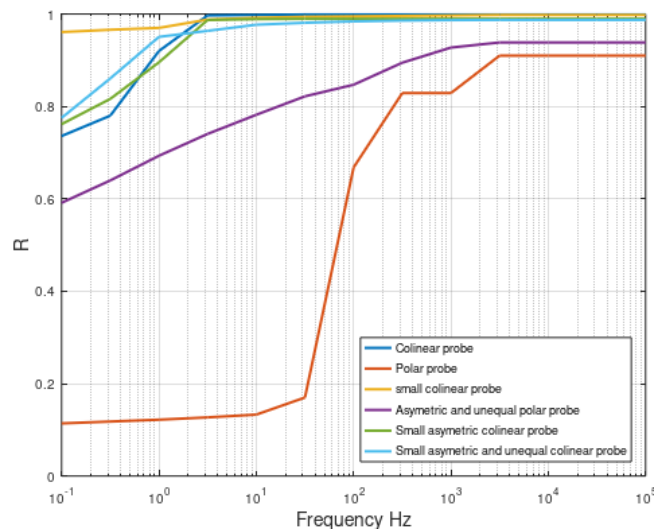


Figure 3. 6 Pearson correlation coefficient (R) as a function of the frequency range for the proposed probes. R represents the experimental response of the probes to the calibration solutions and reflects the working frequency of the probes

3.3.3 Measurement accuracy

The accuracy of a tetrapolar probe refers to its ability to provide measurements that align with the true values of the physical quantities being measured. It is a measure of the precision of the probe to acquire accurate data. The accuracy of a tetrapolar probe can be influenced by various factors, including the design of the probe, the electrical properties of the sample being measured, and the measurement conditions [118]. Hence, ensuring stable and consistent measurement conditions is crucial. Additionally, accurate measurements depend significantly on the proper calibration of the tetrapolar probe [129], [221], [240]. Calibration involves measuring the response of the probe to a standard sample with known electrical properties and adjusting the calibration of the probe factors accordingly [59], [118], [227], [240].

Chapter 3: Evaluation of Tetrapolar Probes: Investigating the Impact of Probe Typology and Electrode Size on Conductivity Measurements for the Left Atrial Appendage from 0.1 Hz to 100 kHz

The measurement of accuracy in this thesis is represented using the average error. The average error is defined as the difference between the measured conductivity and the reference conductivity values from the literature for standard NaCl solutions [35]. For this thesis, the accuracy of the proposed probes is investigated with measurements taken over the frequency range from 0.1 Hz to 100 kHz with 10 frequency points per decade, 60 points per measurement. The total number of measurements taken for the accuracy test is 15 measurements, 5 measurements for each NaCl concentration solution (0.1 M, 0.05 M and 0.01 M).

The calculation of the average error involves a comparative analysis between the mean frequency-dependent conductivity values acquired for each probe and the corresponding reference conductivity values. Given the inherent frequency dependence and non-linearity (not a perfect straight line) of the experimental conductivity, the average error is computed across the entire frequency range. Notably, the assessment is based on the maximum discrepancy observed between the acquired conductivity and the reference conductivity, serving as the metric for probe comparison.

The measurement of the NaCl phantoms was conducted in a cylindrical container with a diameter of 9 cm and the container was filled with a 1.5 cm depth liquid to match the thickness of the LAA. NaCl phantoms are advantageous for electrical conductivity studies because their stable properties remain constant across different frequencies. The simplicity of NaCl as a basic ionic compound results in minimal changes in conductivity with frequency variations. This frequency-independent behaviour is crucial for experiments involving electrical impedance measurements providing a consistent and predictable conductivity.

3.3.4 Repeatability of measurement

The repeatability of a tetrapolar probe refers to its ability of the probe to produce consistent and reproducible measurements under similar conditions. For this thesis, the influence of the electrode size and typology of the repeatability of the proposed probes is investigated. The repeatability of the probes is assessed based on a total of 15 measurements for each probe through the frequency range then the SD (0.1 HZ to 100 kHz) is averaged to give a singular value of SD that is used to compare the probes. In this analysis, the standard deviation (SD) and the

coefficient of variation (CV) are employed. Specifically, the standard deviation (SD) used in this context pertains to the variability in conductivity measurements. Given that the experiment utilizes saline solutions with an anticipated uniform conductivity across the targeted frequency range, the standard deviation is computed across all frequencies. Subsequently, the obtained standard deviation values are averaged, resulting in a singular representative value for the standard deviation associated with each probe for each saline solution. [27], [241]. The SD and the CV are calculated using (3.7) and (3.8) [241]:

$$SD = \sqrt{\frac{1}{N-1} \sum_{i=1}^N (X_i - \mu)^2} \quad (3.7)$$

$$CV = 100 \frac{SD}{\mu} \quad (3.8)$$

where μ is the mean, N is the total number of measurements, and X_i is the measurement values. These accuracy and repeatability measures are used to identify the best-performing tetrapolar probe from the six proposed custom probes to be used to characterize the LAA.

3.4 Results

3.4.1 Effect of the typology and electrode size of the probe on the accuracy of the acquired conductivity

To evaluate how various factors, such as the typology and electrode size of the probe, impact the accuracy of the acquired data, several design modifications were implemented for a comparative analysis of each design influence. The design alterations investigated are electrode size, asymmetry of the probes, typology and the combination of electrode size, asymmetry and typology in the same probe.

The initial design alteration focused on varying the electrode size while maintaining the same typology, specifically comparing the collinear probe with the smaller collinear probe.

Next, the assessment shifted towards electrode configuration (typology), comparing the collinear probe with the polar probe.

Chapter 3: Evaluation of Tetrapolar Probes: Investigating the Impact of Probe Typology and Electrode Size on Conductivity Measurements for the Left Atrial Appendage from 0.1 Hz to 100 kHz

Another design change involved introducing asymmetry in the spacing of electrodes within the same collinear probe configuration while keeping the electrode size constant. This comparison was made between the small collinear probe and the small asymmetrical collinear probe.

Lastly, the fourth design variation examined the combined effect of electrode size alteration and asymmetry. This was achieved by using both polar and collinear typologies. Consequently, the unequal and asymmetrical polar probe was compared to the polar probe, while the small unequal and asymmetrical collinear probe was compared to the small collinear probe

The maximum average error and SD of the proposed probes were used as metrics over a frequency range of 0.1 Hz to 100 kHz and were compared to the reference conductivity values obtained from the literature [42]. The results are presented in Table 3.3 as follow maximum average error \pm SD.

Table 3.3 Average conductivity (S/m) plus SD of NaCl phantom acquired with the proposed probes with the reference conductivity values

NaCl	0.01 M	0.05 M	0.1 M
Probes	$\sigma \pm SD$ (S/m)	$\sigma \pm SD$ (S/m)	$\sigma \pm SD$ (S/m)
Collinear probe Fig 3. 3 (a)	0.096 \pm 0.003	0.45 \pm 0.02	0.97 \pm 0.01
Polar probe Fig 3.3 (b)	0.079 \pm 0.009	0.33 \pm 0.05	0.94 \pm 0.07
Small collinear probe Fig 3. 3 (c)	0.121 \pm 0.01	0.48 \pm 0.02	1.02 \pm 0.03
Small asymmetrical collinear probe Fig 3. 3 (d)	0.14 \pm 0.01	0.44 \pm 0.02	0.98 \pm 0.02
Small unequal and asymmetrical collinear probe Fig 3. 3 (e)	0.12 \pm 0.007	0.61 \pm 0.06	1.05 \pm 0.06
unequal and asymmetrical polar probe Fig 3. 3 (f)	0.13 \pm 0.01	0.74 \pm 0.02	1.3 \pm 0.1
Ref. [42] σ (S/m)	0.11	0.49	0.96

The polar probe demonstrated a maximum average error of 32% from the literature values, while the collinear probe exhibited a maximum average error of 12%. The small collinear probe showed a maximum average error of 10%, whereas the small unequal collinear probe displayed a maximum average error of 27%. The small asymmetric collinear probe exhibited a maximum average error of 24% from

Chapter 3: Evaluation of Tetrapolar Probes: Investigating the Impact of Probe Typology and Electrode Size on Conductivity Measurements for the Left Atrial Appendage from 0.1 Hz to 100 kHz

the literature values, and the asymmetric and unequal polar probe displayed the highest difference from the literature values with a 51% maximum average error.

The initial design alteration investigates the impact of electrode size on accuracy, the accuracy of a collinear probe with small electrodes to that of a collinear probe is compared. The collinear probe with small electrodes demonstrated an accuracy of 10%, while the standard collinear probe had an accuracy of 12% over a frequency range of 0.1 Hz to 100 kHz. The observed difference in performance can be attributed to the larger size of the electrodes in the standard collinear probe, which increases electrode impedance and reduces the spacing ratio between electrodes, thereby resulting in higher electrode polarization [215], [216], [242], [243].

The next design alteration focusing on electrode configuration (typology), indicates that the accuracy of the collinear probes was superior to that of the polar probe in the frequency range of 0.1 Hz to 100 kHz with NaCl phantoms.

The variance in accuracy among typologies due to the electrode configuration, particularly evident in the collinear probe. This probe features four strategically aligned electrodes, positioning the measuring electrodes within the region of maximum electrical field (maximum current density) between the inducing electrodes.

To comprehensively understand the factors influencing accuracy variations among typologies, a simulation was executed, focusing on the distribution of the electric field. This simulation specifically analysed the electric field distribution using measurement parameters set at 100 μ A. The simulation captured the field generated by the inducing electrodes at two designated points in two different typologies (point A: at the centre of the inducing electrodes ($x=0, y=0$); point B: 10 mm from the centre on the y -axis ($x=0, y=10$)). The investigation of the acquired field from the inducing electrodes was conducted between two proposed typologies, the collinear probe, and the polar probe, with dimensions derived from Fig 3.3 (a) for the collinear probe and Fig 3.3 (b) for the polar probe.

Fig 3.7 illustrates the electric field generated by the electrodes, including the field at points A and B for the polar probe, collinear probe, and small collinear probe. A notable observation is that the measuring electrodes of the collinear probe align with the maximum electrical field, contrasting with the polar probe.

Chapter 3: Evaluation of Tetrapolar Probes: Investigating the Impact of Probe Typology and Electrode Size on Conductivity Measurements for the Left Atrial Appendage from 0.1 Hz to 100 kHz

This misalignment significantly impacts the acquired data. Consequently, the results underscore the influence of typology on the accuracy of data acquired during measurement while indicating not on the repeatability (as CV < 5% for all probes).

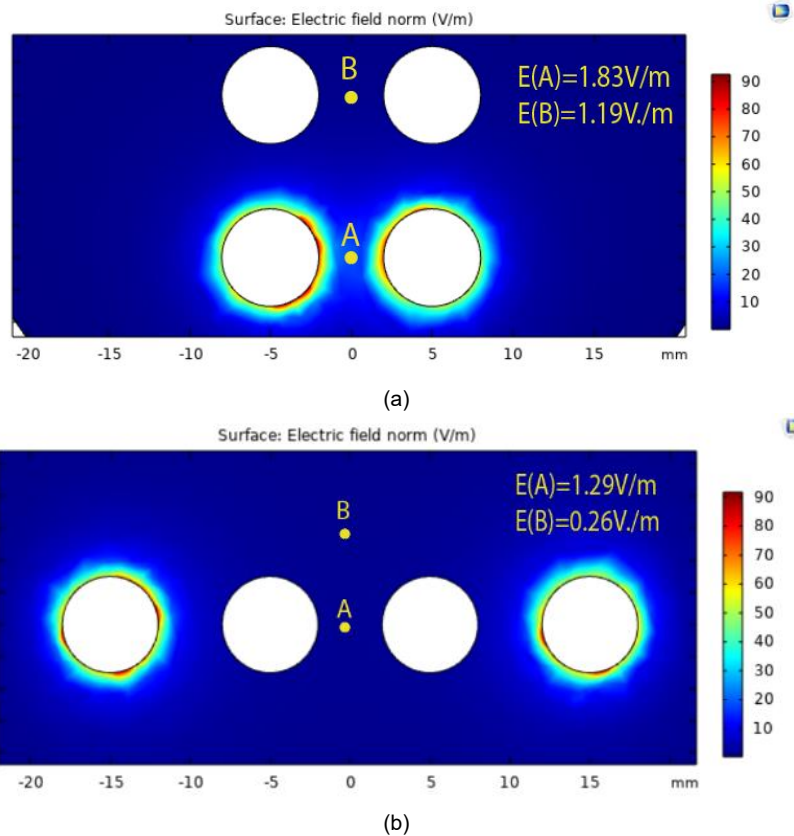


Figure 3. 7 The electric field distribution by the proposed probes focusing on points A and B. (a) field distribution of the polar probe (V m-1). (b) electric field distribution of the collinear probe (V m-1). (c) electric field distribution of the small collinear

The next design change involved introducing asymmetry in the spacing of electrodes and comparing the small collinear probe with the small asymmetrical collinear probe. The larger distance between the electrodes in the asymmetrical collinear probes resulted in a larger measuring area, leading to a higher signal-to-noise ratio that affected the acquired conductivity [216], [236], [242]. The small unequal collinear probe exhibited an accuracy of 24% compared to the small collinear probe with a maximum average error of 10%. Lastly, the fourth design variation is the combined effect of asymmetry and inequality in the polar and collinear probes.

The analysis of the asymmetry and inequality of the electrodes (the inducing electrodes are bigger than the measuring electrodes) in the small collinear probe

indicated that accuracy decreased. Additionally, comparing the collinear probe with the polar probe showed that accuracy decreased with the polar probes [215], [216], [242], [243]. The observations obtained for the asymmetric and unequal polar and collinear probes exhibit the lowest accuracy seen among the polar probes and collinear probes with a maximum average error of 51% and 27% respectively. This difference was attributed to the higher signal-to-noise ratio introduced by the smaller electrodes and the smaller distance between the inducing electrodes (larger electrodes) and the measuring electrodes (smaller electrodes).

3.4.2 Effect of the typology and electrode size of the probe on the repeatability of the acquired conductivity

In this study, the repeatability of the data acquired during the measurement is estimated using the coefficient of variation (CV). The results for all proposed probes are presented in Fig 3.7, where the CV is displayed as a percentage and is considered to be low [27], with errors below 5% for all the probes across 0.1 Hz to 100 kHz. This indicates low intra-observer variability and implies that the measurements are repeatable.

Both the typologies (polar probes and collinear probes) show good CV values (<5% and <1%, respectively), however, it is difficult to assess whether the difference in CV means that the collinear probes provide more repeatable data than the polar probes. Similarly, comparing the proposed collinear probes (collinear probe, small collinear probe, small asymmetrical collinear probe, small unequal and asymmetrical collinear probe), CV is observed to be good with a value of less than 1%, but it is difficult to draw conclusions about the effect of electrode size on repeatability. The resulting data shows that the influence of the typology on repeatability can not be concluded.

Chapter 3: Evaluation of Tetrapolar Probes: Investigating the Impact of Probe Typology and Electrode Size on Conductivity Measurements for the Left Atrial Appendage from 0.1 Hz to 100 kHz

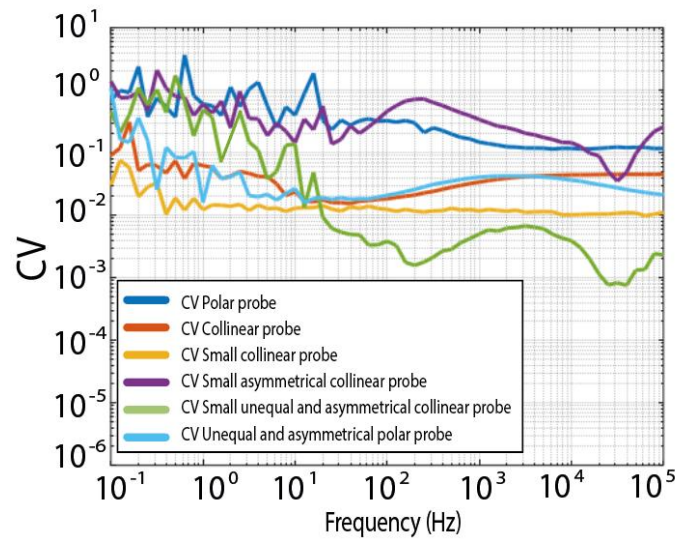


Figure 3. 8 Coefficient of variation (CV) of the polar probe, collinear probe, small collinear probe, unequal collinear probe, asymmetric and unequal probe, and the unequal polar probe. CV shown in the targeted frequency range from 0.1 Hz to 100 kHz

In Fig 3. 8, the coefficient of variation (CV) was less than 5% for all the different probe typologies and electrode sizes tested. This suggests that the proposed typology and electrode size had limited influence on the repeatability of data acquisition in this case. However, the absolute values of conductivity acquired from the NaCl phantoms varied from 10% to 51% among the different probe typologies and electrode sizes, indicating that the electrode size and typology of the probe did affect conductivity acquisition.

Although the small collinear probe was the most accurate among the proposed probes, the collinear probe was only 2% points lower (from 12% to 10%), a value that is likely smaller than the measurement error. However, considering the value of R, which measures the strength of the association between the measured data and the reference data obtained from the literature, the small collinear probe exhibited the best performance with an accuracy of 10%, a high R value of 0.99, and a CV of 1%. Therefore, it was further tested to acquire the conductivity of the left atrial appendage (LAA) in chapter 4 using ten ex-vivo bovine LAA tissue samples over a frequency range of 0.1 Hz to 100 kHz [67].

3.5 Conclusion

Chapter 3 investigated the effect of probe typology and electrode size on the accuracy and repeatability of impedance measurements for the electrical

Chapter 3: Evaluation of Tetrapolar Probes: Investigating the Impact of Probe Typology and Electrode Size on Conductivity Measurements for the Left Atrial Appendage from 0.1 Hz to 100 kHz

characterization of biological tissues. The lack of consistency in the field was demonstrated using different typologies and probe/electrode sizes in previous studies. The design, prototyping, and manufacturing of the six probes presented in this thesis were undertaken by the author. This constitutes an augmented contribution to the thesis, as these probes were not only conceptualized but also fabricated in-house. This distinguishes them from commercially available probes, thereby enhancing the originality of the research. The proposed probes underwent comprehensive testing, further validating their unique contribution to the study.

The repeatability of the measurements using the two typologies and different electrode sizes was consistent, with low variance in the acquired conductivity ($CV < 5\%$). However, the accuracy of the conductivity measurements varied across the proposed probes used on the same phantoms, with maximum average error ranging from 10% to 51%. This suggests that the probe typology can influence the accuracy of the measured electrical conductivity.

The findings suggest that compromising the data acquisition from the electrical characterization of biological tissues can occur when the probe design is not adapted to the specific tissue under study. Based on the results, the collinear probe with small electrodes was identified as the best-performing probe from the proposed probes for the electrical characterization of the LAA and was further tested using ten ex-vivo bovine LAA tissue samples at frequencies ranging from 0.1 Hz to 100 kHz.

In summary, chapter 3 emphasizes the effect of probe typology and electrode size on the accuracy and repeatability of conductivity measurements for the electrical characterization of biological tissue. The collinear probe with small electrodes was identified as the best-performing probe for the electrical characterization of the LAA. Chapter 4 presents a detailed account of the methodology employed to measure the conductivity of the LAA using the small collinear probe, which provides the first data on LAA conductivity and compares it to existing data on cardiac tissue in the literature. The findings of this study highlight the importance of adapting the probe design to the tissue under study and motivate further research in the field.

Chapter 4: Assessing Conductivity of Ex-vivo Left Atrial Appendage from 0.1 Hz to 100 kHz

4.1 Introduction

Chapter 3 introduces six variations of the tetrapolar probes and investigates the effect of probe typology and electrode size on the accuracy and repeatability of the acquired data [216], [218], [220], [236]. Additionally, chapter 3 emphasizes the effect of probe typology and electrode size on the accuracy and repeatability of conductivity measurements. Based on the results, the small collinear probe was identified as the best-performing probe among the proposed probes, and subsequently, the small collinear probe will be used for electrical characterization of the LAA at low frequencies below 100 kHz [118], [227].

In Chapter 4, the goal was to evaluate the initial conductivity measurements of the left atrial appendage (LAA) in an ex-vivo setting, marking the first instance of such assessments in the existing literature. To reach the main objective and to ensure accurate and reproducible measurements, the best-fit tetrapolar probe and rigorous sample acquisition and tissue handling procedures were employed.

In chapter 4, the background on the methodology of biological tissue data acquisition is presented, with a particular focus on cardiac tissue, including the various probes that have been used in previous studies [31], [32], [222]–[224], [244]. Additionally, chapter 4 presents a detailed account of the methodology employed to measure the conductivity of the LAA, which includes the probe used, sample acquisition, tissue handling procedures and data processing. This comprehensive description is based on measurements taken from ten ex-vivo samples. Chapter 4 concludes by providing the first data of the conductivity of the LAA, which is compared to existing data on cardiac tissue in the literature.

4.2 Background on Probes used on cardiac tissue electrical characterisation

This section introduces the probes used in the electrical characterization of cardiac tissues. Cinca et al., 1997 [222], utilized a tetrapolar probe with four platinum electrodes for in-vivo porcine samples. Ellenby et al., 1987 [223], employed a four-electrode method using gold-plated brass pins for ex-vivo left ventricle measurements. Gabriel et al., 2009 [36], studied electrical conductivity in various tissues, including the heart, using a linear four-terminal probe design. Hahn et al., 1980 [224], assessed electrical conductivity in porcine cardiac tissues using a nine-needle electrode probe.

The data acquired using those probes display a range of cardiac tissue conductivity which varies from 0.5 mS cm^{-1} to 9 mS cm^{-1} [31], [32], [36], [222], [223], [244]. The conductivity range varies from study to study and can be explained by the different origins of the samples (ex-vivo or in-vivo, different animal sources, or human) and the difference in tissue samples (measurement in different parts of the heart). However, if only focusing on ex-vivo animal studies, the conductivity averages at $3 \pm 0.5 \text{ mS cm}^{-1}$ in the frequency range from 10 Hz to 100 kHz [31], [32], [36], [222], [223], [244].

4.3 Methodology of Left atrial appendage measurement

4.3.1 Data acquisition of the electrical properties below 100 kHz

This section outlines the methodology used to measure the conductivity of the LAA. The frequency-dependent complex impedance to calculate the conductivity was acquired using similar methods outlined in chapter 3. The set-up consists of a PGSTAT204 (Autolab, Kanaalweg Den Haag, The Netherlands) in galvanostatic mode at room temperature and controlled with Nova 2.1 software. The galvanostatic mode was utilized with a $100 \mu\text{A}$ current flowing between the inducing electrodes. The measurement setup included the PGSTAT204 connected to the small collinear probe ($k = 0.032 \text{ m}$). The PGSTAT204 was connected to a

Chapter 4: Assessing Conductivity of Ex-vivo Left Atrial Appendage from 0.1 Hz to 100 kHz.

computer running Nova 2.1 to control the PGSTAT204. A retort stand was used to maintain the stability of the setup, and the probe was designed to fit into a holder. The new upgrade to the set-up in chapter 3 is a weighing scale (Kern Weighing Scale, METTLER TOLEDO, Columbus, OH, USA) to monitor and ensure constant probe contact with the tissue to avoid tissue movement due to excess contact force [27]. The full setup is illustrated in Fig 4.1.

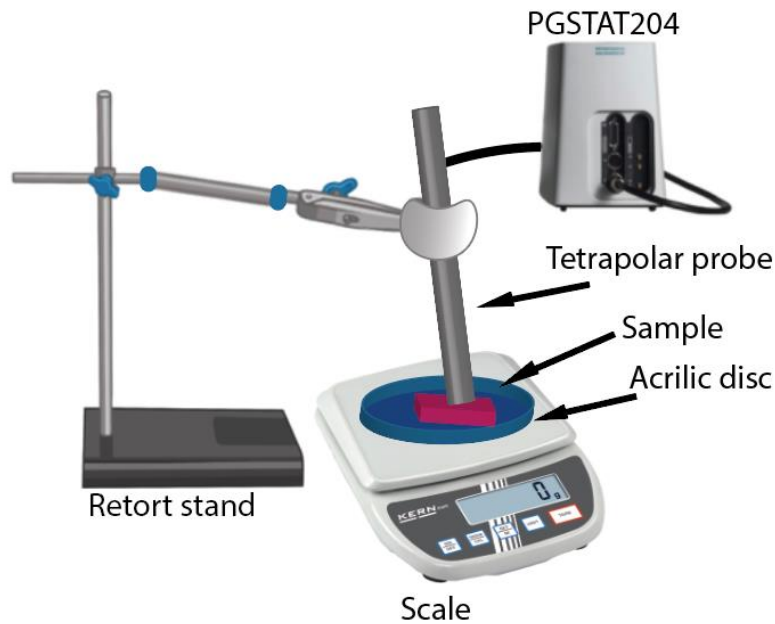
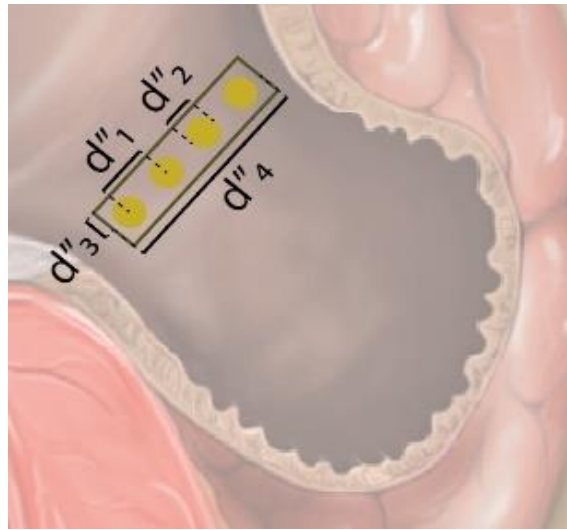


Figure 4. 1 Measurement setup with the probe, the laptop running NOVA 2.1 software in the foreground. PGSTAT204 potentiostat/galvanostat and the probe holder used to lift and keep the probe fixed

4.3.2 Probe description

Based on the results of chapter 3, the small collinear probe was observed to be the best-performing probe regarding accuracy and repeatability of the proposed six probes. The probe has electrodes with a diameter of 3 mm to reduce non-linearities, electrode impedance and electrode polarization [118], [221], [236], [237]. The total footprint of the proposed probe is 20 mm by 4 mm. The fabricated prototype of the small collinear probe is shown in Fig 4.2(b), and a schematic representation overlaid on the LAA in Fig 4.2(a), where the dimensions are $d''1 = 5$ mm, $d''2 = 3$ mm, $d''3 = 2$ mm, $d''4 = 20$ mm.

The collinear probe with small electrodes provides an accuracy of 10%, $R > 0.95$ [29], CV of 1% from 0.1 Hz to 100 kHz [118], [187], [227].



(a)



(b)

Figure 4. 2 Diagram showing the dimensions of the proposed collinear probe with small electrodes. The illustration shows the footprint of the probe on the surface of the LAA, (b) Photo of the manufactured prototype of the proposed collinear probe with small electrodes

4.3.3 Sample acquisition and tissue handling of the LAA

This section elucidates on the process of tissue acquisition with respect to tissue handling and measurement set-up for the experiment. The animal tissue was procured from a local slaughterhouse immediately after excision and was transported to the TMD Laboratory (University of Galway, Ireland) in vacuum-sealed containers. The time of death of the animal was not taken in consideration. The samples were received at the laboratory within two hours of excision. A total

of ten bovine heart samples were obtained, and each heart was embedded in its fat capsule to limit the dehydration of the tissue [62], [227]. The LAA was dissected from the heart, and the internal membrane was removed to allow for direct measurements of the LAA pectinate muscle. The membrane of the LAA can be seen in the left photo in Fig. 4.3 highlighted by a yellow dot.

The position of the measurement was selected to be on the endocardium of the LAA, where IRE treatment is usually administered. The endocardium of the LAA is known to be the optimal location for the administration of IRE treatment because it is in direct contact with the blood flow and has a higher density of muscle fibres, which ensures better contact with the IRE probe and improved treatment efficacy [72], [81], [86], [87], [105], [245]. Therefore, by selecting the position of the measurement to be on the endocardium of the pectinate muscles of the LAA, the aim is to replicate the conditions of IRE treatment and measure the electrical conductivity of the tissue at the site of the intended treatment.

The temperature was monitored throughout all experiments, and the initial and final temperatures of all samples remained stable at room temperature of $20\text{ }^{\circ}\text{C} \pm 0.5\text{ }^{\circ}\text{C}$. Each sample was measured three times at the position displayed in Fig 4. 3. To ensure firm contact while avoiding tissue movement due to excess pressure, a pressure of $2\text{ N} \pm 0.5\text{ N}$ was applied by the probe [27].

Fig 4.3 displays the first bovine heart sample, with the LAA highlighted for reference. The right picture shows the dissected LAA from sample one, with a yellow square indicating the position of the LAA pectinate muscle where the measurements were taken. The pectinate muscles are the muscles that line the pectinate ridge and the inner wall of the LAA [72], [87]

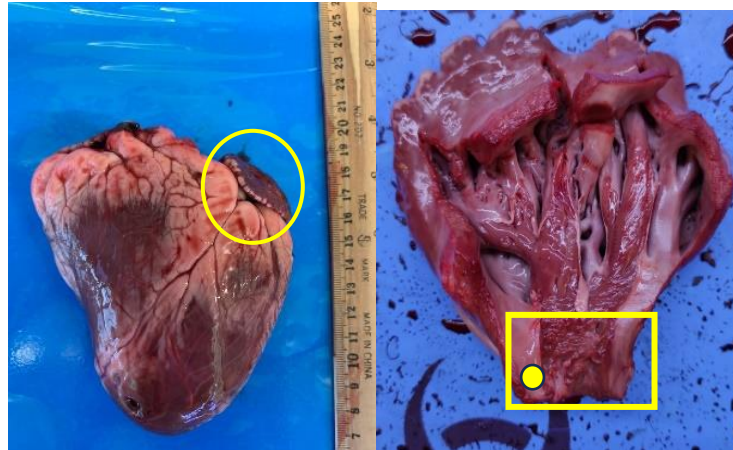


Figure 4. 3 Left picture shows the first sample bovine heart with the LAA highlighted. The right picture shows the dissected LAA from sample one. The yellow square shows the position of the LAA pectinate muscle where the measurements were taken. The yellow dot shows part of the membrane

4.4 Assessing the conductivity of ten ex-vivo samples of LAA from 0.1 Hz to 100 kHz at room temperature

The electrical conductivity of LAA of bovine tissue was measured using a 4- electrode probe method, a similar method described in chapter 3. The electrical conductivity of the LAA was calculated from ten LAA samples. To validate the measurement setup, three pre- and post-validation measurements were acquired using 0.15 M NaCl solution to detect any drift in the measurement setup.

The results of the LAA measurements were compared to the conductivity of cardiac tissue reported in the literature. The conductivity of cardiac tissue in the literature varied widely, ranging from 0.5 mS cm^{-1} to 9 mS cm^{-1} , as discussed in section 2.9. This variation could be explained by factors such as the tissue origin (ex-vivo or in-vivo, different animal sources or human), and differences in tissue samples (measurements taken in different parts of the heart) [23], [24], [27], [38]-[43]. The average of the three measurements of each sample is shown in Fig 4.4, along with reference values from the literature on the conductivity of cardiac tissue. The computed conductivity from the ten bovine samples was 2.5 mS cm^{-1} with a standard deviation of 0.24 mS cm^{-1} .

In addition to comparing the computed conductivity of the LAA to the literature values, further analysis was conducted to investigate the variability of conductivity

across the ten bovine samples. The CV was calculated for the conductivity measurements of each sample, the CV values ranged from 7.8% to 12.2%, indicating a moderate level of variability in conductivity across the samples shown in Table 4.1.

Moreover, the drift observed in the pre-and post-validation measurements showed a characteristic zero drift and sensitivity drift averaging at 2.5%. The computed conductivity from the LAA was observed to be within the range of the conductivity in literature.

To investigate potential sources of variability, the anatomical features of the LAA were examined. It was observed that the size and shape of the LAA varied across the samples, with some samples exhibiting a more elongated and narrow shape, while others had a more rounded and wider shape. These anatomical differences may have contributed to the observed variability in conductivity measurements.

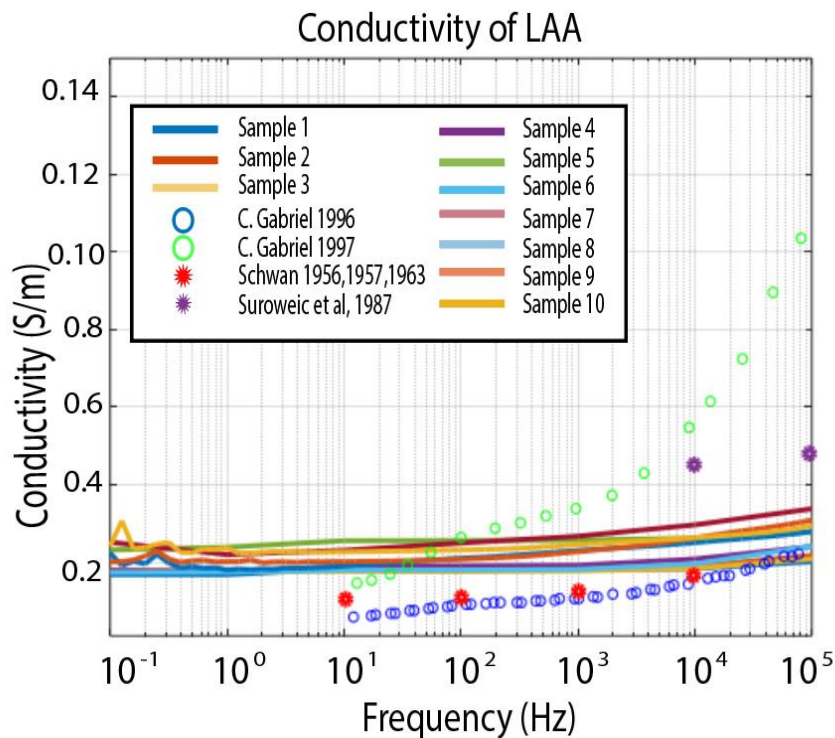


Figure 4. 4 Conductivity acquired from ten bovine LAA samples at room temperature 20 °C and the reference cardiac conductivity

Chapter 4: Assessing Conductivity of Ex-vivo Left Atrial Appendage from 0.1 Hz to 100 kHz.

Table 4.1 Average electrical conductivity of ten bovine LAA samples compared to literature values

Sample Number	Conductivity (mS/cm)	Coefficient of Variation (%)
1	2.4	10.1
2	2.5	8.3
3	2.3	9.2
4	2.6	8.6
5	2.4	7.8
6	2.6	11.2
7	2.5	9.7
8	2.4	8.8
9	2.7	12.2
10	2.5	9.4
Ref [31], [32], [36], [222], [223], [244]	0.5-9 (mean: 3)	N/A

The mean conductivity of the bovine LAA samples was 2.5 mS cm^{-1} , with a standard deviation of 0.24 mS cm^{-1} . The coefficient of variation ranged from 7.8% to 12.2%, indicating a moderate level of variability in conductivity across the samples.

4.5 Conclusion

In this study, the electrical conductivity of ex-vivo bovine LAA tissue was measured using a collinear probe with small electrodes and a 4-electrode probe method at room temperature ($20 \text{ }^\circ\text{C} \pm 0.5 \text{ }^\circ\text{C}$) in the frequency range from 0.1 Hz to 100 kHz. The mean conductivity of the LAA acquired from the ten samples was found to be 2.5 mS cm^{-1} with a standard deviation of 0.24 mS cm^{-1} . The observation from the results suggests that the acquired conductivity of the LAA is in line with the literature values for the conductivity of cardiac tissue.

There are several limitations to consider in the study of LAA conductivity. One significant limitation is the diversity of tissue regarding the anatomical features of the LAA. The size of the LAA varies between samples, and this can affect the LAA during tissue handling and the experiment process, such as hydration and temperature. Another limitation is the number of samples and the fact that the samples are ex-vivo. Although 10 ex-vivo samples are a good starting point, introducing a larger number of samples, and moving towards a more realistic scenario such as an in-vivo scenario, would be beneficial in future studies. A third

limitation is the variation in the contact force of the probe on the LAA during the measurement. The LAA is a semi-solid and slimy structure that can lead to movement during the experiment, potentially affecting conductivity acquisition.

In chapter 5, the limitation of the effect of contact force on the conductivity of the LAA will be investigated in more detail. This is an important limitation to address, as contact force could impact the measurement results. By exploring the effect of contact force, a better understanding of the factors that influence LAA conductivity can be gained and improve the accuracy and reproducibility of the conductivity measurements of the LAA. Ultimately, this will help advance our understanding of LAA conductivity and its potential clinical implications.

In summary, this study offers important insights into the electrical conductivity of the LAA and presents the first reported value of LAA conductivity in the literature. Although the conductivity values provided in this thesis are preliminary, they can serve as initial data for numerical electromagnetic simulations to estimate the outcome of IRE for the LAA which could optimize treatment planning.

Future research could focus on optimizing the measurement protocol and set-up to acquire more precise and consistent LAA conductivity values. By doing so, it can lead to improving the accuracy and reliability of LAA conductivity measurements, which could have significant implications for future clinical applications.

Chapter 5: The Effect of Contact Force on Conductivity Measurement of Ex-vivo Left Atrial Appendage of from 10 Hz to 100 kHz

5.1 Introduction

Chapter 5 explores the influence of probe contact force on the measurement of conductivity of tissue, and how this may affect the conductivity of the LAA. Additionally, chapter 5 introduces a statistical analysis to assess the significance of extracellular fluids as a contributing factor to the observed effects.

The measured electrical properties have been synthesized into several freely available databases, including the Italian National Research Council database and the IT'IS Foundation database [55], [56]. The electrical conductivity using the electrical impedance measurement method is typically acquired using a probe in contact with the tissue to measure the ratio of current and voltage [59], [62], [132], [240], [246].

Communally the contact between the probe and tissue is fixed throughout the experiment. However, the effect of contact force on tissue conductivity is not fully understood and varies between tissue types [27], [40], [132]. For this study, the LAA is used as a test case to evaluate the effect of contact force on conductivity. The limited availability of data and the known issues regarding the impact of the contact force on the measurements motivated the study in chapter 5. The main aim of this chapter is to investigate the frequency-dependent conductivity of the LAA with respect to the contact force of the probe in the range of 2 N to 10 N in the frequency range from 10 Hz to 100 kHz. Potential causes of conductivity variance and the acquired data are statistically compared to investigate if the extracellular fluids are contributors to the conductivity change. The results of this chapter will help

improve the understanding of tissue conductivity measured under different contact forces.

5.2 Background

Researchers often rely on the literature and online databases to obtain electrical property values for over 112 tissues from 10 Hz to 100 GHz [55], [56], which have been widely cited (over 1700 citations). However, the source data for these databases typically do not report, control or monitor probe contact force. In studies where contact force is reported, it is typically qualitatively described as "sufficient contact" or on a scale from "light contact" to "moderate" to "firm" [27], [40], [247]. Of the ten studies reporting the conductivity of heart muscle in the IT'IS Foundation database, only three studies [31] [224] [250] describe the contact force used [56]. Table 5.1 summarizes these ten studies and how the contact pressure during measurement is described.

Table 5.1 Contact force reported by the ten studies investigating heart muscle conductivity from the IT'IS Foundation database and how the contact pressure during the measurement is described

	Year	Species	Number	Ex-vivo	In-vivo	Force
[248]	1967	Various	-	✓	✓	-
[130]	1980	Dog	7	✓	✓	-
[224]	1980	Dog	4		✓	Gentle pressure
[223]	1987	Dog	12		✓	-
[249]	1993	Sheep	39		✓	-
[250]	1995	Pig	10		✓	Electrodes 4 to 6 mm deep
[31]	1996	Various	> 30	✓		Firm
[222]	1997	Pig	26		✓	-
[246]	2002	Pig	8		✓	-
[36]	2009	Pig	> 3		✓	-

The impact of contact force on tissue conductivity may vary depending on the type of tissue, in addition to quantitatively reporting the contact force. Studies that have investigated the effect of contact force on tissue conductivity have reported different trends, ranging from increased conductivity with increased force to decreased conductivity with increased force [27], [226], [247], [251]. These studies are not currently available in online databases. The application of force to biological tissue has a direct impact on its properties, such as the movement of

internal extracellular fluids, tissue deformation, or tissue damage [252]. When measuring biological tissue with mechanical damage, extracellular fluid movement is commonly thought to be the main contributor to changes in tissue conductivity [27], [253]. An increase in contact force applied to the tissue monotonically results in a decrease in conductivity due to the movement of extracellular fluids away from the measuring area. This can be seen in the cervix, where an increase in contact force on the probe displaces a high-conductance mucus film on the cervix, effectively decreasing tissue electrical conductivity [27], [253]. However, for some tissues such as the lung, conductivity increases as more contact force is applied, possibly because air is pushed away from the alveoli [251]. Liver tissue behaves differently, where the contact force applied by the probe has little effect on conductivity [226]. In the liver, a change of +0.8% per 1 N of applied force (per 6.25 kPa of applied pressure) is observed [226]. Table 5.2 displays the different behaviour of various tissues under monotonically increasing contact force.

Table 5.2 Percentage change of the electrical properties of cervix, lung, and liver with monotonically increasing contact force

Tissue	Force range	% Change in electrical properties
Cervix [27]	Soft to firm	-21.7%
Lung [251]	1 N to 10 N	44.9%
Liver [226]	2.9 N to 29 N	-7%
Liver [137]	1 N to 10 N	-8%

Chapter 5 is driven by the different trends in tissue conductivity in relation to contact force, to evaluate the impact on LAA conductivity to obtain accurate and repeatable LAA conductivity measurement. The main objective of this chapter is to examine how LAA conductivity changes when contact force varies between 2 N and 10 N, at frequencies ranging from 10 Hz to 100 kHz. Furthermore, various experiments are explored to determine the underlying factors contributing to the changes observed in conductivity measurements.

5.3 Methodology

To achieve the goal of this study, three different experiments were conducted: the forward experiment, the reverse experiment, and the hyperhydration experiment.

5.3.1 Forward experiment description

In the forward experiment, the aim was to measure the conductivity of the LAA by applying incremental levels of contact force with the tetrapolar probe. Specifically, LAA conductivity was measured at contact forces ranging from 2 N to 10 N, in intervals of +1 N, with the contact force being increased monotonically between each measurement. The forward experiment was conducted using ten ex-vivo LAA bovine samples. The initial contact force of 2 N was chosen to ensure sufficient contact between the LAA and the probe [27]. It should be noted that a contact force above 10 N is typically higher than what the tissue would experience in-vivo [4], [253]. For each sample, the conductivity was measured at the pectinate muscle in the opening of the LAA.

5.3.2 Reverse experiment description

The reverse experiment sought to measure the conductivity of the LAA by applying incremental levels of contact force in the opposite direction of the forward experiment. The reverse experiment involved measuring the LAA conductivity at contact forces ranging from 10 N to 2 N, in intervals of 1 N. The measurements were performed in the opposite direction the forward experiment, with the contact force being first increased to 10 N before being gradually reduced back to the starting value of the forward experiment (2 N).

By reversing the order of the measurements, this experiment aimed to investigate if the changes observed in the forward experiment were due to alterations in tissue conductivity caused by contact force. The reverse experiment was conducted on five ex-vivo LAA samples, using the same procedure as the forward experiment.

It has been suggested in the literature that the contact force can cause a change in the concentration of extracellular fluid in the tissue, resulting in differences between the forward and reverse experiments. However, as the contact force is decreased, there may be a partial increase in fluids in the measurement area due to tissue relaxation [253]. Therefore, the hyperhydration experiment was designed to address the limitation of partial extracellular fluids flowing back into the measuring area.

5.3.3 Hyperhydration experiment description

The hyperhydration experiment aimed to investigate the effect of extracellular fluid concentration on LAA conductivity changes in response to contact force. To this end, the LAA samples were preprocessed to reduce extracellular fluid concentration, which in turn reduces the number of charge carriers in the fluid. This would lead to a decreased effect of extracellular fluid movement on the measured conductivity changes due to the contact force. Therefore, if constant conductivity measurements are obtained in this experiment, it would suggest that extracellular fluid movement is indeed a contributor to the effects observed in the forward experiment [254]. The hyperhydration experiment involved submerging each of the five LAA samples in deionized water for one hour, which reduces the ion content of the extracellular fluid [255]. Following this process, the sample is removed from the water and the experiment proceeds as per the forward experiment.

5.3.4 Data acquisition

The LAA conductivity measurements were obtained using the same set-up in chapter 4, using the small collinear probe connected with the PGSTAT204 (Autolab, Kanaalweg Den-Haag, The Netherlands) in Galvanostat mode (100 μ A) at room temperature with Nova 2.1 software, and the weighing scale (Kern Weighing Scale, METTLER TOLEDO, Columbus, OH, USA) was used to monitor the contact force applied to the LAA.

The method for acquiring conductivity is described in chapter 3. The targeted frequencies of 10 Hz, 100 Hz, 1 kHz, 10 kHz, and 100 kHz were used for the conductivity measurements. The acquired frequency points were updated from 10 points per decade to 1 per decade, to make the measurement faster (160 s to 20 s) lowering the variation of the contact force during the measurement. The frequency range used for conductivity measurements with the small collinear probe in previous studies was from 0.1 Hz to 100 kHz. However, during the investigation of the relationship between contact force and conductivity in this study, the frequency range used was from 10 Hz to 100 kHz. This was because it was found that the frequency range from 0.1 Hz to 10 Hz was not reliable as it contained a lot of noise under different contact forces. It should be noted that the limitation of the probe's

frequency range in this study is acknowledged by the authors, and future studies should aim to optimize the probe design to expand the frequency range for more accurate and reliable conductivity measurements.

5.3.5 Force Monitoring

The contact force applied by the probe is measured by placing a weighing scale underneath the LAA. The required probe contact force is determined by calculating the mass recorded by the scale as follows:

$$F = m \times g \quad (5.1)$$

The applied contact force by the probe is expressed as F [N], and it is the weight force exerted by the probe on the sample. The mass of the sample is denoted as m [kg], and it is determined by measuring the weight recorded by the weighing scale with an accuracy of 0.1 g after being zero-ed. The acceleration due to gravity, g , is 9.801 m s^{-2} in Galway, Ireland, where the measurements were performed. To achieve a 2 N applied contact force on the LAA, a mass of 0.20406 kg should be measured on the weighing scales.

However, the semi-solid nature of the samples and the finite measurement time may cause deformation of the sample during measurement, which can lead to a change in the contact force. Therefore, monitoring the contact force during and after the measurement is essential. To monitor the contact force, the following measurement protocol was followed:

- Firstly, the sample was placed on the weighing scales, and the scale was zero-ed.
- The probe was brought into contact with the sample and adjusted until the mass read the appropriate value for the desired probe contact force as per equation 5.1.
- The mass was monitored during the conductivity measurement, and if the mass varied by more than 2% during the conductivity measurement, the measurement was repeated.

5.3.6 Statistical analyses

To assess the significance of conductivity changes observed in the present study, two paired T-tests are employed. Specifically, the T-tests aim to compare the

conductivity changes observed in the forward experiment, which utilized a high extracellular fluid concentration in the measurement area, to those observed in the reverse and hyperhydration experiments, which both employed a lower extracellular fluid concentration in the measurement area.

The paired t-test is appropriate when you have two sets of related or paired data, such as pre-and post-measurements on the same sample of individuals. It is specifically designed to compare the means of two paired samples while taking into account the correlation between them [256]–[259]. The paired t-test reduces the variability in the data that arise from individual differences between subjects [256]–[259]. Therefore, if you have paired data, the paired t-test is a more appropriate statistical test than an unpaired t-test [259].

T1, the first T-test, is designed to test the hypothesis that the conductivity change resulting from the contact force applied in the forward experiment is greater than that observed in the reverse experiment. A significant result for T1 would support the notion that fluid concentrations play a role in the observed conductivity differences. Similarly, T2 tests the hypothesis that the conductivity change resulting from the contact force applied in the forward experiment is greater than that observed in the hyperhydration experiment. The significance level for both T-tests is set at 5%, and a p-value less than 1% ($p < 0.01$) is deemed significant, consistent with previous research. Each frequency is tested separately, as changes in conductivity are known to be dependent on frequency [256]–[258].

5.3.7 Tissue handling

Twenty ex-vivo bovine LAA samples were investigated. Specifically, ten samples were used for the forward experiment, five for the reverse experiment, and another five for the hyperhydration experiment. The tissue handling protocol is similar to the protocol described in chapter 4. The LAA was dissected from the heart and the internal membrane was removed to directly measure the LAA pectinate muscle. The measurements were performed on the endocardium of the LAA, where IRE treatment typically occurs. The LAA dissection and its position in sample 1 can be observed in Fig 5.2(a). The experiments were carried out at the opening of the LAA, as indicated in Fig 5.2(b), and the temperature was monitored

throughout all experiments. The initial and final temperatures remained within the range of 20 ± 0.5 °C for all samples.

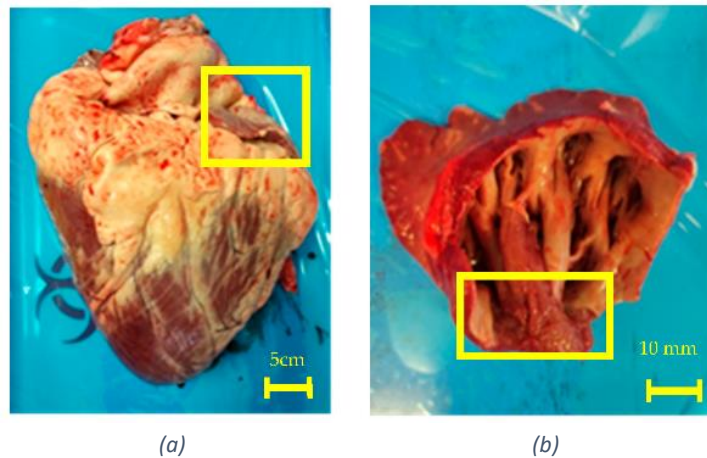


Figure 5. 1 (a) Left picture shows the first sample bovine heart with the LAA highlighted; (b) The right picture shows the dissected LAA from sample one. The yellow square shows the position of the LAA pectinate muscle where the measurements were taken

5.4 Results: Assessing the conductivity of the LAA change due to probe contact force

Fig 5.3 displays the mean conductivity and standard deviation obtained from the forward, reverse, and hyperhydration experiments at frequencies of 10 Hz, 100 Hz, 1 kHz, 10 kHz, and 100 kHz as a function of contact force. The mean conductivity values at all contact forces fall within the range of literature values, with a minimum of 0.15 S m^{-1} for the hyperhydration experiment and a maximum of 0.24 S m^{-1} at low contact force for the forward experiment. The standard deviation for all three experiments is high, at $\pm 14\%$. According to reports, the drift error is less than +2% for all measurements, suggesting that the high standard deviation is mostly due to differences between samples and the probe-sample contact rather than errors in the acquisition hardware sensitivity of the tissue in frequencies below 100 kHz [30], [260]. The observed variability in measurements can be attributed to inherent differences in tissue properties across samples. Worth noting is that the drift error, reflecting subtle shifts in readings over time, remains within a modest range of +2% between pre- and post-validation measurements for all experiments. This phenomenon, influenced by factors such as environmental conditions, aging components, or calibration variations, underscores the importance of vigilance in understanding and mitigating drift for sustained

Chapter 5: The Effect of Contact force on Conductivity Measurement of Ex-vivo Left Atrial Appendage of from 10 Hz to 100 kHz

measurement accuracy, particularly in contexts where tissue characteristics may vary.

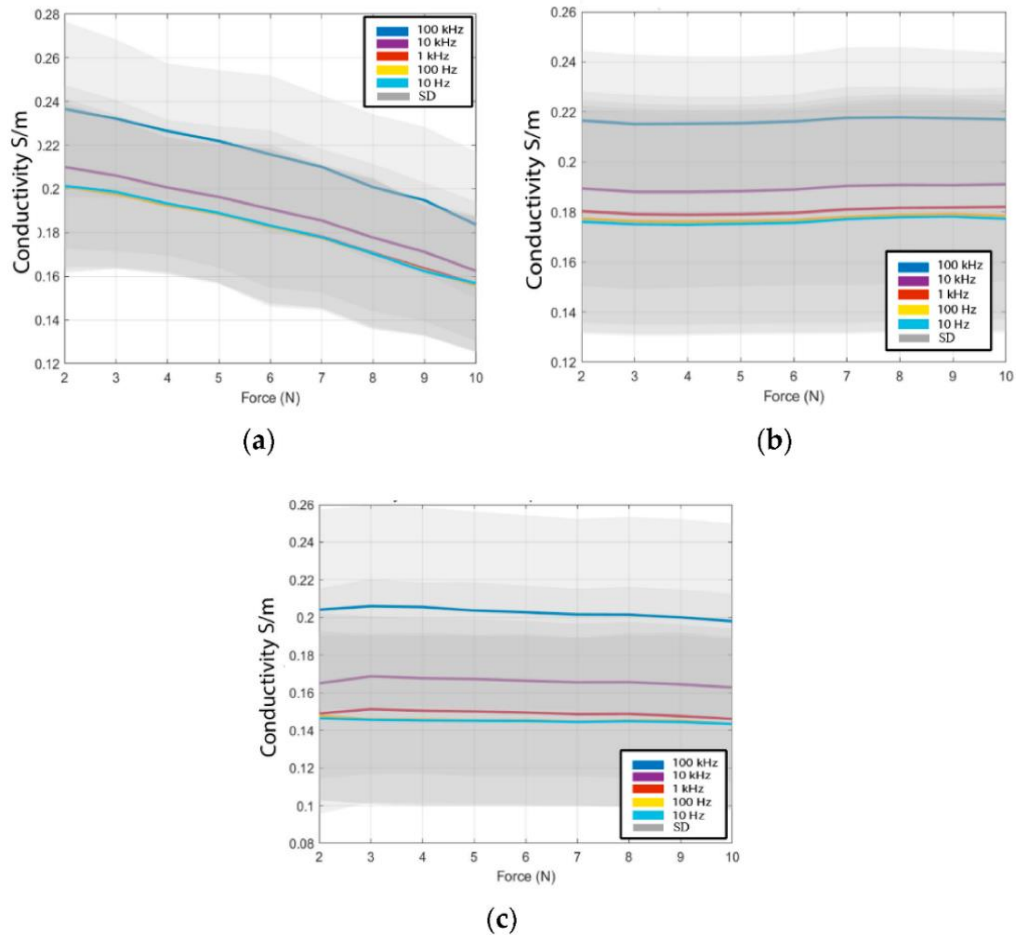


Figure 5.2 The average variation of the conductivity with the contact force for (a) forward experiment (b) reverse experiment (c) hyperhydration experiment

The mean conductivity obtained from the 10 LAA samples in the forward experiment, 5 samples in the reverse experiment, and 5 samples in the hyperhydration experiment are computed and subsequently compared. The Pearson coefficient (R) of the mean conductivity with the entire dataset is greater than 0.99 for all three experiments, indicating that the mean conductivity is a suitable representation of each set of samples.

Fig 5.4 displays a summary of all the average conductivities obtained from the forward, reverse, and hyperhydration experiments at the targeted frequencies of 10 Hz, 100 Hz, 1 kHz, 10 kHz, and 100 kHz.

Chapter 5: The Effect of Contact force on Conductivity Measurement of Ex-vivo Left Atrial Appendage of from 10 Hz to 100 kHz

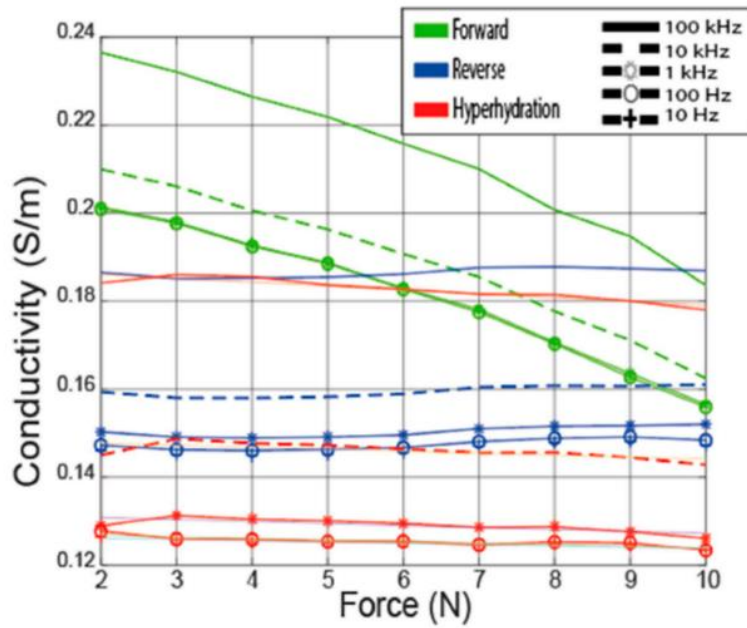


Figure 5. 3 The average variation of the conductivity with the force for the forward, reverse, and hyperhydration experiment at 10 Hz, 100 Hz, 1 kHz, 10 kHz, and 100 kHz

The slopes of the average conductivities obtained from the forward, reverse, and hyperhydration experiments are presented in Table 5.3. The observed conductivity change in the forward experiment was significantly greater than the changes observed in the reverse and hyperhydration experiments. To assess the statistical significance of this change, the statistical analysis outlined in the statistical analyses section was used. The p-values obtained from T1 and T2 were calculated and are displayed in Table 5.4. The results reveal that the p-values are <0.01, which suggests that the change observed in the forward experiment is highly significant when compared to the changes seen in the reverse and hyperhydration experiments.

Table 5.3 The measured conductivity changes by -21% and -2.5% due to the increase of force contact for the set of samples in the forward and the hyperhydration experiment, respectively, +1.3% change is seen in the conductivity in the samples in the reverse experiment

Experiment	y-intercept [S/m]	x-intercept [N]	Slope [S/(m×N)]	σ change (%)
Forward	0.239	0.187	-6.45×10^{-3}	-21%
Reverse	0.185	0.187	2.64×10^{-4}	1.3%
hyperhydration	0.186	0.179	-8.8×10^{-4}	-2.5%

Chapter 5: The Effect of Contact force on Conductivity Measurement of Ex-vivo Left Atrial Appendage of from 10 Hz to 100 kHz

Table 5. 4 p-Values from the two tests conducted to assess the significance of the variation between the forward experiment, the reverse, and the hyperhydration experiment

	Frequencies				
	10 Hz	100 Hz	1 kHz	10 kHz	100 kHz
p-value T1	0.23×10^{-3}	0.08×10^{-3}	0.088×10^{-3}	0.13×10^{-3}	0.25×10^{-3}
p-value T2	0.59×10^{-3}	0.19×10^{-3}	0.24×10^{-3}	0.34×10^{-3}	0.48×10^{-3}

The LAA conductivity in the forward experiment is found to decrease with an increasing contact force, with a slope of $-6.5 \times 10^{-3} \text{ S m}^{-1} \text{ N}^{-1}$. The average conductivity decreases due to the contact force increase during the forward experiment (-21%) is seen as similar to the cervix ([27] in Table 5.2), which is also identified as muscle tissue. This similarity is expected as both tissues exhibit decreasing fluid concentration with an increasing contact force.

In contrast, the conductivity changes due to the contact force in the reverse and hyperhydration experiments are observed to be small, with slopes of $2.64 \times 10^{-4} \text{ S m}^{-1} \text{ N}^{-1}$ and $-8.8 \times 10^{-4} \text{ S m}^{-1} \text{ N}^{-1}$, respectively. These results support the hypothesis that changes in fluid concentration in the measurement area are responsible for the conductivity changes due to the contact force.

Fig 5.5(a) shows the percentage variation in conductivities of each sample in the forward experiment from the initial force of 2 N to the final force of 10 N at frequencies ranging from 10 Hz to 100 kHz. The average variation of the conductivity between the ten samples is -21%.

Fig 5.5(b) displays the results of the reverse experiment from the initial force of 10 N to the final force of 2 N at the same frequencies. The conductivity is observed to have an average change of +1.3% due to the contact force from the five measured LAA samples.

Fig 5.5(c) shows the percentage variation in conductivities of the hyperhydrated LAA samples (with extracellular fluids partially removed) from the initial force of 2 N to the final force of 10 N at the same frequencies. The average conductivity change is -2.5% in the five clarified LAA samples.

Chapter 5: The Effect of Contact force on Conductivity Measurement of Ex-vivo Left Atrial Appendage of from 10 Hz to 100 kHz

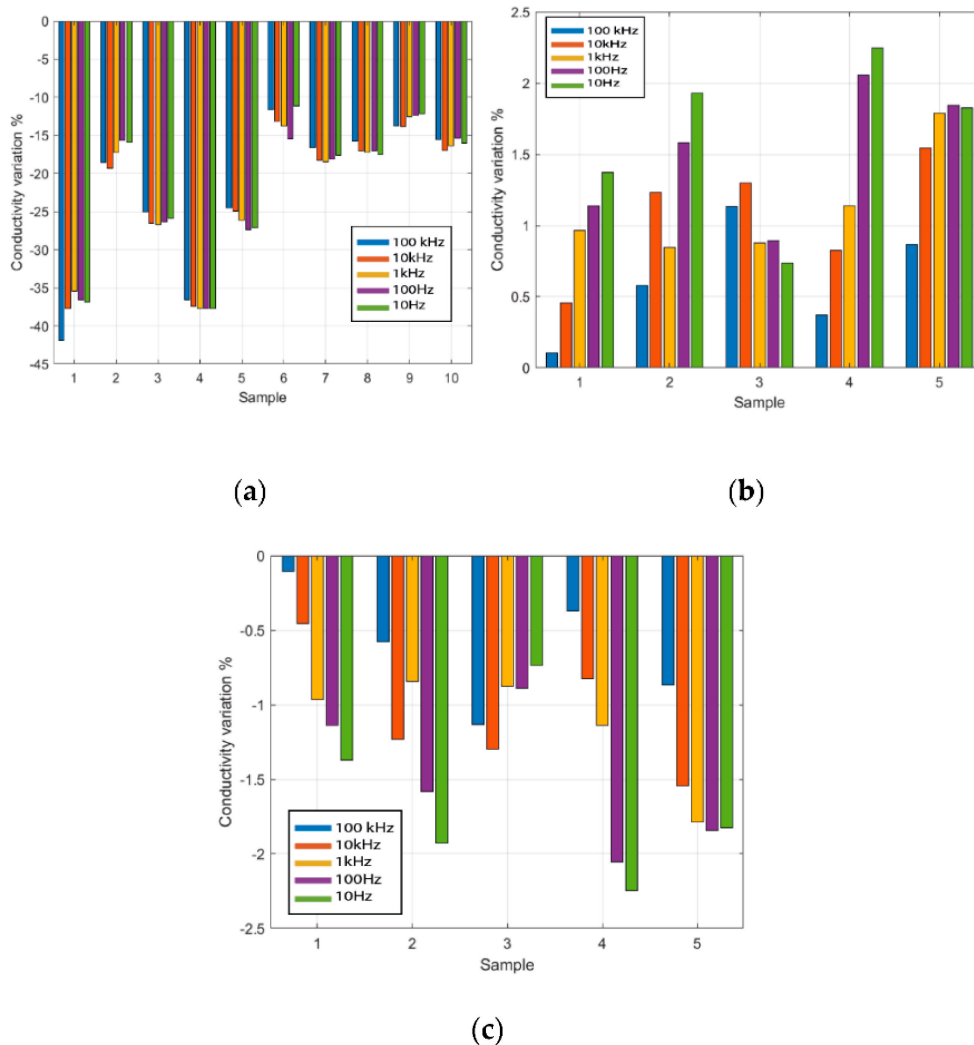


Figure 5.4 The percentage variation of the conductivity from the proposed experiment at 10 Hz, 100 Hz, 1 kHz, 10 kHz, and 100 kHz (a) Forward experiment with ten LAAs, contact force from 2 N to 10 N (b) Reverse experiment with five LAAs, contact force from 10 N to 1 N (c) the hyperhydration experiment with five LAAs, contact force from 1 N to 10 N

Interestingly, significant variability in the conductivity changes due to contact force is observed across each set of samples. In the forward experiment, for instance, the largest and smallest conductivity changes are observed in sample 1 and sample 6, with a -41% decrease and -12% decrease, respectively. The initial extracellular fluid concentration in the sample may play a role in the observed changes in conductivity due to contact force, although this is not always known in ex-vivo samples. Higher initial fluid concentrations would be expected to result in larger conductivity changes. Overall, the conductivity of the samples decreases as the contact force increases, and these changes are more substantial compared to the smaller changes observed in the reverse and hyperhydration experiments.

5.5 Conclusion

The study reported in chapter 5 on the measurement of conductivity in twenty ex-vivo bovine hearts, specifically in the LAA, over a frequency range between 10 Hz and 100 kHz. The contact force of the measurement probe on the samples was monitored and recorded. The measurements were conducted for nine distinct forces ranging from 2 N to 10 N. The obtained conductivity values ranged between 0.14 S m^{-1} and 0.24 S m^{-1} , which are consistent with values reported in the literature for cardiac muscle. An average decline of -21% in conductivity was observed as the contact force was raised from 2 N to 10 N.

In addition, this study investigated the potential causes of the observed conductivity changes. Prior research has suggested that changes in the concentration of extracellular fluids in the measurement region are a critical factor in alterations in measured conductivity that occur due to variations in contact force. To explore this hypothesis, the twenty samples were divided into three experiments: the forward experiment, reverse experiment, and hyperhydration experiment (forward experiment with processed LAA).

In comparison to the average decline of -21% in measured conductivity in the forward experiment, the reverse and hyperhydration experiments showed an average increase of +1.3% and a decrease of -2.5%, respectively, in conductivity. These results suggest that the high initial contact force in the reverse experiment decreased the extracellular fluid content in the measurement area, resulting in minimal changes in conductivity across the contact force range. Similarly, the considerably smaller change observed in the hyperhydration experiment indicates that the removal of ionic extracellular fluids during sample processing was partly responsible for the changes in conductivity due to the contact force observed in the forward experiment.

Furthermore, these findings indicate that the contact force of the probe in tissue conductivity measurements must be regulated, monitored, and recorded. A variety of methods exist for controlling contact force, but the setup used in this study is simple to use and precise. More complicated approaches, such as using a strain gauge or other sensors to regulate contact force, are also available.

Chapter 6: Effects of IRE on Conductivity of Hydrogel with Cells: IRE Implications for Atrial Fibrillation

6.1 Introduction

Validating the outcome of the IRE has been investigated through multiple feasibility studies [14], [24], [30], [66], and several detection techniques have been suggested to validate the success of the IRE [20], [66], [261]–[263]. These techniques include the use of dyes such as fluorophores or colour stains [264], functional molecules [265], the measurement of the efflux of biomolecules [266], impedance measurements [173], [267], voltage clamp techniques [268], and monitoring cell swelling [269]. The detection techniques can be broadly classified into three categories: the in-vivo and ex-vivo measurement techniques, and the situ measurement technique. The detection techniques such as dyes, functional molecules, the measurement of the efflux of biomolecules, voltage clamp and monitoring cell swelling are used for situ measurement. The impedance monitoring is more suitable for the in-vivo and ex-vivo [173], [267].

To monitor the IRE in-vivo during treatment, initial data and insights need to be gathered. Therefore, the ex-vivo scenarios are commonly proposed. However, in the case of IRE, ex-vivo tissue cannot be used due to the absence of physiological factors such as blood flow and neural input, which are vital in understanding cellular behaviour and responses to IRE. This emphasizes the importance of using living models for accurate research results [270].

Therefore, to monitor the IRE and investigate if the electrical properties of the LAA could be utilized to validate IRE in an LAA, a benchtop LAA model is introduced. The benchtop LAA model is a hydrogel-based model with myocardial cells to mimic in-vivo IRE in the LAA. This model will allow us to observe and analyse

living cell behaviour and physiological responses in a controlled environment, which will provide valuable insights for future in-vivo studies.

The monitoring of the outcome of IRE on the benchtop LAA model is done in the frequency range below 100 kHz, therefore the conductivity is going to be used as a metric. The monitoring involves measuring the conductivity at two different times, before and after ablation of the benchtop LAA model, and calculating the difference to assess the occurrence of the IRE treatment via cell death. While the focus is on the change in conductivity, there is still value in the absolute measurements taken at each time point.

Chapter 6 comprises a methodology section, which outlines the cell culturing techniques, hydrogel fabrication and embedding of cells. A hydrogel stress test and validation test are proposed to ensure the mechanical robustness and stability of the hydrogel during IRE and conductivity measurements. An IRE protocol, as well as its validation, is also described. Data acquisition of conductivity from the experimental setup used for data computation is presented. A statistical analysis is proposed to evaluate the significance of the conductivity change. The third section reports the pre- and post-IRE conductivity measurements and their significance. Chapter 6 concludes with a summary and discussion of future work.

6.2 Methodology

6.2.1 Cell culture

To simulate the LAA, hydrogel-embedded with human cardiomyocyte cells (AC16, Merck Life Science Limited, Vale Road, Arklow Y14EK18 Ireland) was proposed. The protocol presented in [66] was utilized for culturing the cells, and the cells were cultured in T75 flasks. The cardiomyocytes were cultured in Dulbecco's Modified Eagle's Medium/Ham's Nutrient Mixture F-12 (DMEM/F-12) (Sigma Aldrich), supplemented with 2 mM L-glutamine (Sigma Aldrich), 1% penicillin/streptomycin (Sigma Aldrich), and 12.5% fetal bovine serum (FBS) (Gibco, Dublin, Ireland). The cells were passaged (split into new culture vessels) every 2-3 days with trypsin-EDTA 0.025% (Sigma-Aldrich, Arklow, Ireland) for maintenance. For the cell adherence experiment, 6 well plates were coated with 0.1 (mg mL⁻¹) of gelatin, and cardiomyocytes were seeded at a cell density of 7.5×10^5 cells per well, allowing for complete confluence overnight.

6.2.2 Hydrogel

The hydrogel utilized in this investigation was prepared according to the following protocol. The hydrogel was composed of lyophilized HA-TA and phosphate-buffered saline (PBS) (Sigma Aldrich). To prepare the hydrogel, lyophilized HA-TA was added to PBS at a concentration of 15 mg mL^{-1} and rehydrated overnight on a rotational rocker at 4°C . The polymer solution was separated into two equal volumes, with the first half mixed with Horseradish Peroxidase (HRP) and the cardiomyocyte cells. The second half of the solution was mixed with $0.1\% \text{ H}_2\text{O}_2$ to match the HRP solution's volume. Equal volumes of the HRP and H_2O_2 polymer solutions were drawn into separate Luer lock syringes, which were attached to an extension mixer that synchronously expelled the two solutions into a custom cylinder mould positioned inside a 6-well plate. The custom cylinder mould had dimensions of 24 mm in diameter by 2 mm in height and could hold a volume of 1 mL of the mixed HRP and H_2O_2 polymer solutions. Following the expulsion of the HRP and H_2O_2 polymer solutions into the mould, the hydrogel was formed almost instantaneously. Culture media was added until complete coverage of the gel, which was then placed in an incubator at 37°C for 24 hours to ensure full jellification of the hydrogel. The final cell concentration in each gel was 2 million. The cardiomyocyte cell had an average volume of $33726 \mu\text{m}^3$, as reported in [66], [271], representing 3% of the total volume of the samples under investigation (hydrogel with 2 million cells).

The hydrogel embedded cells can provide a useful in-vivo model for studying cell behaviour and interactions, but the hydrogel can introduce limitations [272]. Hydrogels have limitations in mimicking real tissue mechanical properties due to their softness, uniformity, and lack of dynamic properties [273]. Real tissues are heterogeneous in mechanical properties and contain significantly more cells than can be embedded in the current hydrogel, constantly undergoing stresses and strains, which hydrogels cannot replicate effectively [272]. However, hydrogels remain a valuable tool for studying many aspects that occur in-vivo scenarios. The total samples used in the study are 16 hydrogels, 6 for validation purposes and 10 for monitoring the conductivity change pre- and post-IRE.

6.2.3 Conductivity acquisition

The electrical conductivity acquisition set-up utilized is similar to the method used in chapters 4 and 5. The conductivity was measured using the small collinear probe connected with the PGSTAT204 (Autolab, Kanaalweg Den Haag, The Netherlands) in Galvanostat mode with a fixed current of 100 μ A at ambient temperature with Nova 2.1 software and a weighing scale (Kern Weighing Scale, METTLER TOLEDO, Columbus, OH, USA). The targeted frequencies for conductivity measurement are 10 Hz to 100 kHz (10 points per decay). Similarly, to chapter 4 and chapter 5, the conductivity acquired from 0.1 Hz to 10 kHz for this experiment were observed to be unreliable as the data is very noisy and the conductivity cannot be separated from the noise.

6.2.4 Statistical analysis

A paired t-test was used to compare the conductivity change between the pre-treatment hydrogel with living cells and the post-treatment hydrogel with dead cells in the treatment area. The paired t-test is appropriate when you have two sets of related or paired data, such as pre-and post-measurements on the same sample of individuals. It is specifically designed to compare the means of two paired samples while taking into account the correlation between them [256]–[259]. The paired t-test reduces the variability in the data that arise from individual differences between subjects [256]–[259]. Therefore, if you have paired data, the paired t-test is a more appropriate statistical test than an unpaired t-test [259].

The null hypothesis was that there is no significant difference between the measured conductivity variations of the pre-and post-treatment stages. The T-test was performed under the hypothesis at a 5% significance level, and the resulting p-value was used to measure the probability of obtaining the observed results assuming that the null hypothesis is true. A lower p-value ($p < 0.01$ indicating strong evidence against the null hypothesis) would indicate greater statistical significance of the observed difference. The T-test was conducted for each frequency as the variation of conductivity in frequency dependence. References [256]–[259] were consulted for guidance on statistical analysis.

6.2.5 Hydrogel testing

The hydrogel plays a focal role in the experiment as it serves as the primary support structure for the cells, and any alterations made to it can significantly impact the final results. As such, it is imperative to evaluate the stability of the hydrogel via stress and validation tests. The stress test seeks to identify the point at which the hydrogel breaks due to probe contact, while the validation test assesses whether any changes occur to the hydrogel due to treatment in the absence of cells. These tests aim to ensure the stability of the hydrogel and minimize errors caused by probe contact force and potential formula changes.

6.2.6 Hydrogel validation stress test

The stress test seeks to identify the point at which the hydrogel breaks due to probe contact. The stress test commences with using the forward experiment from chapter 5. A starting contact force of 1 N to ensure contact, then gradually increasing by +1 N until the hydrogel breaks. The hydrogel is defined with a break when a fracture is observed in the hydrogel. The contact force is measured the same way as in chapter 5. This test assesses the robustness of the hydrogel during IRE and is conducted with cells present. Examples of a damaged hydrogel are shown in Fig 6.1.

Fig 6.1 displays the first sample of hydrogel after each probe contact force increment, indicating that the hydrogel begins to exhibit damage at 4 N, as seen by the probe imprint on the surface. Higher contact forces result in more pronounced indentations on the hydrogel. At 8 N, the hydrogel breaks. Three different hydrogel samples underwent the stress test, with the second and third samples exhibiting major damage (hydrogel breaks) at 9 N and 9 N, respectively, after showing minimal damage (indents) at 4 N. The stress test results demonstrate that probe contact can affect the hydrogel, necessitating the use of adequate contact force to ensure contact without introducing damage to the hydrogel. During IRE and conductivity measurement, probes are placed atop the hydrogel with a contact force of 2 N to guarantee probe-hydrogel contact and prevent hydrogel damage.

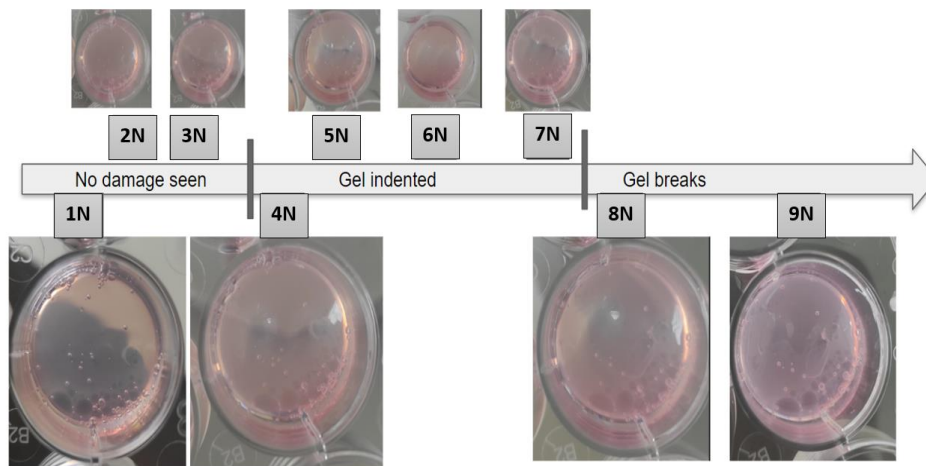


Figure 6. 1 The figure shows the effects of probe contact force on the surface of the hydrogel during the stress test. The photos illustrate that the hydrogel starts exhibiting damage at 4N, with more pronounced indentations at higher contact forces. The first sample of hydrogel shown in this figure is breaks at 8N

6.2.7 Hydrogel validation test

The hydrogel validation test is designed to evaluate the change in conductivity of a hydrogel resulting from IRE. The primary objective of this validation test is to establish a baseline conductivity of the hydrogel pre- and post-electroporating, to verify that any observed changes in conductivity after electroporating when introducing the cells are solely due to the presence of cells. To perform the test, the hydrogel is prepared without cells one day prior to the experiment. The conductivity of the hydrogel is then measured before IRE, after which the hydrogel is subjected to the IRE protocol described in the IRE protocol section. The validation test is done on three hydrogel samples. Finally, the conductivity of the hydrogel post-IRE is measured. The hydrogel validation test is performed on three separate hydrogel samples without cells.

Following the IRE, the electrodes used for the treatment leave visible marks on the surface of all three samples, which were not present prior to treatment. The marks on the hydrogel and the probe used for IRE are seen in Fig 6.2. A comparison of pre-and post-IRE conductivity measurements with standard deviation is seen in Fig 6.3. Fig 6.3 indicates that the conductivity change in all three samples was insignificant (T-test with p value 9.67×10^{-13}). This observation suggests that the IRE

did not have a significant effect on the conductivity of the hydrogel, thus demonstrating the stability of the conductivity of the hydrogel in response to IRE.

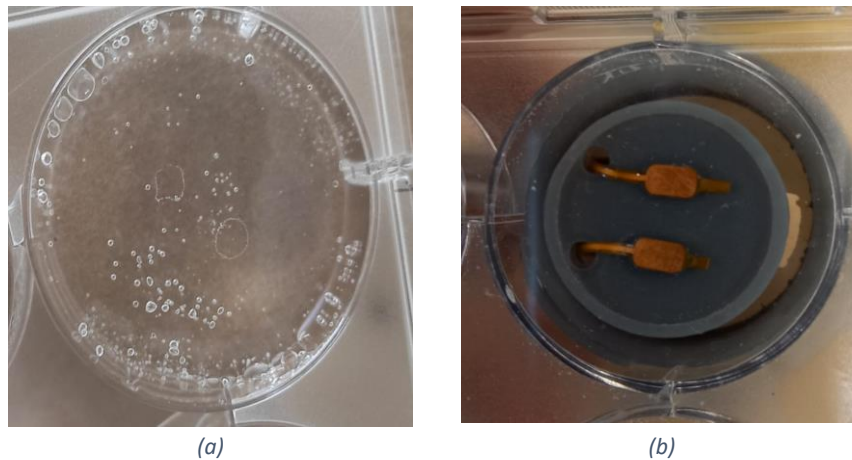


Figure 6. 2 shows visible marks on the surface of all three hydrogel samples following IRE. These marks are from the electrodes used for the treatment and were not present prior to treatment. (a) shows the marks on sample 1 (b) shows the probe used for IRE

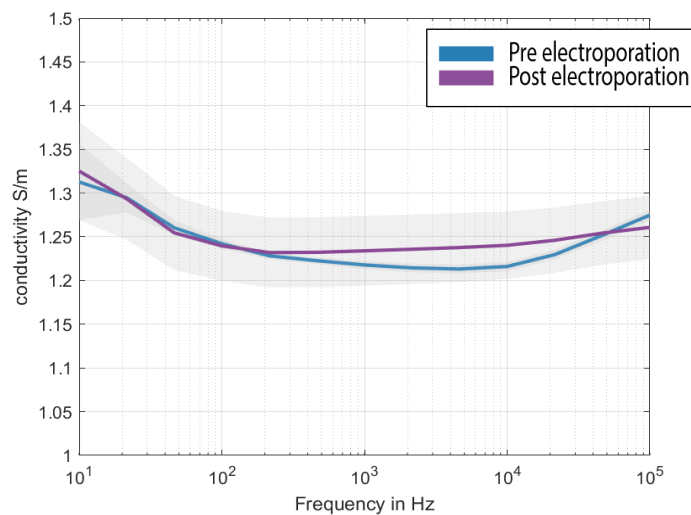


Figure 6. 3 compares pre- and post-IRE conductivity measurements with the standard deviation of the hydrogel. The results show that there was no significant change in conductivity between pre- and post-IRE

6.2.8 Ablation protocol

The IRE pulse parameters have been shown to have a direct correlation with the treatment outcome, including cell death, treatment zone, treatment depth, and more [15], [30], [66], [274]. To ensure successful treatment, an established protocol that has been proven to be effective with myocardial cells with a minimum threshold of 70% cell death and a minimum of 500 V cm^{-1} is followed [66]. The IRE setup consists of a two-electrode probe connected to a signal generator, as shown in Fig 6.5. The IRE probe is composed of two $50 \text{ }\mu\text{m}$ thick copper electrodes with

Chapter 6: Effects of IRE on Conductivity of Hydrogel with Cells: IRE Implications for Atrial fibrillation

dimensions of 3×5 mm and a 5 mm gap as seen in Fig 6.3 (b). The IRE is delivered using a biphasic 60 ms on-time waveform consisting of 100 μ s negative followed by 100 μ s positive phase with electric field strengths of 1000 V cm^{-1} through an ECM 830 square wave IRE system (Massachusetts, United States). To validate the treatment, the treatment was performed on three hydrogel samples with cells, and the EVOS M7000 Imaging System was used to 3D scan the hydrogel. The imaging system provides an image of the treatment zone, with green indicating living cells in the hydrogel and red indicating the treated area with dead cells. The ablation parameters, including area, perimeter, and diameter, match the expected results from [66]. The resulting images from the three hydrogel samples after treatment are shown in Fig 6.6.

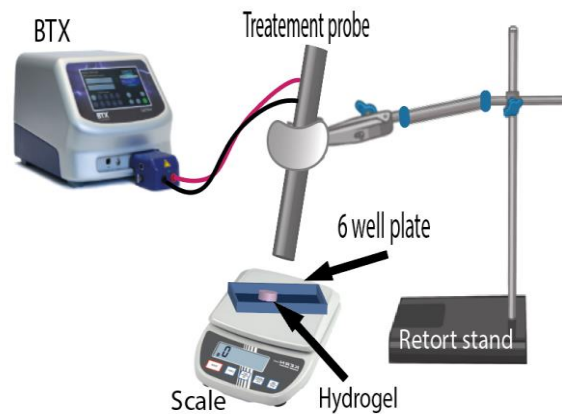


Figure 6. 4 Schematic diagram of the IRE setup, consisting of a two-electrode probe connected to a signal generator. The probe is composed of two $50 \mu\text{m}$ thick copper electrodes with dimensions of 3×5 mm and a 5 mm gap

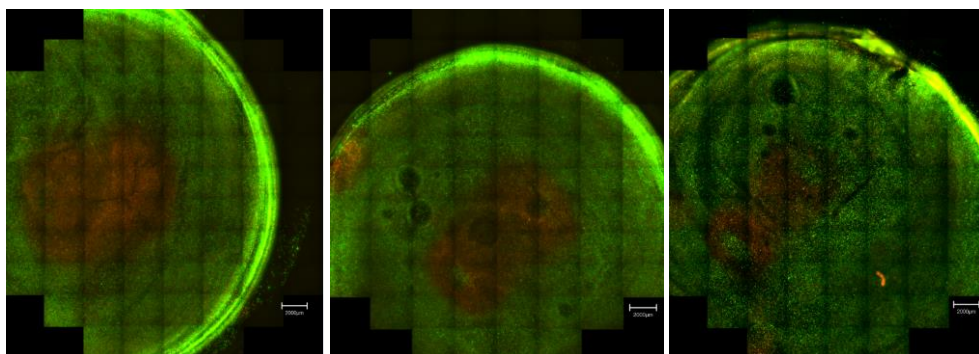


Figure 6. 5 3D scanned images of three hydrogel samples with cells after IRE treatment, as visualized by the EVOS M7000 Imaging System. The green area indicates living cells, and the red area indicates dead cells in the treated zone. The ablation parameters, including area, perimeter, and diameter, match the expected results from a successful treatment protocol

6.3 Results and Discussion

Before monitoring the outcome of IRE on the benchtop LAA model in the frequency range below 100 kHz and assessing whether the conductivity could be utilized as a means of validating IRE. The methodology of chapter 6 examined the effect of IRE on the conductivity of hydrogels with and without cells, and the impact of cell presence on the conductivity of the hydrogel.

The results show that the presence of cells influenced the conductivity of the hydrogel, whereas IRE had no significant effect on the conductivity. Upon introducing cells to the hydrogel, a noticeable decrease in conductivity occurred, dropping from an average of 1.25 S m^{-1} to 0.65 S m^{-1} . However, it remains inconclusive whether the observed drop in conductivity directly correlates with the presence of cells. The hydrogel with cells shown in Fig 6.6(a) is seen with a pink tint, indicating the potential of cell media absorption by the hydrogel. The hydrogel with and without cells are shown in Fig 6.6(a).

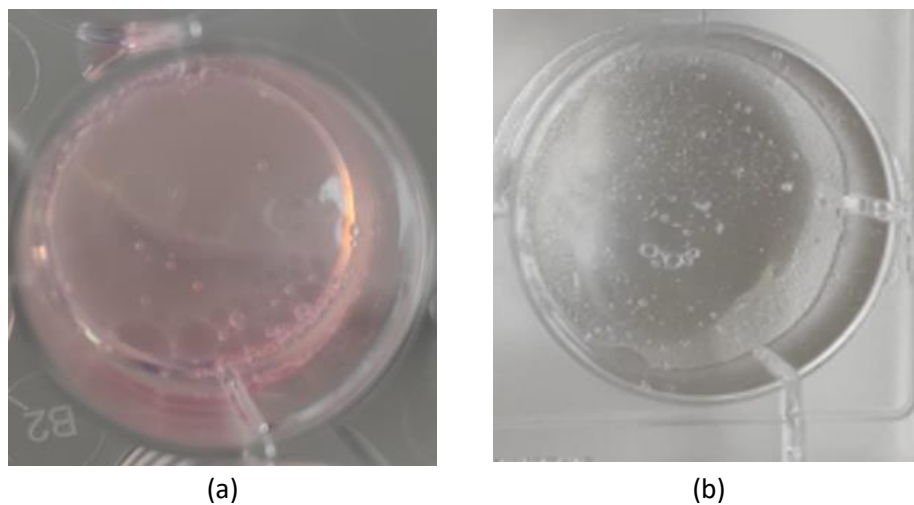


Figure 6. 6 hydrogel sample with and without cells (a) hydrogel with cells the pink tint is introduced by the cells and cell media (b) hydrogel without cells

Fig 6.7 presents the conductivity measurements of hydrogel samples with cells, taken before and after IRE, in the frequency range below 100 kHz. These measurements were conducted to monitor the effects of IRE on the benchtop LAA model and evaluate the potential utility of conductivity as a validation method. A total of ten samples were analysed, and the conductivity data was recorded within the frequency range of 10 Hz to 100 kHz.

The mean conductivity of the hydrogel with cells before treatment is 0.65 S m^{-1} , whereas, after treatment, it is 0.79 S m^{-1} , showing an average change of 17% among ten samples. To examine the statistical significance of this change, a T-test was performed, yielding a p-value of 8.59×10^{-12} , below the threshold. This result indicates that the change in the conductivity of the hydrogel before and after treatment is statistically significant.

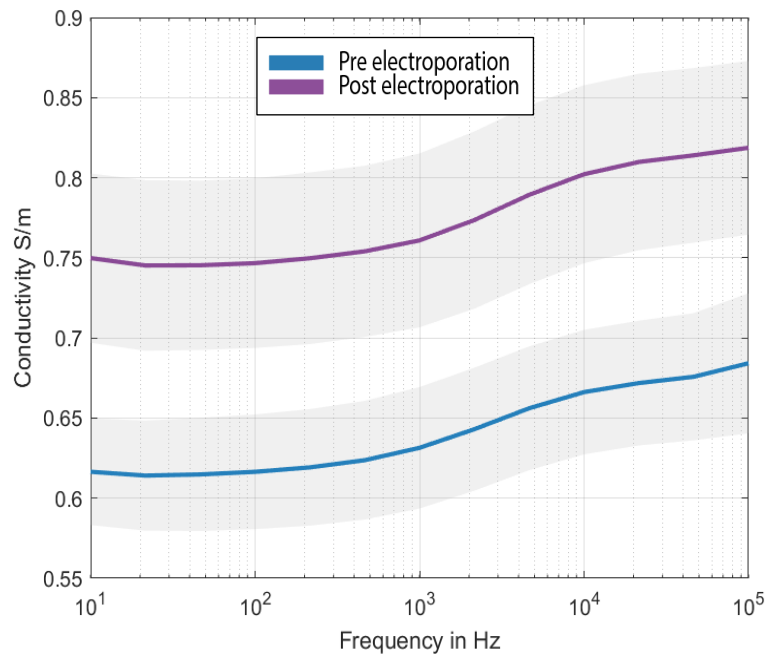


Figure 6. 7 shows the comparison of the mean conductivity with the standard deviation of the hydrogel with cells before and after IRE. The graph displays the conductivity measurements from ten different samples at various frequencies ranging from 10 Hz to 100 kHz

The observed change in conductivity of the hydrogel pre- and post-treatment suggests that the treatment alters the conductivity of the sample, with cell death being a contributing factor. The goal of IRE is to disrupt the cellular structure, such as the cell membrane, leading to the release of cytoplasm, which is a conductive liquid [15], [19], [22], [30], [66], [274]. This release of cytoplasm increases the conductivity of the treatment area. Despite cells accounting for only 3% of the treatment area, a significant change in conductivity is observed after IRE, partially due to the low measuring frequency (below 100 kHz) used in this study. Measurements below 100 kHz can be challenging, but their sensitivity to electrical stimulation increases as the conductivity is affected by the cellular level of the tissue. Electrical currents below 100 kHz primarily flow in the extracellular spaces, with the charges flowing around cells rather than penetrating the cell membrane,

emphasizing the importance of choosing the appropriate measuring frequency. Additionally, if conductivity changes can be seen in a scenario where cells represent only 3% of the total sample, the results could be extrapolated in in-vivo LAA samples, where approximately 70-80% of the tissue volume is made up of cardiomyocytes [275], [276].

6.4 Conclusion

Based on the results of chapter 6, the conductivity of the hydrogel with cells is affected by IRE, and the main contributor to the change in conductivity is the release of conductive liquid from dead cells. The significant change in conductivity pre- and post-treatment was confirmed through statistical analysis using a T-test. In the case of hydrogel model the expectation for a significant change is typically based on the experimental design as the hydrogel is adapted the targeted cell and the anticipated effects of the treatment on conductivity cannot be hypothesized.

Furthermore, this study highlighted the importance of the choice of frequency when measuring conductivity. This finding suggests that the conductivity measurement is highly sensitive to the cellular level of the tissue. However, some limitations of this study include the lack of investigation into the relationship between the conductivity change and the number of dead cells in the hydrogel. Additionally, the study only examined the conductivity change in a scenario where cells represent 3% of the total sample, and it remains unknown how this result would be affected in tissues where cells represent a higher percentage.

Future work could involve investigating the relationship between conductivity change and dead cell concentration in the hydrogel, as well as examining the effects of IRE on tissues where cells represent a higher percentage of the total sample. These studies could lead to a better understanding of the impact of pulse field IRE treatment on tissue conductivity.

Chapter 7: Conclusions and Future Work

Chapter 7 provides a summary of the key conclusions and findings of this thesis. The motivation of this work, the principal findings and the overall conclusions are presented in Section 7.1. Furthermore, the potential for future work to build upon and improve the results of this thesis is discussed in Section 7.2.

7.1 Summary of the main conclusions

AF and its consequences are a growing challenge facing health services with complex long-term effects for patients. In addition to current treatments, IRE is an emerging potential treatment for AF with promising preclinical results from early studies. However, there is a need to better understand the electrical conductivity of biological tissues at low frequencies used by IRE and specifically the LAA which is a common target for IRE treatment. Improved knowledge of the conductivity can help refine and improve the electromagnetic simulations used to develop and refine IRE treatments for AF.

Despite several studies in the literature measuring the conductivity of heart tissues and muscle tissues, it is difficult to compare studies due to variations in data acquisition methods in terms of probe typologies, electrode sizes, probe contact force monitoring and other acquisition and reporting differences. Preliminary studies in the literature and related fields suggest that these factors can impact the measurement results and the accuracy and repeatability of the conductivity measurements [138], [187], [219], [230].

Chapter 3 investigates the impact of probe typology and electrode size on the accuracy and repeatability of conductivity measurements of biological tissues. Six representative probe designs including polar probes and collinear probes were examined in liquid phantoms for repeatability and accuracy. In all cases, results suggest that all designs enabled repeatable measurements due to the consistent and low coefficient of variation and standard deviation measured. However, when comparing the measured conductivity values of the same phantoms, the conductivity measurements acquired varied depending on the probes across the range of 10% to 51%. These results suggest that probe typology and electrode size

can influence the accuracy of the measured electrical conductivity. These findings suggest that the probe design should be adapted and customised to the tissue under study to maximise the accuracy of the acquired conductivity data. In the context of the LAA, it is observed that a probe fitting the size of the LAA, with electrodes smaller than 6mm and larger than 1mm in radius, and adopting a collinear configuration, yields superior results in terms of accuracy and repeatability.

Similarly, these findings suggest that differences in the probe design may help explain some of the variance in reported conductivity values in the literature.

Chapter 4 investigates the average conductivity of the LAA obtained from ten bovine samples between 0.1 Hz and 100 kHz. These values were acquired using a small collinear probe detailed in chapter 3. This probe achieved the most accurate and consistent performance between 0.1 Hz and 100 kHz (10% accuracy, $R > 0.99$, $CV < 1\%$). The mean conductivity of the LAA acquired from the ten samples was found to be 2.5 mS cm^{-1} with a SD of 0.24 mS cm^{-1} . This value is broadly consistent with the literature values for the conductivity of cardiac tissues. Finally, the measurement protocol and probe presented are suitable for the conductivity measurement of biological tissues at these frequencies.

Nevertheless, there are certain challenges associated with the interpretation of the experimental results of conductivity. Firstly, these samples are excised, and the electrical properties may change due to excision and subsequent dehydration. Measurements are performed under strict time limits to minimize these effects; however, sample handling can still potentially affect the conductivity values. Secondly, tissue can vary substantially from sample to sample, even with defined anatomical features such as the LAA. The size and measurement area can vary between samples, which may also affect how the hydration and temperature change during measurement. Thirdly, the studies in this thesis contain 10 ex-vivo bovine samples, which may not fully represent in-vivo human conditions.

The measurement protocol in chapter 4 includes a method to measure and report the probe contact force used during measurement. However, in many studies in the literature, the contact force is either not measured or not controlled. Chapter 5 examines the potential impact of contact force on acquired conductivity measurements. The conductivity of LAA samples was measured in three different

sets of experiments to consider the effect of contact force on the conductivity measurement: firstly, with monotonically increasing contact force, secondly, with increasing then decreasing force, and thirdly where the tissues have been first hyperhydrated to reduce the concentration of extracellular fluids. Measurements were acquired at nine distinct contact forces from 2 N to 10 N. The measured conductivity for all samples ranged between 0.14 S m^{-1} and 0.24 S m^{-1} , which are consistent with literature values for cardiac muscle and the results in chapter 3. On average, the measured conductivity of the sample changed as the contact force increased monotonically (forward experiment) by on average -21% in conductivity. However, when the force was decreased in the reverse experiment or the tissue had been preprocessed to alter the extracellular fluid concentration in the hyperhydration experiment, the average change in conductivity was +1.3% and -2.5%, respectively. These findings suggest that the high initial contact force in the reverse experiment decreased the extracellular fluid concentration in the measurement area, resulting in minimal changes in conductivity across the contact force range. Similarly, the considerably smaller change observed in the hyperhydration experiment indicates that the removal of ionic extracellular fluids during sample processing was partly responsible for the changes in conductivity due to the contact force observed in the forward experiment. Furthermore, these results support the regulation, monitoring and recording of the contact force of the probe in tissue conductivity measurements.

The study in chapter 6 investigates the potential use of the conductivity of LAA tissue as an indicator of the success of the IER treatment. A benchtop LAA model consisting of a hydrogel embedded with myocardial cells was used to model living LAA tissue. The electrical conductivity was measured before and after IRE treatment and the extent of the treated area was measured using EVOS M7000 Imaging System. The electrical conductivity of the model was found to change significantly due to the IRE treatment, likely due to the increasing concentration of ions in the extracellular fluid after IRE. These results suggest that conductivity may be suitable for assessing the success of IRE treatments.

Future studies could focus on investigating the correlation between conductivity change and dead cell concentration in the hydrogel, and on examining the effects of pulse field IRE treatment on tissues with higher percentages of cells

in the sample. Such studies could potentially contribute to a better understanding of the impact of pulse field IRE treatment on tissue conductivity and could have implications for the development of new therapies for various medical conditions.

7.2 Future work

This thesis presents accurate and reliable measurements of the conductivity of the LAA below 100 kHz and highlight adapting the proposed protocol for measuring the conductivity of different tissues at this frequency range. Furthermore, the impact of contact force on the measured conductivity and the change in conductivity due to IRE treatments. This work identifies several areas where the results could be extended or improved and highlights a number of questions.

In terms of the conductivity of the LAA, future studies could explore the relationship between LAA anatomy and conductivity, investigating whether adjusting the position or orientation of the probe could reduce variability in conductivity measurements. Additionally, the effect of animal source, tissue preparation and handling procedures on conductivity measurements could be investigated to further optimize the measurement protocol.

In terms of the measurement set-up, measuring and maintaining contact force over the duration of the measurement can be challenging as the semi-solid biological samples can deform. Methods for controlling the contact force and the sample shape using other sensors such as strain gauges or other sample holders should be considered and investigated. In terms of measurement acquisition, the injected current may impact the measured conductivity due to polarisation at the electrodes and other effects. Characterisation of the repeatability and accuracy with respect to measurement current would improve the proposed protocol.

To improve the generalisation of the results, the proposed protocol should be used to acquire conductivity data of other excised tissue from a range of representative tissues to better understand the ranges and limits of the conductivity of these tissues. These studies could be supported by in-vivo measurements to improve the overall understanding of the conductivity of the LAA. Conducting in-vivo measurements would enhance the overall comprehension of the conductivity of the LAA within a more realistic and dynamic physiological

scenario. In-vivo data would provide insights into how the LAA behaves in a living organism, accounting for factors such as blood flow, tissue perfusion, and other in-situ conditions. This additional dimension of information would contribute to a more comprehensive understanding of the electrical conductivity properties of the LAA and its implications in physiological contexts. Similarly, the model used in chapter 6 could be refined and enhanced to include a higher proportion of cardiac cells to minimise the confounding effect of the hydrogel.

Finally, based on the proposed protocol, further studies should carefully consider the acquisition protocol to improve the reliability, accuracy, repeatability, and reproducibility of the conductivity results in the literature.

References

- [1] L. Staerk, J. A. Sherer, D. Ko, E. J. Benjamin, and R. H. Helm, "Atrial Fibrillation: Epidemiology, Pathophysiology, Clinical Outcomes," *Circulation Research*, vol. 120, no. 9. Lippincott Williams and Wilkins, pp. 1501–1517, . 28, 2017. doi: 10.1161/CIRCRESAHA.117.309732.
- [2] Y. Guo, G. Y. H. Lip, and S. Apostolakis, "Inflammation in atrial fibrillation," *J Am Coll Cardiol*, vol. 60, no. 22, pp. 2263–2270, 2012, doi: 10.1016/j.jacc.2012.04.063.
- [3] R. N. Doshi, "The state of atrial fibrillation in 2020," *Journal of Innovations in Cardiac Rhythm Management*, vol. 12, no. 1. MediaSphere Medical LLC, pp. 4350–4353, . 01, 2021. doi: 10.19102/ICRM.2021.120105.
- [4] J. Xu, J. G. Y. Luc, and K. Phan, "Atrial fibrillation: Review of current treatment strategies," *J Thorac Dis*, vol. 8, no. 9, pp. E886–E900, 2016, doi: 10.21037/jtd.2016.09.13.
- [5] B. P. Krijthe *et al.*, "Projections on the number of individuals with atrial fibrillation in the European Union, from 2000 to 2060," *Eur Heart J*, vol. 34, no. 35, pp. 2746–2751, 2013, doi: 10.1093/eurheartj/eh280.
- [6] N. J. Patel *et al.*, "Contemporary trends of hospitalization for atrial fibrillation in the United States, 2000 through 2010 implications for healthcare planning," *Circulation*, vol. 129, no. 23, pp. 2371–2379, 2014, doi: 10.1161/CIRCULATIONAHA.114.008201.
- [7] G. Lippi, F. Sanchis-Gomar, and G. Cervellin, "Global epidemiology of atrial fibrillation: An increasing epidemic and public health challenge," *International Journal of Stroke*, vol. 16, no. 2, pp. 217–221, . 2020, doi: 10.1177/1747493019897870.
- [8] C. A. Morillo, A. Banerjee, P. Perel, D. Wood, and X. Jouven, "Atrial fibrillation: The current epidemic," *Journal of Geriatric Cardiology*, vol. 14, no. 3. Science Press, pp. 195–203, 2017. doi: 10.11909/j.issn.1671-5411.2017.03.011.
- [9] S. Saygi, "Atrial fibrillation and the role of LAA in pathophysiology and clinical outcomes?," *J Atr Fibrillation*, vol. 5, no. 3, pp. 153–160, 2012, doi: 10.4022/jafib.480.
- [10] M. L. Yarmush, A. Golberg, G. Serša, T. Kotnik, and D. Miklavčič, "Electroporation-based technologies for medicine: Principles, applications, and challenges," *Annu Rev Biomed Eng*, vol. 16, pp. 295–320, 2014, doi: 10.1146/annurev-bioeng-071813-104622.
- [11] I. P. Temple, S. Inada, H. Dobrzynski, and M. R. Boyett, "Connexins and the atrioventricular node," *Heart Rhythm*, vol. 10, no. 2, pp. 297–304, . 2013, doi: 10.1016/j.hrthm.2012.10.020.
- [12] A. Brandes *et al.*, "Cardioversion of atrial fibrillation and atrial flutter revisited: Current evidence and practical guidance for a common procedure," *Europace*, vol. 22, no. 8. Oxford University Press, pp. 1149–1161, Aug. 01, 2020. doi: 10.1093/europace/euaa057.
- [13] K.-H. Kim, "Modern treatment of atrial fibrillation," *Korean J Thorac Cardiovasc Surg*, vol. 47, no. 6, pp. 499–503, 2014, doi: 10.5090/kjtcs.2014.47.6.499.
- [14] A. Wojtaszczyk, G. Caluori, M. Pešl, K. Melajova, and Z. Stárek, "Irreversible electroporation ablation for atrial fibrillation," *J Cardiovasc Electrophysiol*, vol. 29, no. 4, pp. 643–651, 2018, doi: 10.1111/jce.13454.
- [15] G. Narayanan, "Irreversible Electroporation," *Semin Intervent Radiol*, vol. 32, no. 4, pp. 349–355, 2015, doi: 10.1055/s-0035-1564706.
- [16] K. N. Aycock and R. V. Davalos, "Irreversible Electroporation: Background, Theory, and Review of Recent Developments in Clinical Oncology," *Bioelectricity*, vol. 1, no. 4, pp. 214–234, 2019, doi: 10.1089/bioe.2019.0029.
- [17] A. Di Monaco *et al.*, "Pulsed Field Ablation to Treat Atrial Fibrillation: A Review of the Literature," *Journal of Cardiovascular Development and Disease*, vol. 9, no. 4. MDPI, 01, 2022. doi: 10.3390/jcdd9040094.
- [18] D. R. Shah, S. Green, A. Elliot, J. P. McGahan, and V. P. Khatri, "Current oncologic applications of radiofrequency ablation therapies," *World J Gastrointest Oncol*, vol. 5, no. 4, pp. 71–80, 2013, doi: 10.4251/wjgo.v5.i4.71.
- [19] J. C. Weaver and Y. A. Chizmadzhev, "Theory of electroporation: A review," *Bioelectrochemistry and Bioenergetics*, 1996, doi: 10.1016/S0302-4598(96)05062-3.

References

- [20] T. Kotnik, W. Frey, M. Sack, S. Haberl Meglič, M. Peterka, and D. Miklavčič, "Electroporation-based applications in biotechnology," *Trends Biotechnol*, vol. 33, no. 8, pp. 480–488, 2015, doi: <https://doi.org/10.1016/j.tibtech.2015.06.002>.
- [21] J. C. Weaver, K. C. Smith, A. T. Esser, R. S. Son, and T. R. Gowrishankar, "A brief overview of electroporation pulse strength-duration space: A region where additional intracellular effects are expected," *Bioelectrochemistry*, vol. 87, pp. 236–243, 2012, doi: [10.1016/j.bioelechem.2012.02.007](https://doi.org/10.1016/j.bioelechem.2012.02.007).
- [22] P. G. K. Wagstaff *et al.*, "Irreversible electroporation: State of the art," *Onco Targets Ther*, vol. 9, pp. 2437–2446, 2016, doi: [10.2147/OTT.S88086](https://doi.org/10.2147/OTT.S88086).
- [23] B. McDermott *et al.*, "Stable tissue-mimicking materials and an anatomically realistic, adjustable head phantom for electrical impedance tomography," *Biomed Phys Eng Express*, vol. 4, no. 1, 2018, doi: [10.1088/2057-1976/aa922d](https://doi.org/10.1088/2057-1976/aa922d).
- [24] T. Y. Tsong, "Electroporation of cell membranes," *Biophys J*. 1991 Aug;60(2):297-306., pp. 297–306, 1991.
- [25] R. Matsumura, H. Yamamoto, T. Hayakawa, S. Katsurabayashi, M. Niwano, and A. Hirano-Iwata, "Dependence and Homeostasis of Membrane Impedance on Cell Morphology in Cultured Hippocampal Neurons," *Sci Rep*, vol. 8, no. 1, pp. 1–10, 2018, doi: [10.1038/s41598-018-28232-0](https://doi.org/10.1038/s41598-018-28232-0).
- [26] N. Ištuk, A. La Gioia, H. Benchakroun, and A. Lowery, "Measurement of Electrical Conductivity of Human Blood at Frequencies Below 100 kHz with Four-electrode Probe Method," *URSI GASS 2021*, no. Galway, Ireland, March, 2021.
- [27] R. P. Jokhi, V. V. Ghule, B. H. Brown, and D. O. C. Anumba, "Reproducibility and repeatability of measuring the electrical impedance of the pregnant human cervix-the effect of probe size and applied pressure," *Biomed Eng Online*, vol. 8, no. May 2014, doi: [10.1186/1475-925X-8-10](https://doi.org/10.1186/1475-925X-8-10).
- [28] B. H. Brown, J. A. Tidy, K. Boston, A. D. Blackett, R. H. Smallwood, and F. Sharp, "Relation between tissue structure and imposed electrical current flow in cervical neoplasia," *Lancet*, vol. 355, no. 9207, pp. 892–895, 2000, doi: [10.1016/S0140-6736\(99\)09095-9](https://doi.org/10.1016/S0140-6736(99)09095-9).
- [29] S. C. Quek, T. Mould, K. Canfell, A. Singer, V. Skladnev, and M. Coppleson, "The Polarprobe - Emerging technology for cervical cancer screening," *Ann Acad Med Singap*, vol. 27, no. 5, pp. 717–721, 1998.
- [30] Q. Castellví, B. Mercadal, and A. Ivorra, *Handbook of Electroporation*. Springer International Publishing, 2016. doi: [10.1007/978-3-319-26779-1](https://doi.org/10.1007/978-3-319-26779-1).
- [31] C. Gabriel, S. Gabriel, and E. Corthout, "The dielectric properties of biological tissues: I. Literature survey" *Phys Med Biol*, vol. 41, no. 11, pp. 2231–2249, 1996, doi: [10.1088/0031-9155/41/11/001](https://doi.org/10.1088/0031-9155/41/11/001).
- [32] S. Gabriel, R. W. Lau, and C. Gabriel, "The dielectric properties of biological tissues: II. Measurements in the frequency range 10 Hz to 20 GHz," *Phys Med Biol*, vol. 41, no. 11, pp. 2251–2269, 1996, doi: [10.1088/0031-9155/41/11/002](https://doi.org/10.1088/0031-9155/41/11/002).
- [33] C. Gabriel, "Compilation of the Dielectric Properties of Body Tissues At Rf and Microwave Frequencies." 1996. [Online]. Available: <http://www.dtic.mil/dtic/tr/fulltext/u2/a303903.pdf>
- [34] A. Peyman and C. Gabriel, "Changes in the dielectric properties of rat tissue as a function of age at microwave frequencies," *Phys Med Biol*, vol. 55, no. 15, 2010, doi: [10.1088/0031-9155/55/15/N02](https://doi.org/10.1088/0031-9155/55/15/N02).
- [35] A. Peyman, C. Gabriel, and E. H. Grant, "Complex permittivity of sodium chloride solutions at microwave frequencies," *Bioelectromagnetics*, vol. 28, no. 4, pp. 264–274, 2007, doi: [10.1002/bem.20271](https://doi.org/10.1002/bem.20271).
- [36] C. Gabriel, A. Peyman, and E. H. Grant, "Electrical conductivity of tissue at frequencies below 1 MHz," *Phys Med Biol*, vol. 54, no. 16, pp. 4863–4878, 2009, doi: [10.1088/0031-9155/54/16/002](https://doi.org/10.1088/0031-9155/54/16/002).
- [37] E. Dunne, A. Santorelli, B. McGinley, M. O. Halloran, G. Leader, and E. Porter, "EIT Image-Based Bladder State Classification for Nocturnal Enuresis," *19th International Conference on*

References

- Biomedical Applications of Electrical Impedance Tomography*, Edinburgh, United Kingdom, 2018.
- [38] Hahn, G. M., Kernahan, P., Martinez, A., Pounds, D., Prionas, S., Anderson, T., & Justice, G. (1980). Some heat transfer problems associated with heating by ultrasound, microwaves, or radio frequency. *Annals of the New York Academy of Sciences*, 335, 327–351. <https://doi.org/10.1111/j.1749-6632.1980.tb50757.x>
- [39] N. K. Nikolova, "Microwave Imaging for Breast Cancer," in *IEEE Microwave Magazine*, vol. 12, no. 7, pp. 78-94, 2011, doi: 10.1109/MMM.2011.942702.
- [40] N. Ištuk *et al.*, "Dielectric properties of ovine heart at microwave frequencies," *Diagnostics*, vol. 11, no. 3, 2021, doi: 10.3390/diagnostics11030531.
- [41] J. C. Lin, "Frequency Optimization for Microwave Imaging of Biological Tissues.," *Proceedings of the IEEE*, vol. 73, no. 2, pp. 374–375, 1985, doi: 10.1109/PROC.1985.13151.
- [42] A. Peyman, C. Gabriel, and E. H. Grant, "Complex permittivity of sodium chloride solutions at microwave frequencies," *Bioelectromagnetics*, vol. 28, no. 4, pp. 264–274, 2007, doi: 10.1002/bem.20271.
- [43] K. B. Yu, S. G. Ogourtsov, V. G. Belenky, A. B. Maslenikov, and A. S. Omar, "Accurate microwave resonant method for complex permittivity measurements of liquids [biological]," *IEEE Trans Microw Theory Tech*, vol. 48, no. 11, pp. 2159–2164, 2000, doi: 10.1109/22.884209.
- [44] M. Tlili, F. Deshours, G. Alquié, H. Kokabi, S. Hardinata, and F. Koskas, "Microwave Resonant Sensor for Non-invasive Characterization of Biological Tissues," *IRBM*, vol. 39, no. 6, pp. 445–450, 2018, doi: <https://doi.org/10.1016/j.irbm.2018.10.013>.
- [45] S. Laufer, A. Ivorra, V. E. Reuter, B. Rubinsky, and S. B. Solomon, "Electrical impedance characterization of normal and cancerous human hepatic tissue," *Physiol Meas*, vol. 31, no. 7, pp. 995–1009, 2010, doi: 10.1088/0967-3334/31/7/009.
- [46] S. Laufer, A. Ivorra, V. E. Reuter, B. Rubinsky, and S. B. Solomon, "Electrical impedance characterization of normal and cancerous human hepatic tissue," *Physiol Meas*, vol. 31, no. 7, pp. 995–1009, 2010, doi: 10.1088/0967-3334/31/7/009.
- [47] S. Burke *et al.*, "Feasibility Study of Plaque Detection using Electrical Impedance Techniques," 2022 16th European Conference on Antennas and Propagation (EuCAP), Madrid, Spain, 2022, pp. 1-4, doi: 10.23919/EuCAP53622.2022.9769600.
- [48] KAY, C. F., & SCHWAN, H. P. (1956). Specific resistance of body tissues. *Circulation research*, 4(6), 664–670. <https://doi.org/10.1161/01.res.4.6.664>
- [49] D. Miklavčič, N. Pavšelj, and F. X. Hart, "Electric Properties of Tissues," *Wiley Encyclopedia of Biomedical Engineering*, pp. 1–12, 2006, doi: 10.1002/9780471740360.ebs0403.
- [50] J. Malvern Benjamin, H. Schwan, C. F. Kay, and J. H. Hafkenschiel, "The Electrical Conductivity of Living Tissues as it Pertains to Electrocardiography I. Review of the Problem of Homogeneity vs. Nonhomo-geneity, an Outline of the Technical Aspects of Tissue Resistivity Measurements, and a Critical and Experimental Analysis of Certain Pertinent Experiments," 1950. [Online]. Available: <http://ahajournals.org>
- [51] W. Kuang and S. O. Nelson, "Low-frequency dielectric properties of biological tissues: A review with some new insights," *Transactions of the American Society of Agricultural Engineers*, vol. 41, no. 1, pp. 173–184, 1998, doi: 10.13031/2013.17142.
- [52] D. A. Dean, T. Ramanathan, D. Machado, and R. Sundararajan, "Electrical impedance spectroscopy study of biological tissues," *J Electrostat*, vol. 66, no. 3–4, pp. 165–177, 2008, doi: 10.1016/j.elstat.2007.11.005.
- [53] R. v. Davalos, D. M. Otten, L. M. Mir, and B. Rubinsky, "Electrical Impedance Tomography for Imaging Tissue Electroporation," *IEEE Trans Biomed Eng*, vol. 51, no. 5, pp. 761–767, 2004, doi: 10.1109/TBME.2004.824148.
- [54] G. S. J. Peters M. Hendriks M., "Estimation of the Electrical Conductivity of Human Tissue," *Electromagnetics*, vol. 21, no. 7–8, pp. 545–557, Sep. 2001, doi: 10.1080/027263401752246199.
- [55] "Dielectric Properties of Body Tissues." <http://niremf.ifac.cnr.it/tissprop/>

References

- [56] "Dielectric Properties » IT'IS Foundation." <https://itis.swiss/virtual-population/tissue-properties/database/dielectric-properties/>
- [57] L. Galvani and M. G. Foley, "Review Reviewed Work(s): Commentary on the Effects of Electricity on Muscular Motion by," 1955. [Online]. Available: <https://about.jstor.org/terms>
- [58] O. Heaviside, "Electrical Papers." New York and London: Macmillan and co, 1894.
- [59] N. Istuk, A. la Gioia, H. Benchakroun, A. Lowery, B. McDermott, and M. O'Halloran, "Relationship Between the Conductivity of Human Blood and Blood Counts," *IEEE J Electromagn RF Microw Med Biol*, vol. PP, pp. 1–7, 2021, doi: 10.1109/JERM.2021.3130788.
- [60] M. Wolf, R. Gulich, P. Lunkenheimer, A. Loidl, "Broadband dielectric spectroscopy on human blood, *Biochimica et Biophysica Acta (BBA)*" - General Subjects, Volume 1810, Issue 8, 2011, Pages 727-740, ISSN 0304-4165, <https://doi.org/10.1016/j.bbagen.2011.05.012>.
- [61] N. Istuk, H. Benchakroun, E. Dunne, and M. O. Halloran, "Pressure Dependency of Conductivity Measurements: The Specific Case of the Pressure Dependency of Conductivity Measurements : The Specific Case of the Lung," 2021, 21st International Conference on Biomedical Applications of Electrical Impedance Tomography, July, pp. 1–2, 2021.
- [62] H. Benchakroun, E. Dunne, D. O. Loughlin, and M. O. Halloran, "Measurement of the Left Atrium Appendage Electrical Conductivity with a Tetrapolar Probe over 0 . 1 Hz to 100 kHz," 2021, 21st International Conference on Biomedical Applications of Electrical Impedance Tomography.
- [63] L. Santamaría, L. Alonso, I. Ingelmo, J. M. Pozuelo, and R. Rodriguez, "Electrical Impedance Spectroscopy of the Human Prostate," *Adv Anat Embryol Cell Biol*, vol. 194, no. 7, pp. 2–11, 2007, doi: 10.1007/978-3-540-69816-6_2.
- [64] A. R. Liboff, "Toward an Electromagnetic Paradigm for Biology and Medicine," *Journal of Alternative and Complementary Medicine*, vol. 10, no. 1, pp. 41–47, 2004, doi: 10.1089/107555304322848940.
- [65] C. J. Bradley and D. E. Haines, "Pulsed field ablation for pulmonary vein isolation in the treatment of atrial fibrillation," *J Cardiovasc Electrophysiol*, vol. 31, no. 8, pp. 2136–2147, 2020, doi: 10.1111/jce.14414.
- [66] J. M. Baena-Montes *et al.*, "Electroporation Parameters for Human Cardiomyocyte Ablation In Vitro," 2022.
- [67] O. Casas *et al.*, "In vivo and in situ ischemic tissue characterization using electrical impedance spectroscopy." *Ann N Y Acad Sci*, 1999. doi: 10.1111/j.1749-6632.1999.tb09448.x.
- [68] M. Amini, J. Hisdal, and H. Kalvøy, "Applications of bioimpedance measurement techniques in tissue engineering," *J Electr Bioimpedance*, vol. 9, no. 1, pp. 142–158, 2018, doi: 10.2478/joeb-2018-0019.
- [69] K. R. Foster, "Dielectric properties of tissues and biological materials: A critical review," 1989. [Online]. Available: <https://www.researchgate.net/publication/20505222>
- [70] Miklavčič, D., Pavšelj, N. and Hart, F.X. (2006). "Electric Properties of Tissues". In *Wiley Encyclopedia of Biomedical Engineering*, M. Akay (Ed.). <https://doi.org/10.1002/9780471740360.ebs0403>
- [71] Magnano, M., Devecchi, C., Oriente, D., Occhetta, E., & Rametta, F. (2023). Proarrhythmic effect of bipolar epicardial left ventricular stimulation in CRT resolved maintaining biventricular pacing with unipolar-cathodal configuration: A peculiar case report. *Journal of arrhythmia*, 39(2), 192–197. <https://doi.org/10.1002/joa3.12818>
- [72] R. J. Bajwa *et al.*, "Left atrial appendage occlusion for stroke prevention in patients with atrial fibrillation," *Clin Cardiol*, vol. 40, no. 10, pp. 825–831, 2017, doi: 10.1002/clc.22764.
- [73] P. Safavi-Naeini and A. Rasekh, "Left Atrial Appendage Closure and Pulmonary Vein Isolation," *Tex Heart Inst J*, vol. 47, no. 1, pp. 60–62, . 2020, doi: 10.14503/THIJ-19-7061.
- [74] Markides, Vias, and Richard J Schilling. "Atrial fibrillation: classification, pathophysiology, mechanisms and drug treatment." *Heart (British Cardiac Society)* vol. 89,8 (2003): 939-43. doi:10.1136/heart.89.8.939

References

- [75] S. Gelsomino *et al.*, "Pharmacological management of atrial fibrillation: One, none, one hundred thousand," *Cardiology Research and Practice*, vol. 1, no. 1. 2011. doi: 10.4061/2011/874802.
- [76] I. Cakulev, I. R. Efimov, and A. L. Waldo, "Cardioversion: Past, present, and future," *Circulation*, vol. 120, no. 16. pp. 1623–1632, 2009. doi: 10.1161/CIRCULATIONAHA.109.865535.
- [77] T. Weimar *et al.*, "The cox-maze procedure for lone atrial fibrillation a single-center experience over 2 decades," *Circ Arrhythm Electrophysiol*, vol. 5, no. 1, pp. 8–14, . 2012, doi: 10.1161/CIRCEP.111.963819.
- [78] A. Belalcazar, "Safety and efficacy aspects of pulsed field ablation catheters as a function of electrode proximity to blood and energy delivery method," *Heart Rhythm O2*, vol. 2, no. 6, pp. 560–569, 2021, doi: 10.1016/j.hroo.2021.10.004.
- [79] J.-B. le Polain de Waroux *et al.*, "Pulmonary vein isolation for the treatment of atrial fibrillation: past, present and future," *Future Cardiol*, vol. 6, no. 1, pp. 51–66, 2009, doi: 10.2217/fca.09.55.
- [80] A. Akinapelli *et al.*, "Left Atrial Appendage Closure-The WATCHMAN Device," 2015.
- [81] Al-Saady, N. M., Obel, O. A., & Camm, A. J. (1999). Left atrial appendage: structure, function, and role in thromboembolism. *Heart (British Cardiac Society)*, 82(5), 547–554. <https://doi.org/10.1136/hrt.82.5.547>.
- [82] K. Benali *et al.*, "Recurrences of Atrial Fibrillation Despite Durable Pulmonary Vein Isolation: The PARTY-PVI Study," *Circ Arrhythm Electrophysiol*, vol. 16, no. 3, p. e011354, 2023, doi: 10.1161/CIRCEP.122.011354.
- [83] J. E. Poole *et al.*, "Recurrence of Atrial Fibrillation After Catheter Ablation or Antiarrhythmic Drug Therapy in the CABANA Trial," *J Am Coll Cardiol*, vol. 75, no. 25, pp. 3105–3118, 2020, doi: 10.1016/j.jacc.2020.04.065.
- [84] Chang, D.C. (2006). Electroporation and Electrofusion. In *Reviews in Cell Biology and Molecular Medicine*, R.A. Meyers (Ed.). <https://doi.org/10.1002/3527600906.mcb.200300026>
- [85] N. M. Al-Saady, O. A. Obel, and A. J. Camm, "Left atrial appendage: Structure, function, and role in thromboembolism," *Heart*, vol. 82, no. 5, pp. 547–554, 1999, doi: 10.1136/hrt.82.5.547.
- [86] G. Ernst *et al.*, "Morphology of the left atrial appendage," *Anat Rec*, vol. 242, no. 4, pp. 553–561, 1995, doi: 10.1002/ar.1092420411.
- [87] D. Regazzoli *et al.*, "Left Atrial Appendage: Physiology, Pathology, and Role as a Therapeutic Target," *Biomed Res Int*, vol. 2015, 2015, doi: 10.1155/2015/205013.
- [88] L. Bonfanti *et al.*, "Effectiveness and safety of electrical cardioversion for acute-onset atrial fibrillation in the emergency department: a real-world 10-year single center experience," *Clin Exp Emerg Med*, vol. 6, no. 1, pp. 64–69, 2019, doi: 10.15441/ceem.17.286.
- [89] G. E. Mead, A. Elder, A. D. Flapan, and J. Cordina, "Electrical cardioversion for atrial fibrillation and flutter," *Cochrane Database of Systematic Reviews*, vol. 2017, no. 11. John Wiley and Sons Ltd, 2017. doi: 10.1002/14651858.CD002903.pub3.
- [90] A. S. Tang *et al.*, "Canadian Cardiovascular Society/Canadian Heart Rhythm Society position paper on implantable cardioverter defibrillator use in Canada," 2005.
- [91] I. G. Stiell *et al.*, "Electrical versus pharmacological cardioversion for emergency department patients with acute atrial fibrillation (RAFF2): a partial factorial randomised trial," *The Lancet*, vol. 395, no. 10221, pp. 339–349, 2020, doi: [https://doi.org/10.1016/S0140-6736\(19\)32994-0](https://doi.org/10.1016/S0140-6736(19)32994-0).
- [92] S. T. Nguyen *et al.*, "Techniques improving electrical cardioversion success for patients with atrial fibrillation: a systematic review and meta-analysis," *EP Europace*. 2022, doi: 10.1093/europace/euac199.
- [93] H. bin Gwag *et al.*, "Which antiarrhythmic drug to choose after electrical cardioversion: A study on non-valvular atrial fibrillation patients," *PLoS One*, vol. 13, no. 5, 2018, doi: 10.1371/journal.pone.0197352.

References

- [94] S. M. Cobbe, "Using the right drug: A treatment algorithm for atrial fibrillation," *Eur Heart J*, vol. 18, no. suppl_C, pp. 33–39, 1997, doi: 10.1093/eurheartj/18.suppl_C.33.
- [95] M. Mirowski, "The automatic implantable cardioverter-defibrillator: An overview," *J Am Coll Cardiol*, vol. 6, no. 2, pp. 461–466, 1985, doi: [https://doi.org/10.1016/S0735-1097\(85\)80186-8](https://doi.org/10.1016/S0735-1097(85)80186-8).
- [96] Sankaranarayanan, Rajiv et al. "How does Chronic Atrial Fibrillation Influence Mortality in the Modern Treatment Era?." *Current cardiology reviews* vol. 11,3 (2015): 190-8. doi:10.2174/1573403x10666140902143020
- [97] E. R. Jessurun, N. M. Van Hemel, J. A. M. T. Defauw, M. A. M. Stofmeel, and J. C. Kelder, "Results of Maze Surgery for Lone Paroxysmal Atrial Fibrillation," 2000. [Online]. Available: <http://www.circulationaha.org>
- [98] S. Lönnerholm, ; P Blomström, ; L Nilsson, ; S Oxelbark, ; L Jideus, and ; C Blomström-Lundqvist, "Effects of the Maze Operation on Health-Related Quality of Life in Patients With Atrial Fibrillation," 2000. [Online]. Available: <http://www.circulationaha.org>
- [99] C. P. Lawrance, M. C. Henn, and R. J. Damiano, "Surgical ablation for atrial fibrillation: Techniques, indications, and results," *Current Opinion in Cardiology*, vol. 30, no. 1. Lippincott Williams and Wilkins, pp. 58–64, . 12, 2015. doi: 10.1097/HCO.0000000000000125.
- [100] O. A. García-Villarreal, "Standardization in maze procedure: A step towards a better future," *Journal of Thoracic Disease*, vol. 10. AME Publishing Company, pp. S3887–S3889, 2018. doi: 10.21037/jtd.2018.08.131.
- [101] K. Tanaka *et al.*, "A new radiofrequency thermal balloon catheter for pulmonary vein isolation," *J Am Coll Cardiol*, vol. 38, no. 7, pp. 2079–2086, 2001, doi: [https://doi.org/10.1016/S0735-1097\(01\)01666-7](https://doi.org/10.1016/S0735-1097(01)01666-7).
- [102] A. Bisignani *et al.*, "Long-Term Outcomes of Pulmonary Vein Isolation in Patients With Brugada Syndrome and Paroxysmal Atrial Fibrillation," *J Am Heart Assoc*, vol. 11, no. 15, 2022, doi: 10.1161/JAHA.122.026290.
- [103] J. G. Andrade *et al.*, "Cryoablation or Drug Therapy for Initial Treatment of Atrial Fibrillation," *New England Journal of Medicine*, vol. 384, no. 4, pp. 305–315, 2021, doi: 10.1056/nejmoa2029980.
- [104] D. Lakkireddy *et al.*, "Amplatzer Amulet Left Atrial Appendage Occluder Versus Watchman Device for Stroke Prophylaxis (Amulet IDE): A Randomized, Controlled Trial," *Circulation*, vol. 144, no. 19, pp. 1543–1552, 2021, doi: 10.1161/CIRCULATIONAHA.121.057063.
- [105] C. Gianni, A. Anannab, A. Sahore Salwan, D. G. Della Rocca, A. Natale, and R. P. Horton, "Closure of the left atrial appendage using percutaneous transcatheter occlusion devices," *J Cardiovasc Electrophysiol*, vol. 31, no. 8, pp. 2179–2186, 2020, doi: <https://doi.org/10.1111/jce.14471>.
- [106] A. Rasekh, P. Safavi-Naeini, M. Razavi, M. Saeed, and A. Massumi, "A Review of the LARIAT Suture Delivery Device for Left Atrial Appendage Closure," 2015. [Online]. Available: <http://jthc.tums.ac.ir>
- [107] Schellinger, Peter D et al. "Percutaneous Left Atrial Appendage Occlusion for the Prevention of Stroke in Patients with Atrial Fibrillation: Review and Critical Appraisal." *Journal of stroke* vol. 20,3 (2018): 281-291. doi:10.5853/jos.2018.02537
- [108] J. Z. Tsai *et al.*, "Error analysis of tissue resistivity measurement," *IEEE Trans Biomed Eng*, vol. 49, no. 5, pp. 484–494, 2002, doi: 10.1109/10.995687.
- [109] Miklavčič, D., Pavšelj, N. and Hart, F.X. (2006). Electric Properties of Tissues. In *Wiley Encyclopedia of Biomedical Engineering*, M. Akay (Ed.). <https://doi.org/10.1002/9780471740360.ebs0403>
- [110] Djajaputra, D. (2005), *Electrical Impedance Tomography: Methods, History and Applications*. *Med. Phys.*, 32: 2731-2731. <https://doi.org/10.1118/1.1995712>
- [111] Lobo, Beatriz et al. "Electrical impedance tomography." *Annals of translational medicine* vol. 6,2 (2018): 26. doi:10.21037/atm.2017.12.06
- [112] A. Bottiglieri, E. Dunne, B. McDermott, M. Cavagnaro, E. Porter and L. Farina, "Monitoring Microwave Thermal Ablation using Electrical Impedance Tomography: an experimental

References

- feasibility study," 2020 14th European Conference on Antennas and Propagation (EuCAP), Copenhagen, Denmark, 2020, pp. 1-5, doi: 10.23919/EuCAP48036.2020.9135226.
- [113] A. Santorelli *et al.*, "Investigation of Anemia and the Dielectric Properties of Human Blood at Microwave Frequencies," *IEEE Access*, vol. 6, pp. 56885–56892, 2018, doi: 10.1109/ACCESS.2018.2873447.
- [114] S. Meng, M. Rouabhia, and Z. Zhang, "Electrical stimulation and cellular behaviors in electric field in biomedical research," *Materials*, vol. 15, no. 1, 2022, doi: 10.3390/ma15010165.
- [115] Dildar, Mehwish *et al.* "Skin Cancer Detection: A Review Using Deep Learning Techniques." *International journal of environmental research and public health* vol. 18,10 5479. 20 May. 2021, doi:10.3390/ijerph18105479
- [116] R. P. Braun, J. Mangana, S. Goldinger, L. French, R. Dummer, and A. A. Marghoob, "Electrical Impedance Spectroscopy in Skin Cancer Diagnosis," *Dermatol Clin*, vol. 35, no. 4, pp. 489–493, 2017, doi: 10.1016/j.det.2017.06.009.
- [117] V. Narayanamurthy *et al.*, "Skin cancer detection using non-invasive techniques," *RSC Adv*, vol. 8, no. 49, pp. 28095–28130, 2018, doi: 10.1039/c8ra04164d.
- [118] H. Benchakroun, D. O'Loughlin, N. Ištuk, M. O'Halloran and A. L. Gioia, "Evaluation of the Feasibility of Three Custom-made Tetrapolar Probes for Electrical Characterization of Cardiac Tissue," 2021 15th European Conference on Antennas and Propagation (EuCAP), Dusseldorf, Germany, 2021, pp. 1-5, doi: 10.23919/EuCAP51087.2021.9410978.
- [119] L. Yang *et al.*, "Ex-vivo characterization of bioimpedance spectroscopy of normal, ischemic and hemorrhagic rabbit brain tissue at frequencies from 10 Hz to 1 MHz," *Sensors (Switzerland)*, vol. 16, no. 11, 2016, doi: 10.3390/s16111942.
- [120] S. M. Feynman RP, Leighton RB, "The Feynman Lectures on Physics. Mainly Electromagnetism and Matter," *The New Millennium Ed. Basic Books*, vol. 2, p. 566, 2010, doi: 10.1558/jsrnc.v4il.24.
- [121] R. Pethig and I. Schmueser, "Marking 100 years since Rudolf Höber's discovery of the insulating envelope surrounding cells and of the β -dispersion exhibited by tissue," *J Electr Bioimpedance*, vol. 3, no. 1, pp. 74–79, 2012, doi: doi:10.5617/jeb.401.
- [122] L. A. Geddes and L. E. Baker, "The specific resistance of biological material—A compendium of data for the biomedical engineer and physiologist," *Med Biol Eng*, vol. 5, no. 3, pp. 271–293, 1967, doi: 10.1007/BF02474537.
- [123] T. Watson, "Key Concepts in Electrotherapy." [Online]. Available: www.electrotherapy.org
- [124] Plonsey, Robert & Barr, Roger. (2007). "Bioelectricity: A Quantitative Approach". 10.1007/978-0-387-48865-3.
- [125] Rutkove, Seward. (2007). Introduction to Volume Conduction. 10.1007/978-1-59745-271-7_4.
- [126] Medina, L. E., & Grill, W. M. (2014). Volume conductor model of transcutaneous electrical stimulation with kilohertz signals. *Journal of neural engineering*, 11(6), 066012. <https://doi.org/10.1088/1741-2560/11/6/066012>
- [127] V. Daněk, "Chapter 8 - Electrical Conductivity," in *Physico-Chemical Analysis of Molten Electrolytes*, V. Daněk, Ed., Amsterdam: Elsevier Science, 2006, pp. 327–357. doi: <https://doi.org/10.1016/B978-044452116-3/50009-X>.
- [128] A. Revil, "Effective conductivity and permittivity of unsaturated porous materials in the frequency range 1 mHz-1GHz," *Water Resour Res*, vol. 49, no. 1, pp. 306–327, 2013, doi: 10.1029/2012WR012700.
- [129] Heaney, Michael B. "Electrical Conductivity and Resistivity." *Electrical Measurement, Signal Processing, and Displays*. Ed. John G. Webster. CRC Press, 2003. 7-1.
- [130] H. P. Schwan and C. F. Kay, "the Conductivity of Living Tissues," *Ann N Y Acad Sci*, vol. 65, no. 6, pp. 1007–1013, 1957, doi: 10.1111/j.1749-6632.1957.tb36701.x.
- [131] R. Singh, M. J. Bathaei, E. Istif, and L. Beker, "A Review of Bioresorbable Implantable Medical Devices: Materials, Fabrication, and Implementation," *Advanced Healthcare Materials*, vol. 9, no. 18. Wiley-VCH Verlag, 2020. doi: 10.1002/adhm.202000790.

References

- [132] A. la Gioia *et al.*, "Open-Ended Coaxial Probe Technique for Dielectric Measurement of Biological Tissues: Challenges and Common Practices," *Diagnostics*, vol. 8, no. 2, p. 40, 2018, doi: 10.3390/diagnostics8020040.
- [133] Kovacsova, Z., Bale, G., Mitra, S., de Roever, I., Meek, J., Robertson, N., & Tachtsidis, I. (2018). Investigation of Confounding Factors in Measuring Tissue Saturation with NIRS Spatially Resolved Spectroscopy. *Advances in experimental medicine and biology*, 1072, 307–312. https://doi.org/10.1007/978-3-319-91287-5_49
- [134] T. Phan *et al.*, "Quantifying the confounding effect of pigmentation on measured skin tissue optical properties: a comparison of colorimetry with spatial frequency domain imaging," *J Biomed Opt*, vol. 27, no. 03, 2022, doi: 10.1117/1.jbo.27.3.036002.
- [135] P. Bertemes Filho, "Assessing Applied Pressure in Impedance Probe by Single-zone Force Sensing Resistors," *Athens Journal of Technology & Engineering*, vol. 4, no. 1, pp. 7–16, 2017, doi: 10.30958/ajte.4-1-1.
- [136] H. Benchakroun *et al.*, "Probe Contact Force Monitoring during Conductivity Measurements of the Left Atrial Appendage to Support the Design of Novel Diagnostic and Therapeutic Procedures," *Sensors*, vol. 22, no. 19, p. 7171, Sep. 2022, doi: 10.3390/s22197171.
- [137] G. Maenhout, T. Markovic, I. Ocket, and B. Nauwelaers, "Effect of open-ended coaxial probe-to-tissue contact pressure on dielectric measurements," *Sensors*, vol. 20, no. 7, pp. 1–13, 2020, doi: 10.3390/s20072060.
- [138] H. Benchakroun *et al.*, "Probe Contact Force Monitoring during Conductivity Measurements of the Left Atrial Appendage to Support the Design of Novel Diagnostic and Therapeutic Procedures," *Sensors*, vol. 22, no. 19, p. 7171, Sep. 2022, doi: 10.3390/s22197171.
- [139] Benchakroun, H.; Ištuk, N.; Dunne, E.; Elahi, M.A.; O'Halloran, T.; O'Halloran, M.; O'Loughlin, D. Probe Contact Force Monitoring during Conductivity Measurements of the Left Atrial Appendage to Support the Design of Novel Diagnostic and Therapeutic Procedures. *Sensors* 2022, 22, 7171. <https://doi.org/10.3390/s22197171>
- [140] R. Oliveira, P. Georgieva, S. Feye de Azevedo, "Plant and Equipment | Instrumentation and Process Control: Instrumentation", 2002, Pages 234-241, ISBN 9780123744074, <https://doi.org/10.1016/B978-0-12-374407-4.00412-X>.
- [141] H. P. Schwan and C. F. Kay, "the Conductivity of Living Tissues," *Ann N Y Acad Sci*, vol. 65, no. 6, pp. 1007–1013, 1957, doi: 10.1111/j.1749-6632.1957.tb36701.x.
- [142] J. Torreblanca González, R. García Ovejero, Á. Lozano Murciego, G. Villarrubia González, and J. F. de Paz, "Effects of Environmental Conditions and Composition on the Electrical Properties of Textile Fabrics," *Sensors*, vol. 19, no. 23, 2019, doi: 10.3390/s19235145.
- [143] C. Rossmanna and D. Haemmerich, "Review of temperature dependence of thermal properties, dielectric properties, and perfusion of biological tissues at hyperthermic and ablation temperatures.," *Crit Rev Biomed Eng*, vol. 42, no. 6, pp. 467–492, 2014, doi: 10.1615/critrevbiomedeng.2015012486.
- [144] M. Foucaud *et al.*, "Sodium-Ion Conductivity and Humidity-Sensing Properties of Na₂O-MoO₃-P₂O₅ Glass-Ceramics," *Nanomaterials*, vol. 12, no. 2, 2022, doi: 10.3390/nano12020240.
- [145] A. Ullah *et al.*, "Garage-Fabricated, Ultrasensitive Capacitive Humidity Sensor Based on Tissue Paper," *Sensors*, vol. 22, no. 20, 2022, doi: 10.3390/s22207885.
- [146] Y.-P. Zheng and A. F. T. Mak, "An ultrasound indentation system for biomechanical properties assessment of soft tissues in-vivo," *IEEE Trans Biomed Eng*, vol. 43, no. 9, pp. 912–918, 1996, doi: 10.1109/10.532125.
- [147] Baker-Jarvis, J. , Kim, S. , Leschallinger, L. , Johnson, J. and Givot, B. (2010), Characterization of Tissue-Equivalent Materials for High-Frequency Applications (200 MHz to 20 GHz), Technical Note (NIST TN), National Institute of Standards and Technology, Gaithersburg, MD (Accessed November 22, 2023)
- [148] A. P. Gregory and R. N. Clarke, "A review of RF and microwave techniques for dielectric measurements on polar liquids," *IEEE Transactions on Dielectrics and Electrical Insulation*, vol. 13, no. 4, pp. 727–743, 2006, doi: 10.1109/TDEI.2006.1667730.

References

- [149] D. K. Ghodgaonkar, V. v Varadan, and V. K. Varadan, "A free-space method for measurement of dielectric constants and loss tangents at microwave frequencies," *IEEE Trans Instrum Meas*, vol. 38, no. 3, pp. 789–793, 1989, doi: 10.1109/19.32194.
- [150] K. J. Lee, S. S. Oh, Y. H. Lee, and Y. S. Kim, "Front-to-back ratio improvement of a short pyramidal horn antenna using metal strips/rods in LTE/cellular band," *IET Microwaves, Antennas and Propagation*, vol. 10, no. 1, pp. 111–118, . 2016, doi: 10.1049/iet-map.2015.0241.
- [151] P. Skocik and P. Neumann, "Measurement of Complex Permittivity in Free Space," *Procedia Eng*, vol. 100, pp. 100–104, 2015, doi: <https://doi.org/10.1016/j.proeng.2015.01.347>.
- [152] N. Tamis, A. Ramli, and D. K. Ghodgaonkar, Free space measurement of complex permittivity and complex permeability of magnetic materials using open circuit and short circuit method at microwave frequencies. 2002. doi: 10.1109/SCORED.2002.1033141.
- [153] Porter, E, La Gioia, A, Salahuddin, S, et al. Minimum information for dielectric measurements of biological tissues (MINDER): A framework for repeatable and reusable data. *Int J RF Microw Comput Aided Eng*. 2018;28:e21201. <https://doi.org/10.1002/mmce.21201>
- [154] K. Y. You, M. S. Sim, H. Mutadza, F. Esa and Y. L. Chan, "Free-space measurement using explicit, reference-plane and thickness-invariant method for permittivity determination of planar materials," 2017 Progress in Electromagnetics Research Symposium - Fall (PIERS - FALL), Singapore, 2017, pp. 222-228, doi: 10.1109/PIERS-FALL.2017.8293139.
- [155] Mir Mohsina Rahman, G.M. Rather, "A simple and accurate FDTD based technique to determine equivalent complex permittivity of the multi-layered human tissue in MICS band, *Journal of Science: Advanced Materials and Devices*", Volume 5, Issue 1, 2020, Pages 134-141, ISSN 2468-2179, <https://doi.org/10.1016/j.jsamd.2020.02.004>..
- [156] S. Bories, C. Delaveaud and H. Jacquinet, "Low profile and directive UWB antenna," 2009 3rd European Conference on Antennas and Propagation, Berlin, Germany, 2009, pp. 1632-1635.
- [157] H. Hong, J. Ahn, J. -g. Jeong and Y. J. Yoon, "Gain enhancement technique for an antipodal vivaldi antenna," 2015 IEEE International Symposium on Antennas and Propagation & USNC/URSI National Radio Science Meeting, Vancouver, BC, Canada, 2015, pp. 2343-2344, doi: 10.1109/APS.2015.7305560.
- [158] H. Benchakroun, A. Fasoula, L. Duchesne, M. O'Halloran and D. O'Loughlin, "Coverage Estimation for Microwave Imaging using Full Multistatic Radar Imaging Algorithms with Restricted Opening," 2020 14th European Conference on Antennas and Propagation (EuCAP), Copenhagen, Denmark, 2020, pp. 1-5, doi: 10.23919/EuCAP48036.2020.9135219.
- [159] H. Benchakroun, A. Fasoula, L. Duchesne, M. O'Halloran and D. O'Loughlin, "Coverage Estimation for Microwave Imaging using Full Multistatic Radar Imaging Algorithms with Restricted Opening," 2020 14th European Conference on Antennas and Propagation (EuCAP), Copenhagen, Denmark, 2020, pp. 1-5, doi: 10.23919/EuCAP48036.2020.9135219.
- [160] H. Benchakroun, S. Castelló-Palacios, A. Nevarez, M. Cabedo-Fabrés and M. Ferrando-Bataller, "Study of penetration ratio using UWB antenna with an in vivo subject," 2019 13th European Conference on Antennas and Propagation (EuCAP), Krakow, Poland, 2019, pp. 1-5.
- [161] Y. Liu, Y. Gu, and X. Yu, "Assessing tissue metabolism by phosphorous-31 magnetic resonance spectroscopy and imaging: a methodology review," *Quant Imaging Med Surg*, vol. 7, no. 6, pp. 707–726, 2017, doi: 10.21037/qims.2017.11.03.
- [162] S. Chen, "Resonant frequency method for the measurement and uncertainty analysis of acoustic and elastic properties," *Ultrasonics*, vol. 38, no. 1, pp. 206–211, 2000, doi: [https://doi.org/10.1016/S0041-624X\(99\)00038-4](https://doi.org/10.1016/S0041-624X(99)00038-4).
- [163] D. Michaeli and Z. H. Rappaport, "Tissue resonance analysis: a novel method for noninvasive monitoring of intracranial pressure: Technical note," *J Neurosurg*, vol. 96, no. 6, pp. 1132–1137, 2002, doi: 10.3171/jns.2002.96.6.1132.
- [164] X. Wang, H. Guo, C. Zhou, and J. Bai, "High resolution probe design for measuring the dielectric properties of human tissues," *Biomed Eng Online*, vol. 20, no. 1, p. 86, 2021, doi: 10.1186/s12938-021-00924-1.

References

- [165] Y. Liu, Y. Gu, and X. Yu, "Assessing tissue metabolism by phosphorous-31 Magnetic resonance spectroscopy and imaging: A methodology review," *Quantitative Imaging in Medicine and Surgery*, vol. 7, no. 6. AME Publishing Company, pp. 707–726, 01, 2017. doi: 10.21037/qims.2017.11.03.
- [166] N. Grenier *et al.*, "Measurement of Glomerular Filtration Rate With Magnetic Resonance Imaging: Principles, Limitations, and Expectations," *Semin Nucl Med*, vol. 38, no. 1, pp. 47–55, 2008, doi: <https://doi.org/10.1053/j.semnuclmed.2007.09.004>.
- [167] R. B. Schwarz and J. F. Vuorinen, "Resonant ultrasound spectroscopy: applications, current status and limitations," *J Alloys Compd*, vol. 310, no. 1, pp. 243–250, 2000, doi: [https://doi.org/10.1016/S0925-8388\(00\)00925-7](https://doi.org/10.1016/S0925-8388(00)00925-7).
- [168] Fleischer, S., Lehmkuhl, S., Lohmann, L. *et al.* Approaching the Ultimate Limit in Measurement Precision with RASER NMR. *Appl Magn Reson* (2023). <https://doi.org/10.1007/s00723-023-01597-w>
- [169] G. R. Morrell and M. C. Schabel, "An analysis of the accuracy of magnetic resonance flip angle measurement methods," *Phys Med Biol*, vol. 55, no. 20, pp. 6157–6174, 2010, doi: 10.1088/0031-9155/55/20/008.
- [170] A J Peyton *et al.*, "An overview of electromagnetic inductance tomography: description of three different systems," *Meas Sci Technol*, vol. 7, no. 3, p. 261, 1996, doi: 10.1088/0957-0233/7/3/006.
- [171] Z. Zakaria *et al.*, "Advancements in transmitters and sensors for biological tissue imaging in Magnetic Induction Tomography," *Sensors*, vol. 12, no. 6. pp. 7126–7156, 2012. doi: 10.3390/s120607126.
- [172] M. S. Raven and M. S. Raven, "Experimental measurements of the skin effect and internal inductance at low frequencies," 2015. Wesite. Available: <http://journal.it.cas.cz>
- [173] R. Bounik, F. Cardes, H. Ulasan, M. M. Modena, and A. Hierlemann, "Impedance Imaging of Cells and Tissues: Design and Applications," *BME Front*, vol. 2022, 2022, doi: 10.34133/2022/9857485.
- [174] C. Rumenapp, B. Gleich, and A. Haase, "Magnetic Nanoparticles in Magnetic Resonance Imaging and Diagnostics," *Pharm Res*, vol. 29, no. 5, pp. 1165–1179, 2012, doi: 10.1007/s11095-012-0711-y.
- [175] Duane, W. (1901). The Absolute Measurement of Self-Inductance. *Physical Review (Series I)*, 13(4), 250–252. <https://doi.org/10.1103/PhysRevSeriesI.13.250>
- [176] B. C. Waltrip, S. Avramov-Zamurovic, and A. Koffman, *Inductance Measurement Using an LCR Meter and a Current Transformer Interface*, vol. 2. 2005. doi: 10.1109/IMTC.2005.1604290.
- [177] N. Chuang, T. J. Gale, and R. A. Langman, "Developing measuring inductance strategies on a direct current machine using a DC source with magnetic saturation," *International Journal of Circuit Theory and Applications*, vol. 44, no. 5, pp. 1094–1111, 2016, doi: <https://doi.org/10.1002/cta.2127>.
- [178] S. Yamaguchi *et al.*, "Required accuracy of inductance measurement for current imbalance phenomena," *Cryogenics (Guildf)*, vol. 41, no. 10, pp. 705–712, 2001, doi: [https://doi.org/10.1016/S0011-2275\(01\)00128-X](https://doi.org/10.1016/S0011-2275(01)00128-X).
- [179] V. Matko and M. Milanovic, "Highly enhanced inductance sensing performance of dual-quartz crystal converter," *Sensors*, vol. 19, no. 9, 2019, doi: 10.3390/s19092188.
- [180] V. Michal, Z. Nicol, and A. Matteo, "Low-complexity inductance estimation for switched-mode power converters using peak-current mode control," *IET Power Electronics*, vol. 13, no. 11, pp. 2269–2273, Aug. 2020, doi: <https://doi.org/10.1049/iet-pel.2019.1234>.
- [181] X. Han, P. Ding, J. Xie, J. Shi and L. Li, "Precise Measurement of the Inductance and Resistance of a Pulsed Field Magnet Based on Digital Lock-in Technique," in *IEEE Transactions on Applied Superconductivity*, vol. 22, no. 3, pp. 9001105-9001105, 2012, Art no. 9001105, doi: 10.1109/TASC.2011.2177056.

References

- [182] G. Giovannetti, F. Frijia, A. Flori, A. Galante, C. Rizza, and M. Alecci, "A Practical Guide to Estimating Coil Inductance for Magnetic Resonance Applications," *Electronics*, vol. 11, no. 13, 2022, doi: 10.3390/electronics11131974.
- [183] J. Zuo, J. Fan, Y. Ouyang, H. Liu, C. Yang, and C. Hao, "Transmission Line Sag Measurement and Simulation Research Based on Non-Contact Electric Field Sensing," *Sensors*, vol. 22, no. 21, p. 8379, 2022, doi: 10.3390/s22218379.
- [184] N. Fontana, E. Canicatti and A. Monorchio, "An application of the virtual transmission line model of an open-ended coaxial probe for dielectric properties characterization of biological tissues," 2019 IEEE International Symposium on Antennas and Propagation and USNC-URSI Radio Science Meeting, Atlanta, GA, USA, 2019, pp. 341-342, doi: 10.1109/APUSNCURSINRSM.2019.8888294.
- [185] J. Sharp, K. Bouazza-Marouf, D. Noronha, and A. Gaur, "Tissue type determination by impedance measurement: A bipolar and monopolar comparison," *Saudi J Anaesth*, vol. 11, no. 1, pp. 15–20, 2017, doi: 10.4103/1658-354X.197334.
- [186] A. R. Boody and M. D. Wongworawat, "Accuracy in the measurement of compartment pressures: a comparison of three commonly used devices.," *J Bone Joint Surg Am*, vol. 87, no. 11, pp. 2415–2422, 2005, doi: 10.2106/JBJS.D.02826.
- [187] H. Benchakroun, D. O'Loughlin, N. Ištuk, M. O'Halloran and A. L. Gioia, "Evaluation of the Feasibility of Three Custom-made Tetrapolar Probes for Electrical Characterization of Cardiac Tissue," 2021 15th European Conference on Antennas and Propagation (EuCAP), Dusseldorf, Germany, 2021, pp. 1-5, doi: 10.23919/EuCAP51087.2021.9410978.
- [188] C. L. Brace and S. Etoz, "An analysis of open-ended coaxial probe sensitivity to heterogeneous media," *Sensors*, vol. 20, no. 18, pp. 1–13, Sep. 2020, doi: 10.3390/s20185372.
- [189] J P Grant, R N Clarke, G T Symm, & N M Spyrou. (1989). A critical study of the open-ended coaxial line sensor technique for RF and microwave complex permittivity measurements. *Journal of Physics E: Scientific Instruments*, 22(9), 757. <https://doi.org/10.1088/0022-3735/22/9/015>
- [190] D. K. Misra, "A quasi-static analysis of open-ended coaxial lines," *IEEE Transactions on Microwave Theory and Techniques*, vol. 35, no. 10. pp. 925–928, 1987. doi: 10.1109/TMTT.1987.1133782.
- [191] N. Ištuk, A. L. Gioia, H. Benchakroun, A. Lowery, B. McDermott and M. O'Halloran, "Relationship Between the Conductivity of Human Blood and Blood Counts," in *IEEE Journal of Electromagnetics, RF and Microwaves in Medicine and Biology*, vol. 6, no. 2, pp. 184-190, 2022, doi: 10.1109/JERM.2021.3130788.
- [192] H. Mayrovitz, A. Grammenos, K. Corbitt, and S. Bartos, "Young adult gender differences in forearm skin-to-fat tissue dielectric constant values measured at 300 MHz," *Skin Research and Technology*, vol. 22, 2015, doi: 10.1111/srt.12232.
- [193] M. Cavagnaro, E. Pittella, and S. Pisa, "UWB pulse propagation into human tissues," *Phys Med Biol*, vol. 58, no. 24, pp. 8689–8707, 2013, doi: 10.1088/0031-9155/58/24/8689.
- [194] H. Benchakroun et al., "Design of a Tetrapolar Probe for Electrical Characterization of the Left Atrial Appendage From 0.1 Hz to 100 kHz," in *IEEE Sensors Journal*, vol. 23, no. 1, pp. 741-749, 1 Jan.1, 2023, doi: 10.1109/JSEN.2022.3218534.
- [195] V. Garcia-Vazquez, "Biased four-point probe resistance," *Review of Scientific Instruments*, vol. 88, no. 11, 2017, doi: 10.1063/1.4995389.
- [196] J. H. Kim, H. K. Yoon, S. H. Cho, Y. S. Kim, and J. S. Lee, "Four electrode resistivity probe for porosity evaluation," *Geotechnical Testing Journal*, vol. 34, no. 6, 2011, doi: 10.1520/GTJ102866.
- [197] P. Bertemes-Filho and P. B. Filho, "Tissue Characterisation using an Impedance Spectroscopy Probe," *Med Phys*, no., pp. 27–35, 2002.
- [198] A. P. Schuetze, W. Lewis, C. Brown, and W. J. Geerts, "A laboratory on the four-point probe technique," *Am J Phys*, vol. 72, no. 2, pp. 149–153, 2004, doi: 10.1119/1.1629085.
- [199] D. H. Petersen, O. Hansen, R. Lin, and P. F. Nielsen, "Micro-four-point probe Hall effect measurement method," *J Appl Phys*, vol. 104, no. 1, 2008, doi: 10.1063/1.2949401.

References

- [200] A. Ramos and P. B. Filho, "Electrode probe modeling for skin cancer detection by using impedance method," *IEEE Latin America Transactions*, vol. 10, no. 2, pp. 1466–1475, 2012, doi: 10.1109/TLA.2012.6187588.
- [201] X. Wang, H. Guo, C. Zhou, and J. Bai, "High-resolution probe design for measuring the dielectric properties of human tissues," *Biomed Eng Online*, vol. 20, no. 1, 2021, doi: 10.1186/s12938-021-00924-1.
- [202] H. Alharbi, M. Khalid, and M. Abido, "Transmission Lines Impedance Fitting Using Analytical Impedance Equation and Frequency Response Analysis," *Mathematics*, vol. 10, no. 15, Aug. 2022, doi: 10.3390/math10152677.
- [203] Sabban, A. (2016). ELECTROMAGNETIC THEORY AND TRANSMISSION LINES FOR RF DESIGNERS. In *Wideband RF Technologies and Antennas in Microwave Frequencies*, A. Sabban (Ed.). <https://doi.org/10.1002/9781119048640.ch2>
- [204] A. Zahedi, F. A. Boroumand, and H. Aliakbrian, "Analytical transmission line model for complex dielectric constant measurement of thin substrates using T-resonator method," *IET Microwaves, Antennas & Propagation*, vol. 14, no. 15, pp. 2027–2034, 2020, doi: <https://doi.org/10.1049/iet-map.2019.1117>.
- [205] N. Ištuk, H. Benchakroun, M. A. Elahi and M. O'Halloran, "The Effect of Contact Pressure on Ex-vivo Measurements of the Conductivity of Liver," 2022 16th European Conference on Antennas and Propagation (EuCAP), Madrid, Spain, 2022, pp. 1-3, doi: 10.23919/EuCAP53622.2022.9769625.
- [206] N. Istuk, H. Benchakroun, E. Dunne, and M. O. Halloran, "Pressure Dependency of Conductivity Measurements: The Specific Case of the Lung," 21st International Conference on Biomedical Applications of Electrical Impedance Tomography, vol. 54, no. 16, p. 4878, 2021.
- [207] B. Kumar, G. Rajita, and N. Mandal, "A review on capacitive-type sensor for measurement of height of liquid level," *Measurement and Control*, vol. 47, no. 7, pp. 219–224, Sep. 08, 2014. doi: 10.1177/0020294014546943.
- [208] D. Manalili, M. Berardi, H. Aardema, K. Asimaki, R. Sarmiento, and B. Imran Akca, "Parallel-plate compression test for soft materials: confocal microscopy-assisted ferrule-top nanoindentation," *Biomed Opt Express*, vol. 13, no. 2, pp. 824–837, 2022, doi: 10.1364/BOE.447147.
- [209] M. Ayyildiz, R. Aktas, and C. Basdogan, "Effect of solution and post-mortem time on mechanical and histological properties of liver during cold preservation," *Biorheology*, vol. 51, 2014, doi: 10.3233/BIR-14007.
- [210] H. P. Schwan, P. H. D. And, and C. F. Kay, "Capacitive Properties of Body Tissues." [Online]. Available: <http://ahajournals.org>
- [211] J.-E. Sigdell, "A Principle for Capacitance Measurement, Suitable for Linear Evaluation of Capacitance Transducers," *IEEE Trans Instrum Meas*, vol. 21, no. 1, pp. 60–64, 1972, doi: 10.1109/TIM.1972.4313959.
- [212] S. A. Klemuk, S. Jaiswal, and I. R. Titze, "Cell viability viscoelastic measurement in a rheometer used to stress and engineer tissues at low sonic frequencies," *J Acoust Soc Am*, vol. 124, no. 4, pp. 2330–2339, 2008, doi: 10.1121/1.2973183.
- [213] S. Abasi, J. R. Aggas, G. G. Garayar-Leyva, B. K. Walther, and A. Guiseppi-Elie, "Bioelectrical Impedance Spectroscopy for Monitoring Mammalian Cells and Tissues under Different Frequency Domains: A Review," *ACS Measurement Science Au*, vol. 2, no. 6. American Chemical Society, pp. 495–516, 21, 2022. doi: 10.1021/acsmeasuresciau.2c00033.
- [214] Sasaki, K., Porter, E., Rashed, E. A., Farrugia, L., & Schmid, G. (2022). Measurement and image-based estimation of dielectric properties of biological tissues -past, present, and future. *Physics in medicine and biology*, 67(14), 10.1088/1361-6560/ac7b64. <https://doi.org/10.1088/1361-6560/ac7b64>
- [215] Mirtaheri, P., Grimnes, S., & Martinsen, O. G. (2005). Electrode polarization impedance in weak NaCl aqueous solutions. *IEEE transactions on bio-medical engineering*, 52(12), 2093–2099. <https://doi.org/10.1109/TBME.2005.857639>

References

- [216] P. Ben Ishai, M. S. Talary, A. Caduff, E. Levy, and Y. Feldman, "Electrode polarization in dielectric measurements: A review," *Meas Sci Technol*, vol. 24, no. 10, 2013, doi: 10.1088/0957-0233/24/10/102001.
- [217] Schwan H. P. (1968). Electrode polarization impedance and measurements in biological materials. *Annals of the New York Academy of Sciences*, 148(1), 191–209. <https://doi.org/10.1111/j.1749-6632.1968.tb2sad>
- [218] D. Padmaraj, J. H. Miller, J. Wosik, and W. Zagodzón-Wosik, "Reduction of electrode polarization capacitance in low-frequency impedance spectroscopy by using mesh electrodes," *Biosens Bioelectron*, vol. 29, no. 1, pp. 13–17, 2011, doi: <https://doi.org/10.1016/j.bios.2011.06.050>.
- [219] Jones, D.M. & Smallwood, Rod & Hose, D.R. & Brown, B.H.. (2002). Constraints on tetrapolar tissue impedance measurements. *Electronics Letters*. 37. 1515 - 1517. 10.1049/el:20011034.
- [220] H. Kalvøy, C. Tronstad, B. Nordbotten, S. Grimnes, and Ø. G. Martinsen, "Electrical impedance of stainless steel needle electrodes," *Ann Biomed Eng*, vol. 38, no. 7, pp. 2371–2382, 2010, doi: 10.1007/s10439-010-9989-2.
- [221] G. J. A. M. Brom-Verheijden, M. H. Goedbloed, and M. A. G. Zevenbergen, "A Microfabricated 4-Electrode Conductivity Sensor with Enhanced Range," in *EUROSENSORS 2018*, in *EuroSensors 2018*. MDPI, Dec. 2018. doi: 10.3390/proceedings2130797.
- [222] J. Cinca *et al.*, "Changes in myocardial electrical impedance induced by coronary artery occlusion in pigs with and without preconditioning: Correlation with local ST-segment potential and ventricular arrhythmias," *Circulation*, vol. 96, no. 9, pp. 3079–3086, 1997, doi: 10.1161/01.CIR.96.9.3079.
- [223] M. I. Ellenby, K. W. Small, R. M. Wells, D. J. Hoyt, and J. E. Lowe, "On-line Detection of Reversible Myocardial Ischemic Injury by Measurement of Myocardial Electrical Impedance," *Annals of Thoracic Surgery*, vol. 44, no. 6, pp. 587–597, 1987, doi: 10.1016/S0003-4975(10)62141-8.
- [224] Hahn, G. M., Kernahan, P., Martinez, A., Pounds, D., Prionas, S., Anderson, T., & Justice, G. (1980). Some heat transfer problems associated with heating by ultrasound, microwaves, or radio frequency. *Annals of the New York Academy of Sciences*, 335, 327–351. <https://doi.org/10.1111/j.1749-6632.1980.tb50757.x>
- [225] M. Amini, J. Hisdal, and H. Kalvøy, "Applications of Bioimpedance Measurement Techniques in Tissue Engineering," *J Electr Bioimpedance*, vol. 9, pp. 142–158, 2018, doi: 10.2478/joeb-2018-0019.
- [226] N. Ištuk, H. Benchakroun, M. A. Elahi and M. O'Halloran, "The Effect of Contact Pressure on Ex-vivo Measurements of the Conductivity of Liver," 2022 16th European Conference on Antennas and Propagation (EuCAP), Madrid, Spain, 2022, pp. 1-3, doi: 10.23919/EuCAP53622.2022.9769625.
- [227] H. Benchakroun *et al.*, "Design of a Tetrapolar Probe for Electrical Characterization of the Left Atrial Appendage from 0.1 Hz to 100 kHz," *IEEE Sens J*, 2022, doi: 10.1109/JSEN.2022.3218534.
- [228] P. Linderholm, T. Braschler, J. Vannod, Y. Barrandon, M. Brouard, and P. Renaud, "Two-dimensional impedance imaging of cell migration and epithelial stratification," *Lab Chip*, vol. 6, pp. 1155–1162, 2006, doi: 10.1039/b603856e.
- [229] P. Kassanos, "Bioimpedance Sensors: A Tutorial," *IEEE Sens J*, vol. 21, no. 20, pp. 22190–22219, 2021, doi: 10.1109/JSEN.2021.3110283.
- [230] P. Kassanos, H. M. D. Ip and G. -Z. Yang, "A tetrapolar bio-impedance sensing system for gastrointestinal tract monitoring," 2015 IEEE 12th International Conference on Wearable and Implantable Body Sensor Networks (BSN), Cambridge, MA, USA, 2015, pp. 1-6, doi: 10.1109/BSN.2015.7299403.
- [231] A. Ramos and P. Bertemes-Filho, "Numerical sensitivity modeling for the detection of skin tumors by using tetrapolar probe," *Electromagn Biol Med*, vol. 30, no. 4, pp. 235–245, 2011, doi: 10.3109/15368378.2011.589555.

References

- [232] A. Abd Ali, H. Fadhil, E. Yousif, Z. Hussain, S. Abdul-Wahab, and D. Zageer, "An Insight Into Measuring Conductivity Of Solutions With Ease: A Review," *Res J Pharm Biol Chem Sci*, vol. 8, pp. 2033–2037, 2017.
- [233] S. Grimnes and Ø. G. Martinsen, "Chapter 7 - Electrodes," in *Bioimpedance and Bioelectricity Basics (Third Edition)*, S. Grimnes and Ø. G. Martinsen, Eds., Oxford: Academic Press, 2015, pp. 179–254. doi: <https://doi.org/10.1016/B978-0-12-411470-8.00007-6>.
- [234] Y. M. Dupertuis *et al.*, "Influence of the type of electrodes in the assessment of body composition by bioelectrical impedance analysis in the supine position," *Clinical Nutrition*, vol. 41, no. 11, pp. 2455–2463, 2022, doi: 10.1016/j.clnu.2022.09.008.
- [235] M. Metshein, V.-R. Tuulik, V. Tuulik, M. Kumm, M. Min, and P. Annus, "Electrical Bioimpedance Analysis for Evaluating the Effect of Pelotherapy on the Human Skin: Methodology and Experiments," *Sensors*, vol. 23, no. 9, p. 4251, 2023, doi: 10.3390/s23094251.
- [236] A. Koklu, A. Mansoorifar, and A. Beskok, "Effects of electrode size and surface morphology on electrode polarization in physiological buffers," *Electrophoresis*, vol. 40, no. 5, pp. 766–775, 2019, doi: <https://doi.org/10.1002/elps.201800303>.
- [237] M. Lech, Z. Skutnik, M. Bajda, and K. Markowska-Lech, "Applications of electrical resistivity surveys in solving selected geotechnical and environmental problems," *Applied Sciences*, vol. 10, no. 7, 2020, doi: 10.3390/app10072263.
- [238] P. Schober, C. Boer, and L. A. Schwarte, "Correlation Coefficients: Appropriate Use and Interpretation," *Anesth Analg*, vol. 126, no. 5, 2018, Website. Available: https://journals.lww.com/anesthesia-analgesia/Fulltext/2018/05000/Correlation_Coefficients__Appropriate_Use_and.50.aspx
- [239] M. M. Mukaka, "Statistics Corner: A guide to appropriate use of Correlation coefficient in medical research," 2012. [Online]. Available: www.mmj.medcol.mw
- [240] H. Ma, Y. Su, and A. Nathan, "Cell constant studies of bipolar and tetrapolar electrode systems for impedance measurement," *Sens Actuators B Chem*, vol. 221, pp. 1264–1270, 2015, doi: 10.1016/j.snb.2015.07.089.
- [241] J. A. Canchola, "Correct Use of Percent Coefficient of Variation (%CV) Formula for Log-Transformed Data," *MOJ Proteom Bioinform*, vol. 6, no. 3, 2017, doi: 10.15406/mojpb.2017.06.00200.
- [242] Yu Feldman, E Polygalov, I Ermolina, Yu Polevaya, and B Tsentsiper, "Electrode polarization correction in time domain dielectric spectroscopy," *Meas Sci Technol*, vol. 12, no. 8, p. 1355, 2001, doi: 10.1088/0957-0233/12/8/351.
- [243] P. Awasthi and S. Das, "Reduced electrode polarization at electrode and analyte interface in impedance spectroscopy using carbon paste and paper," *Review of Scientific Instruments*, vol. 90, no. 12, p. 124103, . 2019, doi: 10.1063/1.5123585.
- [244] C. Gabriel, S. Gabriel, and E. Corthout, "The dielectric properties of biological tissues: I. Literature survey," *Phys Med Biol*, vol. 41, pp. 2231–2249, . 1996, doi: 10.1088/0031-9155/41/11/001.
- [245] P. ga *et al.*, "State Of The Art In Left Atrial Appendage Ligation - The Lariat," *J Atr Fibrillation*, vol. 7, no. 1, p. 1073, 2014, doi: 10.4022/jafib.1073.
- [246] Z. Bohušlávěk, "The measurement method of meat conductivity," *Czech Journal of Food Sciences*, vol. 36, no. 5, pp. 373–377, 2018, doi: 10.17221/164/2018-CJFS.
- [247] G. Maenhout, A. Santorelli, E. Porter, I. Ocket, T. Markovic, and B. Nauwelaers, "Effect of Dehydration on Dielectric Measurements of Biological Tissue as Function of Time," *IEEE J Electromagn RF Microw Med Biol*, vol. 4, no. 3, pp. 200–207, 2020, doi: 10.1109/JERM.2019.2953401.
- [248] L. A. Geddes and L. E. Baker, "The specific resistance of biological material-A compendium of data for the biomedical engineer and physiologist," *Med Biol Eng*, vol. 5, no. 3, pp. 271–293, 1967, doi: 10.1007/BF02474537.

References

- [249] M. A. Fallert *et al.*, "Myocardial electrical impedance mapping of ischemic sheep hearts and healing aneurysms," *Circulation*, vol. 87, no. 1, pp. 199–207, 1993, doi: 10.1161/01.CIR.87.1.199.
- [250] W. T. Smith IV, W. F. Fleet, T. A. Johnson, C. L. Engle, and W. E. Cascio, "The Ib phase of ventricular arrhythmias in ischemic in situ porcine heart is related to changes in cell-to-cell electrical coupling," *Circulation*, vol. 92, no. 10, pp. 3051–3060, 1995, doi: 10.1161/01.CIR.92.10.3051.
- [251] N. Ištuk, H. Benchakroun, E. Dunne, and M. O'Halloran, "Pressure Dependency of Conductivity Measurements: The Specific Case of the Lung," 2021, 21st International Conference on Biomedical Applications of Electrical Impedance Tomography, Galway.
- [252] M. Capurro, F. Barberis, "valuating the mechanical properties of biomaterials, Editor(s): Peter Dubrue, Sandra Van Vlierberghe, Biomaterials for Bone Regeneration", Woodhead Publishing, 2014, Pages 270-323, ISBN 9780857098047, <https://doi.org/10.1533/9780857098104.2.270>.
- [253] K. M. Lebedinskii, "Pressure: Physiological Background," M. Y. Kirov, V. V. Kuzkov, and B. Saugel, Eds., Cham: Springer International Publishing, 2021, pp. 3–9. doi: 10.1007/978-3-030-71752-0_1.
- [254] M. I. Lindinger and G. J. F. Heigenhauser, "Intracellular ion content of skeletal muscle measured by instrumental neutron activation analysis," *J Appl Physiol*, vol. 63, no. 1, pp. 426–433, 1987, doi: 10.1152/jappl.1987.63.1.426.
- [255] Douglas S. Richardson and Jeff W. Lichtman, "Clarifying Tissue Clearing," *HHS Public Access*, vol. 176, no. 5, pp. 139–148, 2018, doi: 10.1016/j.cell.2015.06.067.Clarifying.
- [256] Dahiru, Tukur. "P - value, a true test of statistical significance? A cautionary note." *Annals of Ibadan postgraduate medicine* vol. 6,1 (2008): 21-6. doi:10.4314/aipm.v6i1.64038
- [257] B. Wang, Z. Zhou, H. Wang, X. M. Tu, and C. Feng, "The p-value and model specification in statistics," *Gen Psychiatr*, vol. 32, no. 3, pp. 1–4, 2019, doi: 10.1136/gpsych-2019-100081.
- [258] S. Leem and T. Park, "An approximation method of extremely low p-values using permutation test," 2018 IEEE International Conference on Bioinformatics and Biomedicine (BIBM), Madrid, Spain, 2018, pp. 1759-1763, doi: 10.1109/BIBM.2018.8621082.
- [259] P. Samuels and M. Gilchrist, "Paired Samples t-test," Technical Report, 2014.
- [260] W. Kuang and S. Nelson, "Low-frequency dielectric properties of biological tissues: A review with some new insights," vol. 41, . 1998, doi: 10.13031/2013.17142.
- [261] T. Batista Napotnik and D. Miklavčič, "In vitro electroporation detection methods – An overview," *Bioelectrochemistry*, vol. 120, pp. 166–182, 2018, doi: 10.1016/j.bioelechem.2017.12.005.
- [262] R. Stampfli, "Reversible electrical breakdown of the excitable membrane of a Ranvier node," *Anais da Academia Brasileira de Ciencias*, vol. 30, no. 1, pp. 57–61, 1958, <https://eurekamag.com/research/025/402/025402612.php>
- [263] M. Usaj, D. Torkar, and D. Miklavcic, "Automatic cell detection in phase-contrast images for evaluation of electroporation efficiency in vitro," 2007. [Online]. Available: www.springerlink.com
- [264] G. Lukinavičius *et al.*, "A near-infrared fluorophore for live-cell super-resolution microscopy of cellular proteins," *Nat Chem*, vol. 5, no. 2, pp. 132–139, 2013, doi: 10.1038/nchem.1546.
- [265] C. Rohann, S. Joseph K; M. Michael, P. David,"Stereotactic Body Radiotherapy for Oligometastasis: Opportunities for Biology to Guide Clinical Management". *The Cancer Journal* 22(4): p 247-256, 2016. | DOI: 10.1097/PPO.000000000000202
- [266] M. Ayaz, F. Subhan, A. Sadiq, F. Ullah, J. Ahmed, and R. D. E. Sewell, "Cellular efflux transporters and the potential role of natural products in combating efflux mediated drug resistance," *FBL*, vol. 22, no. 4, pp. 732–756, 2017.
- [267] Y. Xu, X. Xie, Y. Duan, L. Wang, Z. Cheng, and J. Cheng, "A review of impedance measurements of whole cells," *Biosens Bioelectron*, vol. 77, pp. 824–836, 2016, doi: 10.1016/j.bios.2015.10.027.

References

- [268] K. L. Perkins, "Cell-attached voltage-clamp and current-clamp recording and stimulation techniques in brain slices," *J Neurosci Methods*, vol. 154, no. 1, pp. 1–18, 2006, doi: <https://doi.org/10.1016/j.jneumeth.2006.02.010>.
- [269] C. E. Yellowley, J. C. Hancox, and H. J. Donahue, "Effects of cell swelling on intracellular calcium and membrane currents in bovine articular chondrocytes," *J Cell Biochem*, vol. 86, no. 2, pp. 290–301, . 2002, doi: <https://doi.org/10.1002/jcb.10217>.
- [270] D. L. Hughes, A. Hughes, Z. Soonawalla, S. Mukherjee, and E. O'Neill, "Dynamic physiological culture of ex vivo human tissue: A systematic review," *Cancers*, vol. 13, no. 12. 2021. doi: [10.3390/cancers13122870](https://doi.org/10.3390/cancers13122870).
- [271] O. Bergmann *et al.*, "Evidence for cardiomyocyte renewal in humans," *Science (1979)*, vol. 324, no. 5923, pp. 98–102, 2009, doi: [10.1126/science.1164680](https://doi.org/10.1126/science.1164680).
- [272] T. Billiet, M. Vandenhaute, J. Schelfhout, S. Van Vlierberghe, and P. Dubruel, "A review of trends and limitations in hydrogel-rapid prototyping for tissue engineering," *Biomaterials*, vol. 33, no. 26, pp. 6020–6041, 2012, doi: <https://doi.org/10.1016/j.biomaterials.2012.04.050>.
- [273] Luo, T., Tan, B., Zhu, L., Wang, Y., & Liao, J. (2022). A Review on the Design of Hydrogels With Different Stiffness and Their Effects on Tissue Repair. *Frontiers in bioengineering and biotechnology*, 10, 817391. <https://doi.org/10.3389/fbioe.2022.817391>
- [274] J. C. Weaver, "Electroporation: A general phenomenon for manipulating cells and tissues," *J Cell Biochem*, vol. 51, no. 4, pp. 426–435, . 1993, doi: <https://doi.org/10.1002/jcb.2400510407>.
- [275] I. Banerjee, J. W. Fuseler, R. L. Price, T. K. Borg, and T. A. Baudino, "Determination of cell types and numbers during cardiac development in the neonatal and adult rat and mouse," *American Journal of Physiology-Heart and Circulatory Physiology*, vol. 293, no. 3, pp. H1883–H1891, Sep. 2007, doi: [10.1152/ajpheart.00514.2007](https://doi.org/10.1152/ajpheart.00514.2007).
- [276] N. Milani-Nejad and P. M. L. ssen, "Small and large animal models in cardiac contraction research: advantages and disadvantages," *Pharmacol Ther*, vol. 141, no. 3, pp. 235–249, 2014, doi: [10.1016/j.pharmthera.2013.10.007](https://doi.org/10.1016/j.pharmthera.2013.10.007).